



Visible Light Communication using C-OFDM

by

Jummah Abdulwali

School of Engineering

Newcastle University, Newcastle upon Tyne, UK

This thesis is submitted for the degree of Doctor of Philosophy.

January 2023

Abstract

In recent years, new difficulties have been faced in data transmission rates due to advances in next-generation communications. New spectrum resources, including terahertz, millimetre, and visible light, have gained prominence as research topics. Visible light communication (VLC) has a lower deployment cost than the other resources because it allows for concurrent illumination and communication. Unlike conventional wireless communications, VLC operates in the 400-800 THz band and has unique physical characteristics, including superior resistance to electromagnetic interference, secure confidentiality, and high data throughput. This suggests that VLC can be developed as a powerful wireless technique for next-generation communication. VLC utilises light-emitting diodes (LEDs) to modulate the intensity of optical power at the transmitter before transmission over the channel and direct detection at the receiver via a photodetector. The critical challenge in VLC systems is the modulation bandwidth limitation experienced by commercial LEDs, which causes severe reductions in overall throughput. To overcome this challenge, one of the most promising solutions is the adoption of advanced modulation formats such as orthogonal frequency division multiplexing (OFDM). OFDM is a specific case of frequency division multiplexing (FDM) and a popular candidate technology for VLC systems because of its robustness against multipath propagation and high spectral efficiency. Due to the division of available bandwidth into several subcarriers. Moreover, it allows for more extensive data rates without the need for sophisticated equalisers at the receiver. These exceptional features of OFDM mean that it is deemed to be a robust modulation technique capable of significantly improving VLC systems.

Although conventional OFDM modulation has been considered a successful modulation technique for wired and wireless communications systems in several applications, there are still various areas that need to be developed. The large peak-to-average power ratio (PAPR) of the signal is thought to be the main barrier to the achievement of high performance by OFDM systems. In particular, the addition of DC-bias to OFDM symbols and then passing them via the restricted linear dynamic range of the LED renders these schemes unsuitable for some VLC applications where energy economy is paramount.

The primary emphasis of this research is the development of a unique method for OFDM with application to visible light communication (VLC). It is dedicated to improving OFDM performance by reducing the PAPR and computational complexity, thereby enhancing the non-linear region and broadening the limited bandwidth associated with LEDs. In order to address such negative elements of OFDM systems, a novel technique based on an OFDM scheme is proposed in this thesis. Here, the C-transform which combines the Walsh-Hadamard transform (WHT) and discrete cosine transform (DCT) into an orthogonal signal. The proposed transform uses a novel type of optical orthogonal frequency division multiplexing called C-OFDM.

Glossary of Abbreviations

5G	Fifth generation
6G	Sixth generation
(M-PAM)	Multi-level pulse amplitude modulation
ACO-OFDM	Asymmetrically clipped optical OFDM
ADC	Analogue to digital converter
ADO-OFDM	Asymmetrically clipped DC-biased optical OFDM
APD	Avalanche photodiodes
AWGN	Additive white gaussian noise
BDC	Block diagonal structure
BER	Bit error rate
BW	Bandwidth
CA	Complex addition
CAP	Carrier-less amplitude and phase
CCDF	Complementary cumulative distribution Function
CCRR	Computational complexity reduction ratio
CDMA	Code division multiple access
CFO	Carrier frequency offset
CIR	Channel impulse response
CM	Complex multiplication
CP	Cyclic prefix
CT	C-transform
DAB	Digital audio broadcasting
DC	Direct Current
DCO-OFDM	DC-biased optical OFDM
DCT	Discrete cosine transform
DD	Direct detection
DFT	Discrete fourier transform

DHT	Discrete hartley transform
DMT	Discrete multi-tone
DSL	Digital subcarrier loop
DVB	digital video broadcasting
EOC	Electrical to optical converter
EMI	Electromagnetic interference
FDM	Frequency division multiplexing
FFT	Fast fourier transform
FHT	Fast hartley transform
FIR	Finite impulse response
F-OFDM	Fast OFDM
FOV	Field of view
FSO	Free space optical
GaAs	Gallium arsenide
GaN	Gallium nitride
Ge	Germanium
GRO	Gray reverse order
GSM	Global system for mobile communication
HPA	High power amplifier
HS	Hermitian symmetry
IBI	Inter-Block interference
ICI	Inter-Carrier interference
IDCT	Inverse DCT
IDFT	Inverse DFT
IFFT	Inverse FFT
IM	Intensity modulation
IMT	International mobile telecommunications
InGaAs	Indium gallium arsenide
IoT	Internet-of-Things
IR	Infra-red
ISI	Intersymbol interference

ITU	International telecommunication union
LED	Light emitting diode
Li-Fi	Light fidelity
LOS	Line-of-sight
LPF	Low-pass filter
LTE	Long term evolution
MCM	Multicarrier modulation
MIMO	Multiple-input and multiple-output
NLOS	Non-line of sight
NR	New radio
NRZ	Non-return to zero
NTT	Nippon telephone and telegraph
OFDM	Orthogonal frequency division multiplexing
OLED	Organic LED
OWC	Optical wireless communications
P/S	Parallel-to-Serial
PAM	Pulse amplitude modulation
PAPR	Peak-to-average power ratio
PD	Photodetector
PGR	Postgraduate research
PSD	Power spectral density
PTS	Partial transmit sequence
QAM	Quadrature amplitude modulation
RA	Real addition
RF	Radio frequency
RM	Real multiplication
RGB	Red, Green and Blue
RO	Real operation
Rx	Receiver
S/P	Serial-to-parallel
SCs	Subcarriers

SLM	Selective mapping
SNR	Signal-to-noise ratio
SSL	Solid-state lighting
TDMA	Time division multiple access
TI	Tone injection
TR	Tone reservation
TOV	Turn-on voltage
Tx	Transmitter
uHDD	Ultrahigh data density
uHSSLLC	Ultrahigh-speed with low delay communications
uMUB	Universal mobile ultra-broadband
VLC	Visible light communications
WDM	Wavelength division multiplexing
Wi-Fi	wireless fidelity
WiMAX	Worldwide interoperability for microwave access
WPLED	White phosphor LED
ZP	Zero padding

Dedications

To the most important people in my life, my parents, siblings, wife and children. I dedicate this thesis to you.

Acknowledgments

First and foremost, I would like to express my sincere apologies if I inadvertently overlooked anyone in this acknowledgment section. It was never my intention, and I am truly grateful for everyone who contributed to the success of my PhD journey.

I am immensely grateful to the Libyan government for their invaluable financial assistance. Without their generous sponsorship, pursuing this PhD would have been far beyond my means. Their support has made this academic endeavor possible, and I am deeply appreciative.

I extend my heartfelt appreciation to my primary advisor, Professor Said Boussakta, whose unwavering support, guidance, and encouragement have been instrumental throughout my study. At every step, Professor Boussakta has demonstrated unwavering confidence in my abilities, fueling my enthusiasm and patience.

I would like to express my profound gratitude to Dr. Paul Haigh, my second supervisor, for his comprehensive and constructive conversations, valuable advice, and consistent assistance. Dr. Haigh generously dedicated his own time to provide ongoing support, and I am forever indebted to him for his invaluable contributions.

I am thankful to Newcastle University, the School of Electrical and Electronic Engineering, and all the remarkable individuals I have had the privilege of knowing during my academic journey. A special mention goes to my colleagues at the Merz Court building, whose friendliness and efficiency have made my experience all the more enriching. I would also like to extend my gratitude to the school receptionist and the postgraduate research coordinator, Miss Nicola Hawdon, for their invaluable assistance in various aspects.

Lastly, I would like to express my deepest appreciation to my parents and my wife for their unwavering encouragement, patience, understanding, and limitless support throughout my entire PhD study, from day one until the very end. Their constant belief in me has been an invaluable source of strength. Additionally, I would like to acknowledge my children, Khadeejah, Mohammed, Abraheem, and Fatimah, for their understanding and support.

Once again, I offer my sincere gratitude to all the individuals and organisations who have contributed to my academic journey. Your support and encouragement have been truly invaluable, and I am forever grateful for the opportunities and growth that have come my way.

Declaration

I certify that this thesis is entirely my own original work and has never before been presented, by either myself or anyone else, for a degree or certificate at a college or university. This thesis, to the best of my knowledge, does not include any previously published material unless this has been explicitly acknowledged in the list of references.

Jummah Abdulhalim Mohammed Abdulwali

Table of Contents

Abstract	i
Glossary of Abbreviations.....	iii
Dedications.....	vii
Acknowledgments.....	viii
Declaration	ix
Table of Contents	x
List of Figures	xiv
List of Tables.....	xvii
Chapter 1	1
1 Introduction	1
1.1 Background.....	1
1.2 Problem Statement	6
1.3 Research Aims and Objectives	10
1.4 Thesis organisation.....	11
1.5 Original contributions	14
1.6 List of Publications and Awards	15
1.6.1 Peer-reviewed Journal Papers.....	15
1.6.2 Peer-reviewed Conference Papers.....	15
1.6.3 Awards.....	15
2 Visible Light Communication Principles	16
2.1 Evolution of Mobile Communications Networks	16
2.2 Visible Light Communication (VLC)	17
2.2.1 LED Devices	19
2.2.2 Photodetector	23
2.3 Challenges in VLC	25
2.4 Carrier-less Amplitude and Phase Modulation (CAP)	27
2.5 Orthogonal Frequency Division Multiplexing (OFDM)	31

2.5.1	History of OFDM.....	31
2.5.2	OFDM in VLC.....	34
2.5.3	Cyclic prefix (CP).....	36
2.5.4	DC biased optical OFDM (DCO-OFDM).....	40
2.5.5	Asymmetrically clipping optical OFDM (ACO-OFDM)	44
2.6	Advantages and disadvantages of OFDM	46
2.6.1	Drawbacks of OFDM Systems.....	46
2.7	Conclusion	47
Chapter 3		48
3	C-transform.....	48
3.1	Discrete Cosine Transform (DCT)	48
3.2	Walsh-Hadamard Transform (WHT).....	49
3.3	C-transform matrix.....	54
3.4	Computational Complexity.....	57
3.4.1	DCT Computational	57
3.4.2	WHT+DCT Computational Complexity	57
3.4.3	IFFT Computational Complexity	58
3.4.4	CT Computational Complexity.....	60
3.5	Conclusion	66
Chapter 4		67
4	Performance Comparison of C-OFDM, DCO-OFDM and F-OFDM in terms of PAPR Reduction 67	
4.1	Introduction	67
4.2	Fast OFDM.....	68
4.3	PAPR Performance of OFDM Systems.....	70
4.4	VLC Applications of the Proposed Schemes.....	71
4.4.1	Test Set-up.....	71
4.4.1.1	Proposed System Theory.....	74
4.5	Simulation Results and Discussion	74

4.5.1	PAPR Reduction.....	74
4.5.2	BER Performance.....	77
4.5.2.1	BER Performance over AWGN Channel	77
4.5.2.2	BER Performance under the Influence of the Bandwidth Limitation of the LED.	78
4.5.3	Computational Complexity.....	79
4.6	Conclusion.....	81
Chapter 5		82
5	LED Non-linearity Effect on VLC Utilising C-OFDM.....	82
5.1	Introduction	82
5.2	OFDM Systems Model.....	87
5.3	Simulation Results and Discussion	89
5.3.1	BER Performance.....	89
5.3.2	Power Penalties.....	95
5.4	Conclusion	97
6	Performance of C-OFDM with a Multipath Channel.....	98
6.1	Introduction	98
6.2	Channel Model	99
6.2.1	Differences in Propagation Modes.....	99
6.2.2	VLC Channel Model	100
6.3	Multipath Channel.....	110
6.3.1	Channel Impulse Response (CIR).....	110
6.4	System Model.....	111
6.5	Simulation Results and Discussion	113
6.5.1	BER Performance over VLC AWGN Channel.....	113
6.5.2	BER Performance over VLC Multipath Channel	114
6.5.2.1	BER Performance against the Bandwidth Limitations of the LED.....	115
6.5.3	Power Penalties.....	116
6.6	Conclusion.....	118
7	Conclusion and future work	119

7.1	Conclusion	119
7.2	Future Work	122
	References	123

List of Figures

Figure 1-1: Exponential growth in the rate of data transfer in wireless communication.....	2
Figure 1-2: Indoor and outdoor OWC	3
Figure 1-3: VLC in the electromagnetic spectrum.....	4
Figure 1-4: The UK RF spectrum.....	8
Figure 1-5: Thesis plan and structure.....	13
Figure 2-1: Block diagram of a typical VLC system.....	18
Figure 2-2: Block diagram of RGB LED.....	19
Figure 2-3: Block diagram of WPLED.....	20
Figure 2-4: A diagram depicting the optical and electrical bandwidths.	22
Figure 2-5: Relative response of PDs for different materials.....	24
Figure 2-6: The concept of m -CAP demonstrated in terms of the frequency response for $m = 1, 2, 4, 8, 10$	28
Figure 2-7: Block diagram of m -CAP system.	29
Figure 2-8: Impulse Response of the Raised Cosine Filter [71].....	30
Figure 2-9: Frequency domain representation of raised cosine pulse shaping filters [71].	31
Figure 2-10: The history of OFDM has led to the current system stage.	33
Figure 2-11: (a) Flat fading channel (b) Frequency selective	34
Figure 2-12: Frequency spectrums of FDM and OFDM systems with four SCs.....	35
Figure 2-13: OFDM symbol in time domain with four SCs.....	35
Figure 2-14: Cyclic prefix extension.	37
Figure 2-15: Block diagram of the DCO-OFDM.	41
Figure 2-16: Hermitian Symmetry (HS) of DCO-OFDM	42
Figure 2-17: BER performance as a function of E_b/N_0 for DCO-OFDM with DC bias levels of 7, 10 and 13 dB utilising 4, 16, 64 and 256 QAM.....	Error! Bookmark not defined.
Figure 2-18: Block diagram of the ACO-OFDM.....	45
Figure 2-19: Hermitian Symmetry (HS) of ACO-OFDM.	45
Figure 3-1: Discrete Walsh functions, $N = 8$ (a) Hadamard-ordered; (b) Walsh-ordered	53
Figure 3-2: C-transform matrix for $N = 32$	56
Figure 3-3: (a) 8-point 2-radix FFT butterfly flowchart; (b) DIT FFT butterfly.	59
Figure 3-4: (a) BDS transform butterfly; (b) one butterfly structure.	61
Figure 3-5: Computational cost number.	64
Figure 4-1: Subcarrier separation for OFDM (top) and F-OFDM (bottom),	69
Figure 4-2: F-OFDM system.....	70

Figure 4-3: System block diagram	72
Figure 4-4: PAPR performance of the proposed system, F-OFDM, and OFDM.	75
Figure 4-5: Measured PAPR for C-OFDM, F-OFDM and OFDM.....	76
Figure 4-6: BER performance as a function of E_b/N_o for C-OFDM, F-OFDM with 2-PAM, and OFDM with 4-QAM across AWGN channel.	77
Figure 4-7: BER performance as a function of E_b/N_o for C-OFDM, F-OFDM with 2-PAM and OFDM with 16-QAM	78
Figure 4-8: BER performance as a function of E_b/N_o for C-OFDM, F-OFDM with 2-PAM and OFDM with 4-QAM.....	79
Figure 4-9: Computational complexity comparison of CT, DCT and FFT.....	80
Figure 4-10: CCRR shows when N is low, the reduction ratio is approximately 75%, which falls to around 50% when N is increased comparing to FFT,	80
Figure 5-1: Non-linear LED transfer function[2].....	83
Figure 5-2: The measured L-I-V curves of the LED.	85
Figure 5-3: LED measurement data (a) V-I curve; (b) I-V curve; (c) V-L curve; (d) I-L curve.	86
Figure 5-4: Block diagram of the OFDM schemes tested.....	88
Figure 5-5: BER performance as a function of E_b/N_o for OFDM with 4-QAM and 200 AC.....	90
Figure 5-6: BER performance as a function of E_b/N_o for F-OFDM with 2-PAM and 200 AC.	90
Figure 5-7: BER performance as a function of E_b/N_o for C-OFDM with 2-PAM and 200 AC	91
Figure 5-8: BER performance as a function of E_b/N_o for OFDM with 16-QAM and 200 AC.....	92
Figure 5-9: BER performance as a function of E_b/N_o for F-OFDM with 4-PAM and 200 AC.....	92
Figure 5-10: BER performance as a function of E_b/N_o for C-OFDM with 4-PAM and 200 AC.	93
Figure 5-11: BER performance as a function of E_b/N_o for OFDM with 4-QAM and 600 AC.	94
Figure 5-12: BER performance as a function of E_b/N_o for F-OFDM with 2-PAM and 600 AC.	94
Figure 5-13: BER performance as a function of E_b/N_o for C-OFDM with 2-PAM and 600 AC.....	95
Figure 5-14: The net power penalty gains for C-OFDM over F-OFDM at 200 mA.	96
Figure 6-1: Different link configurations (a) directed LOS, (b) non-directed LOS, (c) diffuse	100
Figure 6-2: Geometry of LOS and NLOS propagation model.	101
Figure 6-3: Radiation emission patterns for several Lambertian orders [1].	104
Figure 6-4: Received power distribution for single LED with $\theta=60$ semi-angle at half power illumination.	105
Figure 6-5: Received power distribution for single LED with $\theta=12.5$ semi-angle at half power illumination.	106
Figure 6-6: Signal-to-noise ratio (SNR) distribution for one LED with 60° semi-angle at half power illumination.	106

Figure 6-7: Signal-to-noise ratio (SNR) distribution for one LED with 12.5° semi-angle at half power illumination.	107
Figure 6-8: Received power distribution for multiple LEDs with 60° semi-angle at half power illumination.	108
Figure 6-9 Received power distribution for multiple LEDs with 12.5° semi-angle at half power illumination.	108
Figure 6-10: Signal-to-noise ratio (SNR) distribution for multiple LEDs with 60° semi-angle at half power illumination.	109
Figure 6-11: Signal-to-noise ratio (SNR) distribution for multiple LEDs with 12.5° semi-angle at half power illumination.	109
Figure 6-12: Impulse responses of VLC channels: (a) LED NLOS; (b) LED LOS (c) LED (NLOS+LOS). ...	110
Figure 6-13: Block diagram for the OFDM schemes tested over the VLC CIR.....	112
Figure 6-14: BERs of the proposed C-OFDM, F-OFDM and OFDM systems through the AWGN channel	113
Figure 6-15: BER performance as a function of E_b/N_0 for C-OFDM, F-OFDM and OFDM under VLC channel characteristics.....	114
Figure 6-16: BER performance as a function of E_b/N_0 for C-OFDM, F-OFDM and OFDM with $F_c/B = 1, 0.75, \text{ and } 0.5$	115
Figure 6-17: Measured electrical power penalties for C-OFDM, F-OFDM and OFDM for the BER target of 10^{-3}	117
Figure 6-18: Net power penalty gain for C-OFDM over F-OFDM and OFDM.....	117

List of Tables

Table 1.1: Comparison of light sources.....	5
Table 1.2: Comparison of VLC and RF communication system.....	6
Table 2.1: Typical parameters of silicon PIN PD and Si APD	25
Table 3.1: Relation between the Walsh-ordered and Hadamard-ordered Walsh functions.....	52
Table 3.2: Real additions R_A and multiplications R_M in computational complexity for CT, DCT, DCT-WHT and FFT under different lengths of the transform N	63
Table 3.3: Total computational complexity for CT, DCT, DCT-WHT and FFT under different lengths of the transform N	64
Table 3.4: The computational complexity reduction ratio for CT, DCT, DCT-WHT and FFT under different lengths of the transform N	65
Table 6.1: Parameters for an indoor VLC system.....	103

Chapter 1

Introduction

This chapter provides an overview of the critical aspects that will be addressed and discussed. Specifically, we focus on the following points: the background, problem statement, research aims and objectives, thesis organization, original contributions, and a list of publications and awards.

1.1 Background

Demand for ultra-fast mobile networks has recently increased dramatically, but broadband communication services are still essential. The need to communicate anywhere and at any time has motivated researchers to develop and improve existing infrastructure. They aim to develop future technologies that will meet the needs of next-generation communication networks, such as the sixth generation (6G), which is the next wave of mobile telecommunication following today's 5G standards. Compared with existing 5G systems, 6G is intended to increase capacity, data transmission speed and spectral and power efficiency, and to improve services. Simultaneously, long battery life and the achievement of the lowest possible implementation costs are also deemed essential [3, 4].

Furthermore, developments in modern society have forced researchers to find a novel telecommunications technology that meets essential requirements such as in providing smart homes and cities and smartphones. All of these improvements will result in an expansion of current volumes of mobile and wireless traffic which are expected to be 1000 times greater than current communication levels over the next ten years [5]. Moreover, in its vision of the Network Society, Ericsson predicted that there would be 50 billion connected devices by 2020. More than 15 billion of these would be enabled for video [6], increasing the number of communication devices involved in what is known as the 'Internet of Things' (IoT). That will change users' daily lives which will become more comfortable, safe, and efficient [7].

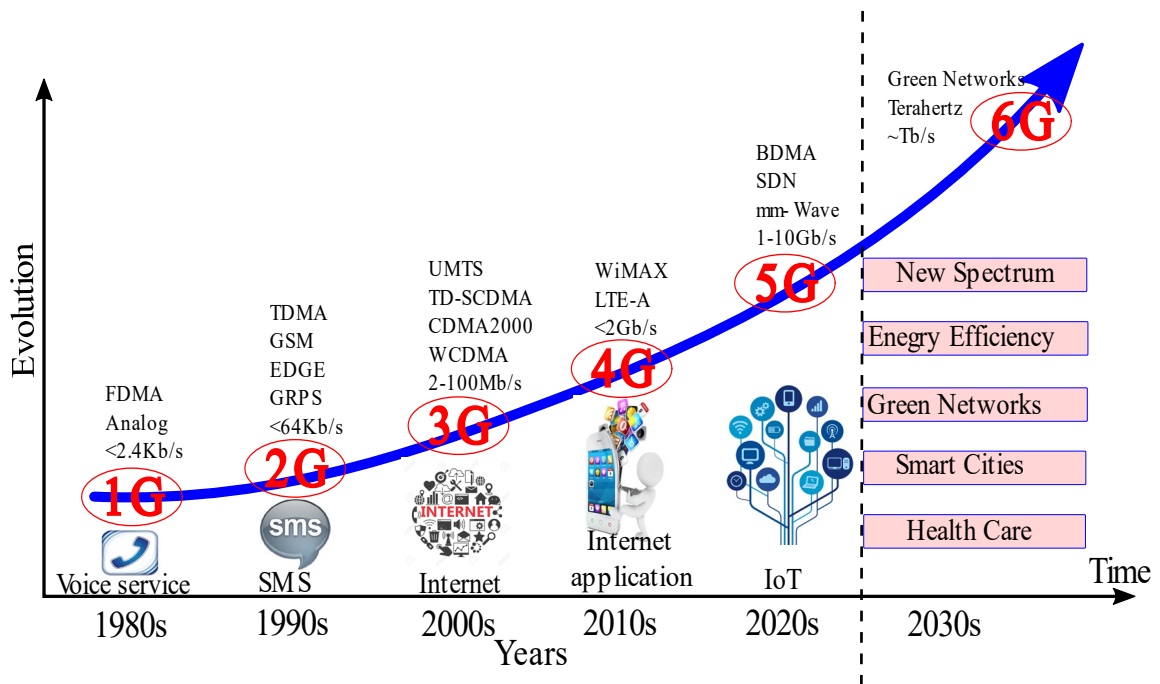


Figure 1-1: Exponential growth in the rate of data transfer in wireless communication

According to one prediction [8], the number of connected devices will reach more than seventy billion worldwide by 2025.

Therefore, 5G networks should include smaller-cell microcells in higher densities, with an extended spectrum in a more power-efficient network with mobile convergence to meet these requirements. It has been claimed [9] that 5G systems may provide Gbps levels at any time and anywhere. Moreover, by 2023, 5G-enabled mobile devices and connections will account for over 10% of all mobile devices worldwide with 1.4 billion 5G-capable smartphones in use bringing the total number to 13.1 billion compared to 8.8 billion in 2018 [10]. This could only be achieved with a lot more spectrum than the currently available for international mobile telecommunications IMT systems via the International Telecommunication Union (ITU) process. As 5G is marketed all over the world, research communities across the globe are beginning to look beyond 5G, and 6G is expected to evolve towards green networks which provide high-quality and energy-efficient service (see Figure 1.1). It is expected that 6G will be available by 2030 [11]. However, significant improvements in the communications network system are necessary in order to achieve the requirements for the next generation of applications. The vision of the next revolution in communication involves unprecedented advances and the integration of traditional land mobile networks with emerging satellite, air, and underwater acoustic networks to provide access to the network at any time, anywhere [12]. Three novel 6G services have been identified [13]: (i) ultrahigh data density (uHDD); (ii) universal mobile ultra-broadband (uMUB), (iii) ultrahigh-speed with low delay

communications (uHSLLC). To accomplish these services, potential and associated beneficial technologies must be considered to form sustainable and socially resilient networks spanning both terahertz and visible-light communication (VLC) [14, 15]. Therefore, scientists are increasingly turning to optical wireless communication (OWC) technologies because of their wide bandwidth, license-free spectra, and inexpensive implementation costs so as to meet the rapidly expanding demand among end-users for data volumes and bandwidth.

A communications technology that utilises light as a transmission medium is commonly known as optical communication technology. This is an area of enormous interest in the telecommunications research community. Optical wireless communication (OWC) is a wireless communication technique that uses an unlicensed spectrum of 670 THz and can give very high data rates. Moreover, OWC can be classified into two categories according to its use of two wavelength spectra: (i) the infrared (IR) spectrum for IR communication; and (ii) the visible light spectrum for VLC [16]. This includes indoor or outdoor OWC with a wide range of applications, as shown in Figure 1.2. For two decades now, VLC has achieved close attention as an important supplementary communications technology for indoor short-distance communication systems to satisfy the demand for a high data rate, R_b , and it is growing exponentially. According to the latest study from Cisco, 24 Exabytes expect to increase monthly. Most of this evolution relates to indoor communications, where the rates of growth of indoor wireless communication are increasing faster than those of outdoor wireless communication by 20% [10]. VLC systems utilise visible light for communication, occupying

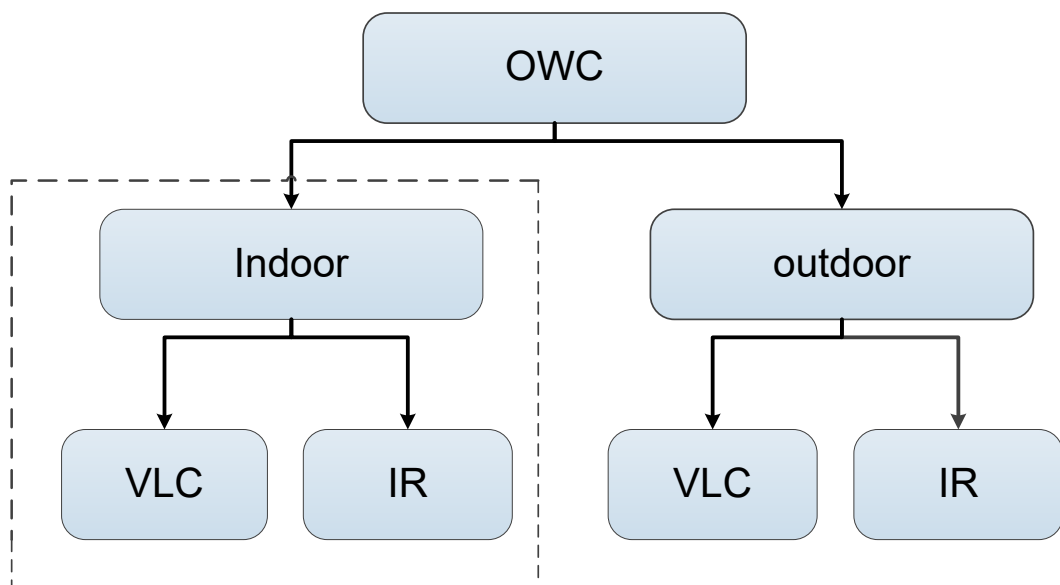


Figure 1-2: Indoor and outdoor OWC

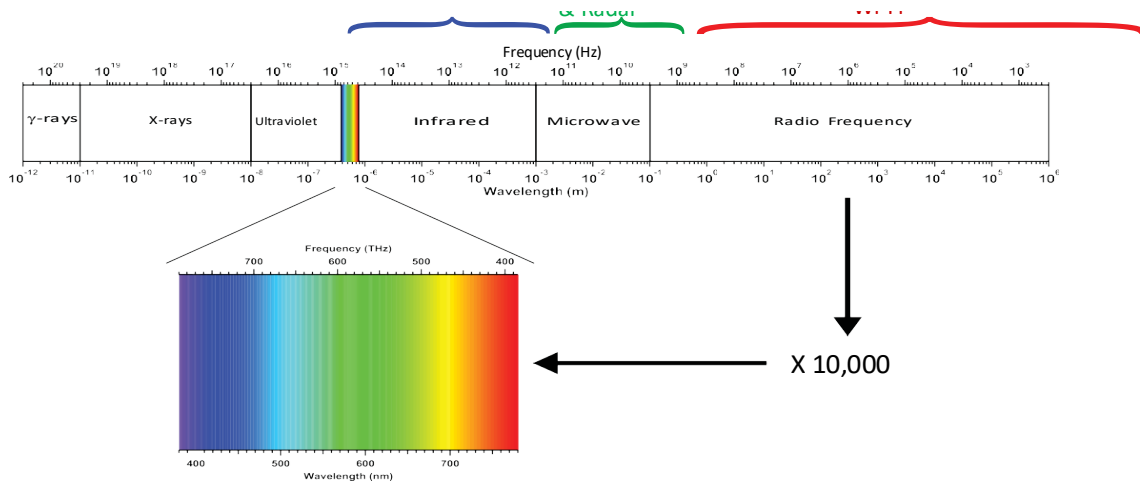


Figure 1-3: VLC in the electromagnetic spectrum




a frequency spectrum of 430–790 THz corresponding to wavelengths of 380 nm to 750 nm. In other words, the bandwidth (BW) is approximately 350 THz. Figure 1.3 depicts the electromagnetic spectrum’s frequency distribution for visible light, RF, and other forms of electromagnetic environment for indoor and outdoor wireless communication. Also, VLC is provided with an unlicensed that is more remarkable than the whole RF spectrum by 10000 and an R_b faster than conventional WiFi by 10 times. As a further benefit, VLC is potentially more energy-efficient, widely available, and ecologically friendly, with no risk to human health or RF interference in communication processes. Several conference papers [17-20] in Japan produced the first reports of VLC utilising light-emitting diodes (LED), but it took several years for a comprehensive scientific paper to be published [21]. LEDs and photodetectors (PD) are used in tandem to transmit data while also lighting up the room, , in processes known as intensity modulation (IM) and direct detection (DD) respectively [16]. The utilisation of LEDs within the VLC system has several advantages compared with general lighting sources such as incandescent bulbs and fluorescent lamps. They can be modified at speeds that surpass the human eye’s perceptual ability (>100 Hz), allowing them to fulfil safety standards for human vision. Moreover, LEDs have a unique capacity to integrate solid-state lighting with data transfer. VLC systems that use LEDs have additional benefits, including high brightness levels, longer lifespan, environmental friendliness, durability, inherent data security, and better transmission speeds. Table 1.1 summarises the comparison between other available lighting sources and LEDs in terms of light levels, luminous efficiency, heat and hours of life. Therefore,

the utilisation of LEDs as light sources results in lower levels of greenhouse gas emissions [22, 23].

In general, there are essentially two ways to generate light using three types of visible LEDs. The first type of LED is known as RGB, which uses a technique of combining the colours red, green and blue with wavelengths of 625, 525 and 470 nm respectively at a precise ratio so that white light can be obtained [16]. Although this LED has a bandwidth of up to 10s MHz, control of the combination of the three colours to produce white light can be difficult [24]. On the other hand, this LED is attractive for applications that involve changes in colour [16]. The utilisation of an RGB LED at Gbps in WDM with a blue filter on the receiver side has been demonstrated [25-27] ; however, the utilisation of the RGB LED leads to colour balancing issues [28]. Blue-chip + phosphor or white phosphor LEDs (WPLEDs) represent a second way to produce white light. In this case, the blue LED is coated with yellow phosphor. This straightforward LED method provides data translation and illumination in a single room [29] but, due to the delayed reactivity of the phosphor layer, WPLED bandwidth is reduced to a few MHz [25, 29]. As mentioned earlier, the VLC technology provides a considerable bandwidth at THz level, but the use of an LED as a transmitter causes a reduction in bandwidth to MHz. According to some studies [30, 31], the bandwidth and data rate might be developed by utilising equalisers and blue filters at the cost of increasing the system’s computational complexity. Digital signal processing algorithms, including equalisers and artificial neural network-based classifiers, have also pushed data rates into the Gb/s region [32, 33].

Bandwidth constraints are the primary obstacle to excellent performance in VLC

Table 1.1: Comparison of light sources

Source of light	Light	Heat	Lifespan (hours)	Luminous efficiency	
Incandescent bulb	5%	95%	1000	51 lm/W	 1 st industrial light source
Fluorescent	25%	75%	10,000	90 lm/W	 Whit light
LED	>50%	< 50%	>50,000	200 lm/W	 Compact

systems. Therefore, advanced modulation formats such as orthogonal frequency division multiplexing (OFDM) and carrier-less amplitude and phase modulation (CAP) have become prevalent due to their higher spectral efficiency and adaptability [34, 35]. CAP is a multi-level, multi-band modulation scheme that is very similar to the quadrature amplitude modulation (QAM) technique in terms of its conception. However, CAP uses two finite impulse response (FIR) band-pass filters, which form Hilbert pairs to enable complex symbol alphabets. Furthermore, both methods have set ultra-high data rates, but more commonly this is achieved with OFDM [36].

OFDM is an exceptional case of frequency division multiplexing (FDM). It is a popular candidate technology for VLC systems because of its robustness against multipath propagation and its high spectral efficiency due to the division of available bandwidth into several subcarriers [37]. Moreover, it allows for more extensive data rates without the need for sophisticated equalisers at the receiver [16, 38]. These exceptional features of OFDM mean that it is deemed to be a robust modulation technique capable of significantly improving VLC systems.

1.2 Problem Statement

As stated in the preceding section, the ever-increasing bandwidth needs of current and upcoming communication systems are driving research in optical wireless communications. VLC ensures a large bandwidth that might be used as a supplementary communication

Table 1.2: Comparison of VLC and RF communication system

Parameter	VLC (indoor system)	RE system
Bandwidth	~ 400THz	Regulated and limited
Power consumption	Low	Medium
Security	High	Low
EM interference	None	Present
Services	Illumination and communication	Communication
Distance	Short	Short and long
Coverage	Narrow and wide	Mostly wide
Mobility	Limited	Good
Noise	Sun light and other ambient lights	All electrical/electronic appliances

technique to alleviate the spectrum congestion that RF communication systems are now experiencing, resulting in faster data rates [37]. Figure 1.4 depicts the overcrowding of the UK RF spectrum which results in premium licencing costs and bandwidth restrictions [39]. In order to compare standard RF-based communication systems to VLC systems, Table 1.2 summarises several of the most crucial characteristics. The ability to control and concentrate the light beam by utilising lenses is another advantage of VLC over RF technology, thereby enhancing power levels at the receiver side.

In addition, VLC is also capable of transmitting communications with little interference since the light beam is not susceptible to RF interference. However, the vast bandwidths accessible in VLC networks which are the backbone of contemporary communication technologies are nevertheless not available to end-users on the access network. This is due to the bandwidth constraints of the LED devices which are at the heart of VLC technology. The benefits listed above have prompted many research investigations into VLC technology in the scientific community in the last two decades. In VLC, the information signal is encoded by modulating the intensity of the light by LED, known as intensity modulation (IM) and direct detection (DD) at the receiver side using a photodetector. As a result, the modulation format used with VLC has to be interoperable with the IM/DD technique, which requires real and positive data.

Short Range Devices (SRDs) Shared Allocations Acronyms

A - Alarms MDA - Movement Detection or Alert
 CA - Cordless Audio NS - Non Specified including Telemetry and Telecommand
 D - Databases RFID - Radio Frequency ID
 DAV - Detection of Avalanche Victims RM - Radio Microphones
 GP - General Purpose SRDs RTTI - Road Transport and Traffic Telematics
 HA - Hearing Aids TTC - Telemetry and Telecommand Commercial
 IA - Induction Applications VLS - Vehicle Location
 ISL - Indoor Data Links VLS - Vehicle Location
 LAN - Local Area Network VLD - Video Distribution
 MB - Medical and Biological VLPAM - Ultra-low Power Active Medical Implants
 MC - Mode Control WA - Wireless Audio
 MD - Metal Detectors WVC - Wireless Video Cameras

Radio Service Legend

- Civil and Military Use
- Civil Use
- Military Use
- Radio Astronomy
- Aeronautical Radionavigation
- Earth Exploration - Satellite
- Amateur
- Aeronautical Mobile
- Maritime Mobile
- Maritime Radionavigation
- Meteorological Aids
- Broadcasting
- Broadcasting - Satellite
- Fixed
- Fixed Satellite Service
- Amateur - Satellite
- Inter - Satellite
- Mobile Satellite
- Land Mobile
- Radio Location
- Space Research
- Space Operation
- Mobile
- Standard Frequency and Time Signal
- Standard Frequency and Time Signal - Satellite
- Meteorological Satellite
- Radionavigation Satellite

Notes

UK6 ISM applications are designated for use within this band

UHF's include bandings S, C, X, Ku, K, Ka and R

SHF's include bandings S, C, X, Ku, K, Ka and R

EHF's include bandings Ka, R, Q, V, W and millimeter (mm)

This chart does not differentiate between primary and secondary allocations. Details may be found in the UK FAT.

Frequencies for distress and safety, search and rescue and emergencies and the protection of frequencies for Radioastronomy are protected bands and should be avoided wherever possible. Details may be found in the UK FAT Annexes H and D.

The authoritative document for spectrum allocations for the UK is the UK Frequency Allocation Table (UK FAT), published by Ofcom (www.ofcom.gov.uk). This UK Frequency Allocation Chart was developed by Rokey Manor Research in accordance with the latest version of this table, published by the Ofcom in 2007. UK spectrum allocations may change over time in accordance with decisions of the ITU, CEPT, European Commission, the UK Government or Ofcom.

The Allocations table does not necessarily imply that the frequencies indicated are available for the use for the purposes allocated. Ofcom publishes a frequency authorization plan on its website which shows the frequencies for particular licence classes or for licence-event use. Ofcom also publishes the UK Spectrum Strategy, which contains guidance on future use on the spectrum in the UK.

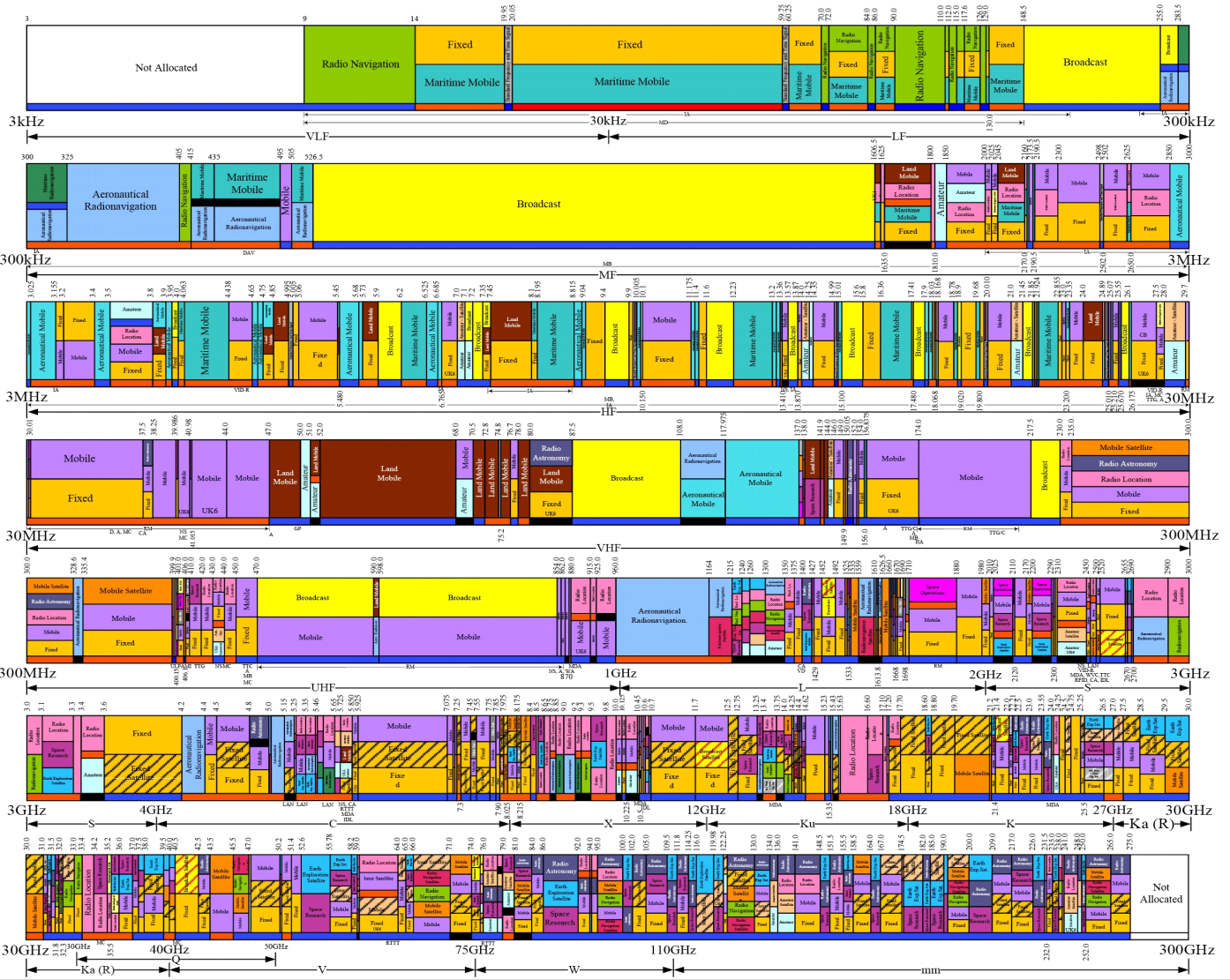


Figure 1-4: The UK RF spectrum.

On the other hand, the available literature shows that the challenges in VLC include: (i) bandwidth limitation, due to the commercial LEDs, the VLC technology could not occupy the entire bandwidth, which is ~ 400 terahertz; (ii) LED non-linearity; (iii) inter-symbol interference (ISI) caused by the multipath channel [16, 30, 40, 41]. The bandwidth limitation is the essential bottleneck preventing the achievement of high performance in visible light communications systems such as in terms of data rates, BER and high capacity. Also, this limitation is a significant barrier in meeting the modern demand for fast communication technology which is growing annually and exponentially. One promising solution is the adoption of an advanced modulation technique such as orthogonal frequency division multiplexing (OFDM). Conventional OFDM utilises an inverse fast Fourier transform (IFFT) at the transmitter to convert frequency domain symbols into the time domain and a fast Fourier transform (FFT) at the receiver to recover the signal. An OFDM technique was first proposed in optical communication in 2001 by Hui [42]. In VLC technology, the electrical power transmitted is converted into the optical domain with the use of intensity modulation (IM) through the LED, which needs a real positive signal.

On the other hand, the output of the IFFT could be imaginary and negative. Half of the spectrum bandwidth is used to achieve the real OFDM signal. The real signal is achieved by inserting Hermitian Symmetry (HS) into the transmitted data as the input to the IFFT. Moreover, a real OFDM signal could be obtained from a real transform as a discrete cosine transform (DCT). Fast OFDM (F-OFDM) was reported for the first time in 2002 [43] using IDCT and DCT to convert frequency domain symbols into the time domain and to recover the signal at the receiver. The issue of negativity can be solved by adding a DC bias which is usually added to the VLC system [44, 45]. It has been shown in the literature that there are two techniques to produce positive OFDM signals with regard to IM/DD modulation [46]:

- DC-biased optical OFDM (DCO-OFDM), which comes at the cost of lower power efficiency.
- Asymmetrically clipping optical OFDM (ACO-OFDM), which entails reductions in spectral efficiency.

Other techniques based on the above schemes are known as asymmetrically clipped DC-biased optical OFDM (ADO-OFDM). This combines the concepts of DCO-OFDM and ACO-OFDM by sending them simultaneously on the even and odd SCs, respectively [44]. One study [46] concluded that “optimal values are found for several configurations and it is shown that in a number of cases ADO-OFDM requires less optical power than existing schemes (DCO-

OFDM) and (ACO-OFDM)”.

Although conventional OFDM modulation has been considered a successful modulation technique for wired and wireless communications systems in several applications, there are still various areas that need to be developed. The large peak-to-average power ratio (PAPR) of the signal is thought to be the main barrier to the achievement of high performance by OFDM systems. In particular, the addition of DC-bias to OFDM symbols and then passing them via the restricted linear dynamic range of the LED renders these schemes unsuitable for some VLC applications where energy economy is critical [47].

The primary emphasis of this research is the development of a unique method for OFDM with application to visible light communication (VLC). It is dedicated to improving OFDM performance by reducing the PAPR and computational complexity, thereby enhancing the non-linear region and broadening the limited bandwidth associated with LEDs. In order to address such negative elements of OFDM systems, a novel technique based on an OFDM scheme is proposed in this thesis. Here, the C-transform combines the Walsh-Hadamard transform (WHT) and discrete cosine transform (DCT) into an orthogonal signal. The proposed transform uses a novel type of optical orthogonal frequency division multiplexing called C-OFDM.

1.3 Research Aims and Objectives

The primary objective of this study is to investigate and evaluate the performance of the proposed C-transform in the context of Visible Light Communication (VLC). The study aims to understand the advantages and drawbacks of OFDM by conducting a thorough literature review on VLC and its technological challenges. The research focuses on utilizing the C-transform to enhance the efficiency of VLC systems. The study also involves developing an optimization tool to analyse DCO-OFDM, F-OFDM, and C-OFDM (using C-transform) design structures in VLC, leading to the creation of new VLC systems. To achieve these research aims, the study outlines the following specific goals:

- Conducting a comprehensive literature review on VLC and the technological challenges it faces to establish a solid foundation for the research.
- Utilizing the C-transform technique to enhance the efficiency of VLC systems, specifically in the context of C-OFDM.
- Developing an optimization tool to analyse and compare the design structures of three different VLC systems: DCO-OFDM, F-OFDM, and C-OFDM (utilizing the C-transform). This step aims to propose novel VLC system

configurations.

- Complete development of the C-OFDM system and gather results for various performance metrics, including BER, PAPR, power penalties, and computational complexity. These results will be compared against existing DCO-OFDM and F-OFDM approaches.
- Assessing and comparing the PAPR and computational complexity of the proposed C-OFDM system with those of other existing optical OFDM schemes, both theoretically and mathematically.
- Investigating the impact of LED non-linearity effects on VLC when employing the C-OFDM technique.
- Analysing the performance of C-OFDM in the presence of multipath channels, and making comparisons with conventional OFDM and F-OFDM in similar scenarios.

1.4 Thesis organisation

There are seven chapters in this thesis, and its structure is depicted in the diagram in Figure 1.5 which offers a general sense of the organisation of the study and how the chapters are linked. An overview of the contents of this thesis is as follows:

Chapter 2: The literature review introduces the most important publications on the topic of OFDM, describing its history, the design of OFDM systems and their merits as well as problems encountered. Moreover, the use of OFDM in VLC and the challenges faced are also discussed.

Chapter 3: The C-transform is explained in terms of implementation, and its advantages and disadvantages based on the OFDM scheme. Furthermore, the computational complexity involved in the use of the C-transform is compared with that of FFT and DCT transforms.

Chapter 4: A comparative study is described of the peak-to-average power ratio and computational complexity of three different orthogonal frequency division multiplexing (OFDM) formats for visible light communication. The schemes investigated are conventional DC-biased OFDM, fast OFDM, and C-transform-based OFDM (C-OFDM) which uses a Walsh-Hadamard matrix in conjunction with a discrete cosine transform. The investigation

considers these systems when transmission occurs over additive white Gaussian noise and band-limited channels. The proposed system results in lower PAPR and computational complexity relative to conventional OFDM. An improvement of 5dB in PAPR is achieved at 10^{-3} of CCDF along with reduced computational complexity.

Chapter 5: A comprehensive investigation is conducted of the effects of the non-linearity of LEDs in VLC utilising C-OFDM. VLC depends on the electro-optical output of the light-emitting diodes commonly used in visible light communication systems that are generally non-linear in nature. This is particularly problematic when using advanced modulation formats such as orthogonal frequency-division multiplexing (OFDM) which have high peak-to-average power ratios due to clipping and distortion. An improvement of ~ 2.5 dB in power penalty at a BER of 10^{-4} in comparison to OFDM has been achieved.

Chapter 6: A study of indoor channel characteristics for VLC taking into consideration multipath channels and various forms of modulation is presented. Performance is evaluated from simulations of different OFDM formats in terms of the ratio E_b/N_o , with BER as a function of energy per bit to noise power spectral density.

Chapter 7: The findings of the study are summarised, discussed and conclusions are drawn. The key accomplishments of the research are addressed, along with comments on the study's objectives as specified in Chapter 1. The chapter ends with a review of the study's achievements and suggestions are made for future work based on the findings. The main conclusion is that C-OFDM has the advantages of resistance to multipath channel dispersion and a lower PAPR than the other OFDM schemes considered.

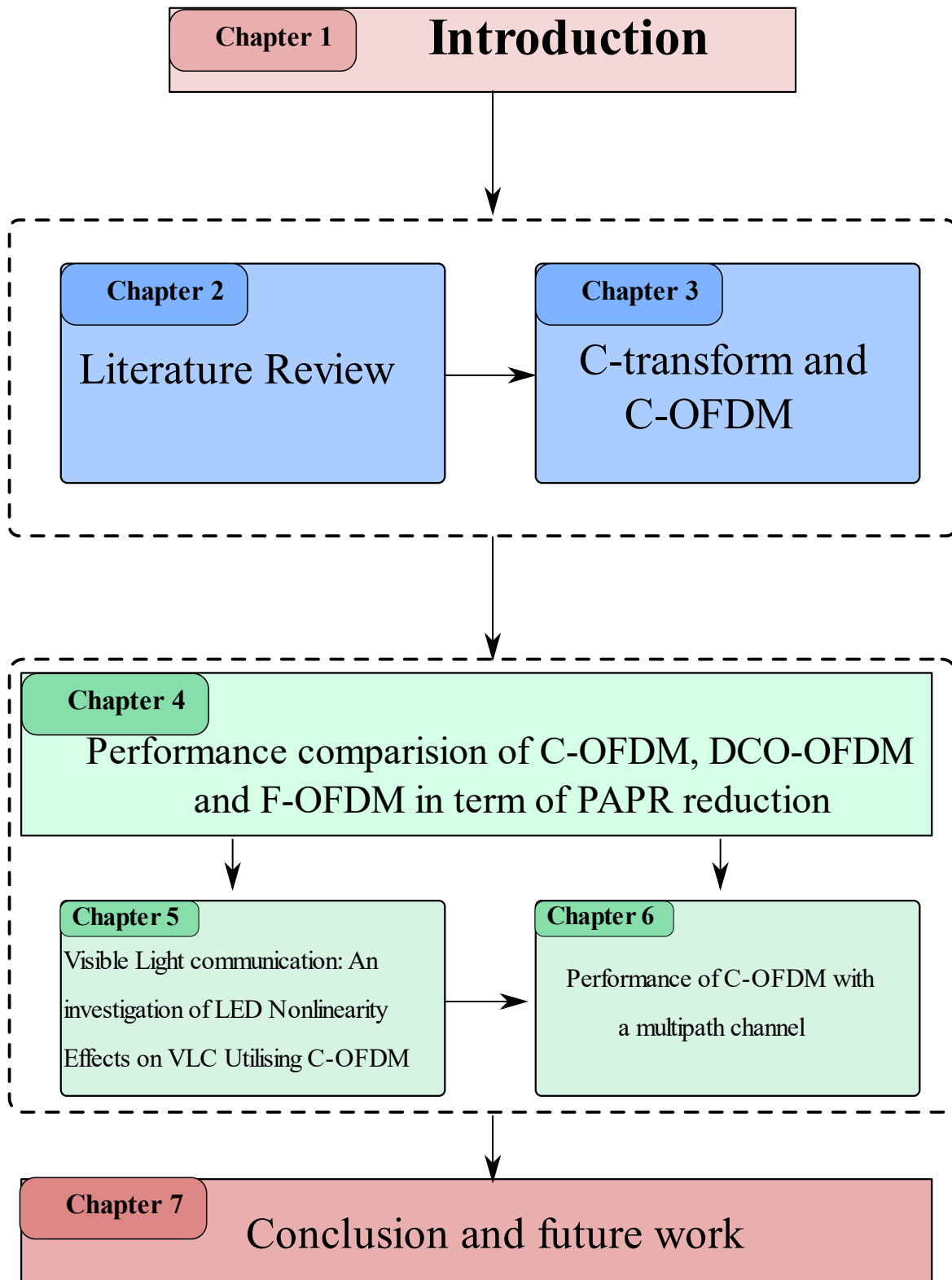


Figure 1-5: Thesis plan and structure.

1.5 Original contributions

The key contributions to knowledge made in this research are as follows:

In Chapter 4, a novel optical OFDM scheme based on the C-transform called C-OFDM is demonstrated and an improvement of 5 dB has been achieved in terms of PAPR at 10^{-4} of CCDF, which is due to the C-transform having the block diagonal structure (BDS). Furthermore, the computational complexity of the C-OFDM system is reduced by 52-75% compared to the FFT. Moreover, despite the influence of the bandwidth limitation of LEDs, the proposed C-OFDM system offers an improvement of several dBs for $f_c=1B$ and $0.5B$.

In Chapter 5, an investigation is detailed of LED non-linearity effects on VLC utilising C-OFDM. The C-OFDM is shown to exhibit the highest degree of independence from non-linearity and yields superior bit-error-rate results. An improvement of ~ 2.5 dB in power penalty at a BER of 10^{-4} compared to OFDM has been achieved.

In Chapter 6, the indoor channel characteristics of the use of C-OFDM for VLC are investigated. Its superiority in performance compared to the other OFDM systems is demonstrated. The proposed system is resistant to multipath channel dispersion and has a lower PAPR than other O-FDM techniques.

1.6 List of Publications and Awards

1.6.1 Peer-reviewed Journal Papers

J. Abdulwali and S. Boussakta, "Visible Light Communication: An Investigation of LED Nonlinearity Effects on VLC Utilising C-OFDM," in *Photonics*, 2022, vol. 9, no. 3: MDPI, p. 192

1.6.2 Peer-reviewed Conference Papers

J. Abdulwali, P. A. Haigh, and S. Boussakta, "New Visible Light Communication Using C-OFDM," in *2020 12th International Symposium on Communication Systems, Networks and Digital Signal Processing (CSNDSP)*, 2020: IEEE, pp. 1-5.

J. Abdulwali, S. Boussakta, " OFDM Based C-transform to Improve LED Non-Linearity for VLC application," in *International Conference on Embedded Systems in Telecommunications and Instrumentation (ICESTI'22)*, 2022. (Accepted).

J. Abdulwali, S. Boussakta, "C-OFDM in Visible Light Communication Systems: Spectral and Energy Efficiency" (will be submitted soon. It is under reviewing).

1.6.3 Awards

- I was given the award for the second-best presentation at the PGR Conference held at Newcastle University in 2021.
- I have been awarded the best poster prize at the SAgE PGR Networking that was held at Newcastle University, on 28th June 2022.

Chapter 2

Visible Light Communication Principles

The literature review introduces the most significant publications on the subject of OFDM in this chapter, including their history, the design of their systems, advantages, and drawbacks. Additionally, the usage of OFDM in VLC and the difficulties encountered are also covered.

2.1 Evolution of Mobile Communications Networks

Since the first analogue communications network appeared in the 1980s, mobile communication networks have advanced tremendously. This revolution is not a one-step operation but a series of generations with varying standards, capabilities, and procedures. Almost every 10 years, a new generation is released. Figure 1.1 shows the exponential growth in the data transfer rate in wireless communication [14, 48].

The first-generation mobile network was built by Nippon Telephone and Telegraph (NTT) in Tokyo, Japan, for voice services and had a data rate of up to 2.4 kbps, was deployed in the 1980s utilising analogue signals to transfer data. There was no uniform wireless standard, which resulted in various problems such as difficult hand-off, poor transmission efficiency, and lack of security [12]. However, 2G has been built on digital modulation techniques such as Time Division Multiple Access (TDMA) and Code Division Multiple Access (CDMA) in comparison to first-generation (CDMA) systems. 2G has a 64kbps data rate, allowing it to offer enhanced voice services and Short Message Services (SMS). The GSM (Global System for Mobile Communication) was the leading mobile communication standard throughout the 2G period [15]. In the year 2000, the third generation was planned with the purpose of allowing for high-speed data transfer. The 3G network offers a 2 Mbps data transmission rate and high-speed Internet access [49]. It provides sophisticated services, such as video services, navigational mapping, and TV streaming that are not enabled by 1G and 2G networks. The 3rd Generation Partnership Project (3GPP) was formed to define technical specifications and

continue the progress being made by developing mobile standards and technologies to accomplish global roaming [50]. In the late 2000s, the fourth generation mobile system was invented, which is an IP-based network system. The goal of moving to an all IP system is to provide a single platform for all of the technologies that have been produced so far. It offers speeds of up to 1Gbps [49, 50]. Latency, computational complexity, power penalty, cost, high-quality performance, and end-to-end dependability are all trade-offs in 5G. In contrast, 6G will be built in a comprehensive manner to fulfil network needs, including ultra-high reliability, capacity, efficiency, and low latency in light of the anticipated economic, social, technical, and environmental backdrop of the coming years.

There is a growing desire for the global system to become entirely wireless, requiring access to information at any time and from any location with the highest quality, speed, and bandwidth as well as cost reductions. Therefore, the new generations of wireless communication will be anticipated to use frequency ranges not previously considered for cellular standards, and especially the terahertz band and visible light communication, in order to achieve the aforementioned criteria.

2.2 Visible Light Communication (VLC)

The concept of light communication has been used since the year 150 BC when smoke signals were implemented. Since then, light communication was improved for the long-range firing relay and insertion encoder techniques through the use of smoke signals in 400 BC. Then, in 800 BC, the ancient Greeks and Romans used fire beacons to communicate [16, 25]. In 1792, the French engineer Claude Chappe built the first optical telegraph network and managed to denote 196 symbols for information. Alexander Graham Bell then implemented the first Free Space Optical (FSO) link in 1880. He was able to modulate a speech signal into a light signal by using a vibrating mirror and crystalline selenium cells in both the transmitter (Tx) and receiver (Rx). However, Bell's system had several disadvantages and, most importantly, it used intermittent sunlight.

However, Bell's work is well known as the first viable illustration of VLC that uses sunlight as a means of transmission [16, 25]. FSO was used mainly in secure military applications in the 1970s. Recent years have seen an increasing use of OWC technology. Subsequently, in 2001, at the Nakagawa Laboratory of Keio University (Japan), the first VLC using the state-of-the-art semiconductor lighting (SSL) technology known as the light-emitting diode (LED) involved a light source and data communication at the same time [20].

VLC is mainly used for indoor applications and provides illumination and data communication simultaneously through the frequency spectrum from ~ 430 up to 790 THz.

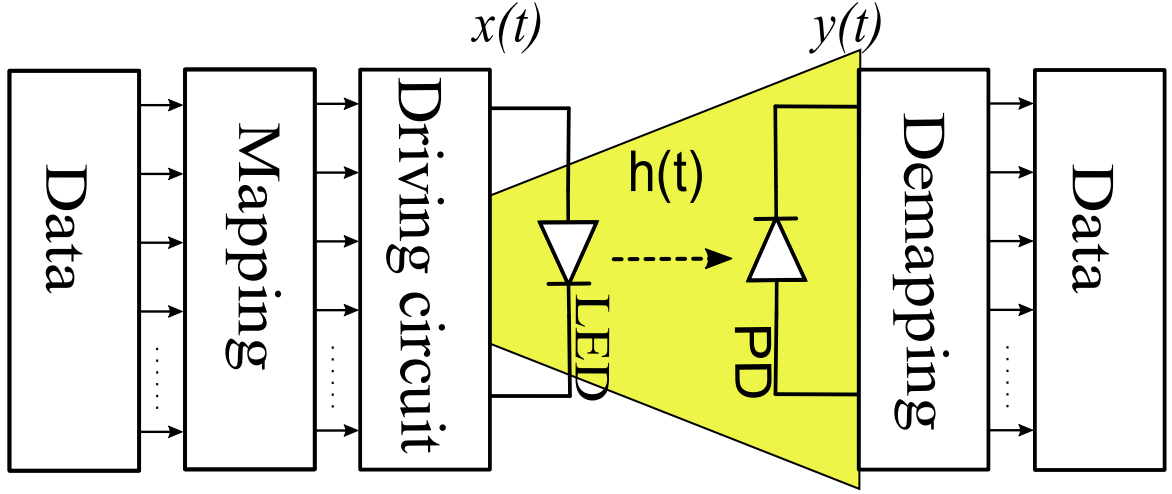


Figure 2-1: Block diagram of a typical VLC system.

Additionally, VLC can be used in indoor situations with a wide range of applications that have attracted considerable research attention over the last two decades. This is due to its many advantages such as huge bandwidths, 10,000 times $>$ RF, the absence of licensing requirements, health hazards or threats to human safety, high power efficiency, and a lack of electromagnetic interference (EMI) as well as low implementation costs when the infrastructure is already present [47].

The field of VLC research activity has seen much recent growth involving the scientific community. VLC provides both data transfer and lighting at the same time, and there are three parts to every communication system: a transmitter, a propagation medium $h(t)$, and a receiver. Figure 2.1 demonstrates a VLC block diagram utilising an LED to modulate the intensity of optical power within the transmitter side, known as the intensity modulation (IM) technique. On the receiver side, the direct detector (DD) technique is used by implementing a photodetector (PD) to detect the received signal $y(t)$. Unlike RF-based communication in VLC, the transmitted signal $x(t)$ should be real and non-negative. Thus, in VLC, the utilisation of a driving circuit guarantees that the optical power output by the LED is constantly positive. The transmitted power P_t has been described mathematically as [51]:

$$P_t \geq \lim_{T \rightarrow \infty} \frac{1}{2T} \int_{-T}^T x(t) dt. \quad (2.1)$$

$$x(t) \geq 0. \quad (2.2)$$

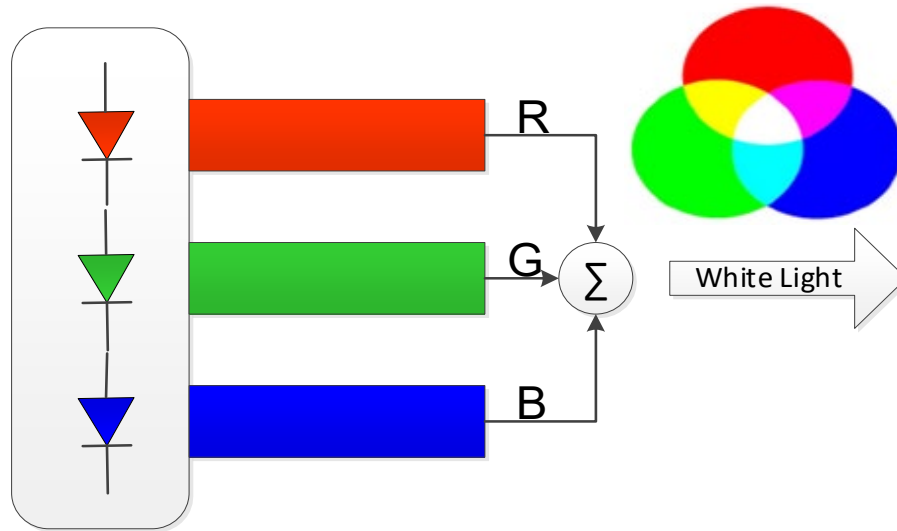


Figure 2-2: Block diagram of RGB LED

2.2.1 LED Devices

LEDs are light sources that emit narrowband light in the ultraviolet, visible, and infrared wavelength regions. Because of Isamu Akasaki and his team's creative efforts [52], white LED lighting is now achievable. Their development of the energy-efficient blue LED has had worldwide influence on lighting energy usage, earning them the Nobel Prize for Physics in 2014.

There are essentially two ways to generate light using three types of visible LEDs. The first type of LED is known as RGB, and this LED uses a technique combining the colours red, green and blue with wavelengths (625, 525 and 470), respectively by a precise ratio so that white light can be obtained [16]. Figure 2.2 shows the RGB LED with three LEDs and one optical combined in single package. Although this LED has a bandwidth of up to 10s MHz, it is difficult to control the combination of the three colours to produce white light [24]. On the other hand, this LED is attractive for changeable colour applications [47].

The second type is the blue chip + phosphor or white phosphor LED (WPLED). In this type, the blue LED will be coated with yellow phosphor because of its low cost and straightforward production procedure [47]. Figure 2.3 illustrates the block diagram of a WPLED. Due to the phosphor layer's slow reaction, the WPLED bandwidth shrinks to a few MHz [25, 29]. However, it has been claimed that up to 20 megahertz could be developed [30].

A VLC system employing a phosphorescent white-LED as a transmitter has been found to allow a data throughput of 2.5 Gbps [53]. This result was accomplished by extending the bandwidth of the utilised phosphorescent white-LED involved using hardware pre-equalisation methods. Due to their ability to send data on parallel streams of wavelength channels, which may be separated using optical filters at the receiver, RGB LEDs enable the system to reach

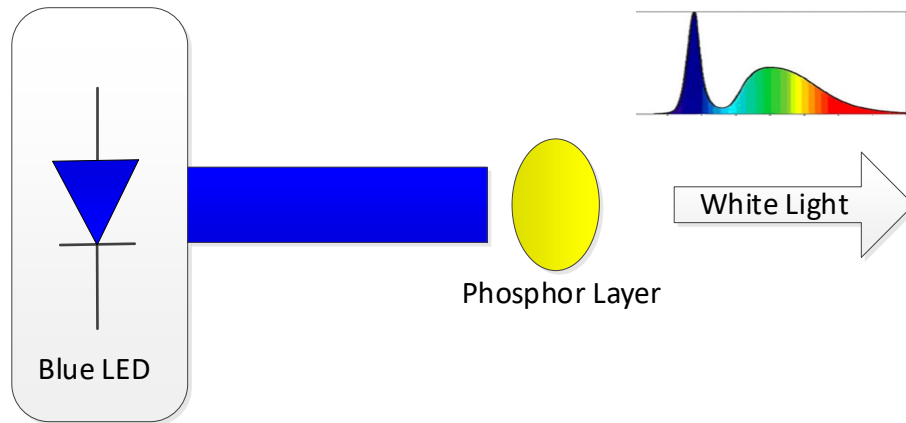


Figure 2-3: Block diagram of WPLED

substantially faster data speeds. With off-the-shelf multicoloured LEDs, a data rate of 15.7 Gbps has been proven experimentally [34]. Furthermore, the micro-LED (μ -LED) has attracted much attention in recent years due to its high 3-dB bandwidth which surpasses 800 MHz [54-56]. A violet μ -LED with an active area of $435 \mu\text{m}^2$ and a 3-dB bandwidth of 370 MHz has been used to achieve a data throughput of 7.9 Gbps [55], and a blue μ -LED was recently used to provide a data throughput of 11.7 Gbps [56].

Finally, the organic light-emitting diode (OLED) is a novel SSL approach that allows lighting and data communication. OLEDs have numerous features that make them attractive for lighting and visualisation applications; in particular, their low-cost manufacture and low power consumption. In addition to the possibility of production in different shapes and sizes, their light weight and flexibility are also fascinating features. Moreover, the efficiency of OLEDs is improving every year [57]. However, low charge mobility and high capacitance restrict the modulation bandwidth for OLEDs to a few tens of MHz, making them slower than other LEDs [58]. Nonetheless, with better design and manufacturing techniques, it has been shown that higher data rates are possible [58, 59]. Rates of 1.13 Gbps were recently achieved at 245 MHz modulation bandwidth within a 2 m distance [59].

The limited modulation bandwidth of LEDs, which acts as a first-order low-pass filter (LPF), is a bottleneck in a VLC network, despite the numerous aforementioned benefits of LEDs, as reported in the literature [2, 16, 28, 47]. This is the primary obstacle to achieving large capacity in VLC systems. The bandwidth is defined as the difference in frequency (Hz) between the highest and lowest signal frequency components, while it may also be defined as the range of frequencies where the signal's power spectral density (PSD) is greater than zero.

Additionally, the -3 dB bandwidth is the most commonly used bandwidth specification in VLC systems (see Figure 2.4). Thus, -3 dB results when the input signal has been attenuated by 70.7 and 50 per cent respectively of its original electrical and optical transmitted signals [60]. This is because the signal power in the electrical domain is proportional to the square of the current $P_{ele} \propto I^2$. Alternatively, in an optical domain, the optical power is proportional to the photocurrent $P_{opt} \propto I_p$ [61]. Thus the -3 dB bandwidth for electrical and optical domains can be defined as follows:

$$(-3dB)_{1/2 Ele Power} = 10 \log_{10} \left(\left(\frac{I_{out}}{I_{in}} \right)^2 \right) = 20 \log_{10} \left(\frac{I_{out}}{I_{in}} \right). \quad (2.3)$$

where I_{in} and I_{out} input and output current.

Then $\left(\frac{I_{out}}{I_{in}} \right)$ at the half-power (-3dB) as:

$$\left(\frac{I_{out}}{I_{in}} \right) = (10)^{-3/20} = 0.707 = 70.7\% .$$

Alternatively, in the optical domain as follows:

$$(-3dB)_{1/2 opt Power} = 10 \log_{10} \left(\frac{I_{out}}{I_{in}} \right). \quad (2.4)$$

then $\left(\frac{I_{out}}{I_{in}} \right)$ at the half-power (-3dB) in the optical domain can be presented by:

$$\left(\frac{I_{out}}{I_{in}} \right) = (10)^{-3/10} = 0.501 = 50.1\% .$$

There are several possible causes of the shrinking LED bandwidth and reduction in frequency response, such as the injected current, junction capacitance and parasitic capacitance. The capacitance values are almost constant; however, the frequency response rises as a function of injected current. Furthermore, it can reduce the effects of the reasons mentioned earlier by superimposing the continuous signal into a constant DC bias current. In this case, if the device's DC output is $P(0)$, the crossbanding optical power output at frequency $P(f)$ is given as [62]:

$$\frac{P(f)}{P(0)} = \frac{1}{\sqrt{1 + (f\tau)^2}}. \quad (2.5)$$

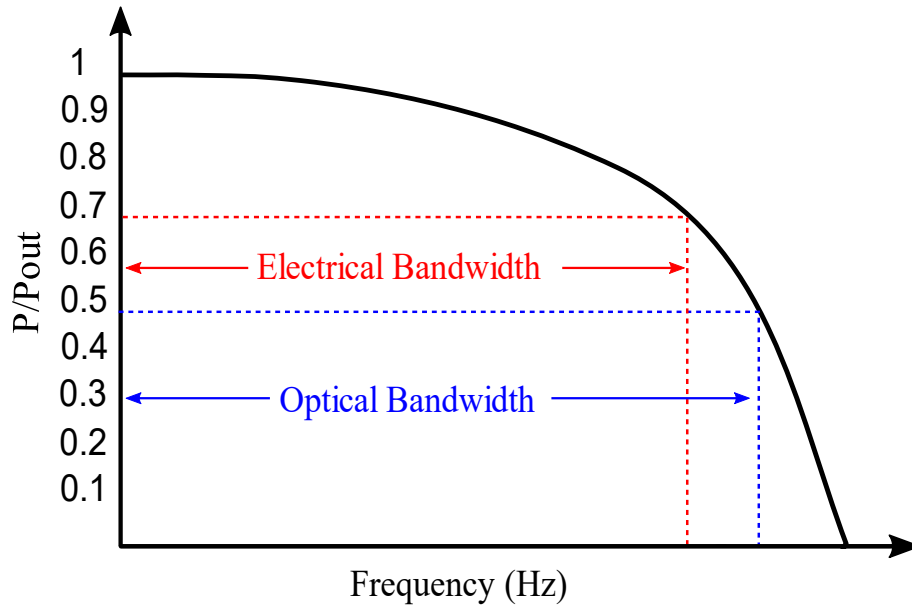


Figure 2-4: A diagram depicting the optical and electrical bandwidths.

where τ is the minority carrier's lifetime, which has two components of a radiative τ_r and a nonradiative τ_{nr} ; note that, in Equation 2.5, a reduction in the effective carrier lifetime leads to increased modulation bandwidth

$$\tau^{-1} = \tau_r^{-1} + \tau_{nr}^{-1}. \quad (2.6)$$

The correct amount of injected current is critical, because the swing of the transmitted signal must be maintained within the linear area of the LED's dynamic range throughout this procedure to prevent clipping the transmitted signal [16]. Also, the transfer function of the 1st order LPF LED is given as

$$H(j\omega) = \frac{1}{1+j\omega RC_j}. \quad (2.7)$$

where R is the resistance of the LED, and C_j is its junction capacitance. Therefore the cut-off frequency (f_c) is given as follows [16]:

$$f_c = \frac{1}{2\pi RC_j}. \quad (2.8)$$

2.2.2 Photodetector

Photodetectors are distinguished by their sensitivity, detection area, frequency and spectrum responses, and field of view (FoV). PDs are diodes that create a photocurrent (I_p) when their depletion area absorbs light, which means that the I_p created is always proportional to optical power (P_r) at the receiver, which is given as [1]:

$$I_p = \eta \frac{qP_r}{hv} [1 - e^{-\alpha l}], \quad (2.9)$$

where q and h are the charge of an electron and Planck's constant, respectively; η represents the quantum efficiency, which is the proportion of created charge carriers that contribute to the generated I_p ; l is the length of the photoactive region; ν is the photon's frequency, and α is the absorption coefficient. The material used for near-infrared to far-infrared light absorption is mainly gallium alloys, whereas an absorption material for visible light is typically silicon (Si). Furthermore, it is critical for PDs to exhibit a high response, since responsivity determines the ratio of incoming photons to the photocurrent produced. A high response is desired for PDs in VLC systems because it naturally leads to a high signal-to-noise ratio, and responsivity \mathfrak{R} is expressed as

$$\mathfrak{R} = \frac{I_p}{P_r} = \frac{q\eta}{hv} [1 - e^{-\alpha l}]. \quad (2.10)$$

The reception of a signal after it has been sent over an optical channel is difficult due to the faint signal received; hence high responsiveness is preferred. Figure 2.5 depicts the responsiveness of several semiconductor materials, including germanium (Ge) and indium gallium arsenide (InGaAs), which are not utilised in VLC due to them not absorbing visible light at all [63]. As shown in Figure 2.5 (adapted from [1]), an organic photodetector (OPD) using polymer semiconductor poly (3-hexylthiophene) (P3HT) provides several advantages over the Si PD. A higher responsivity of around 400 nm and shorter cut-off wavelength of about 650 nm are the most significant advantages of this VLC system compared to the Si PD [1]. P3HT was presented for the first time for VLC technology [64]. The semiconductor materials used are essential since they determine the wavelength range within which devices can operate. As shown in Figure 2.5, the cut-off wavelength of the silicon is 1060 nm and its wavelength range is 400 to 1060 nm.

Due to their excellent linearity and rapid response, P-type intrinsic N-type photodiodes

(PIN PDs) and avalanche photodiodes (APDs) are the most commonly utilised PDs in VLC systems. As the name implies, PIN consists of a p-n semiconductor diode with an extra layer of intrinsic semiconductor inserted between the p-n layers. The APD differs from the PIN PD in that it delivers an essential gain. As can be seen from the Table 2.1, which lists the general properties of PIN PDs and APDs [16], the APD provides responsivity between 77 to 130 in contrast to PIN at 0.6. This is due to the APD's gain of 150-250; however, this gain comes at the cost of additional noise which must be taken into account in terms of system performance.

In addition to the above, noise is always a significant factor in evaluations of system performance. Noise sources in photodetectors set the lower sensitivity limit of the device. The two essential noise sources are shot noise σ_{shot}^2 and thermal $\sigma_{\text{thermal}}^2$ (Johnson) noise. Shot noise

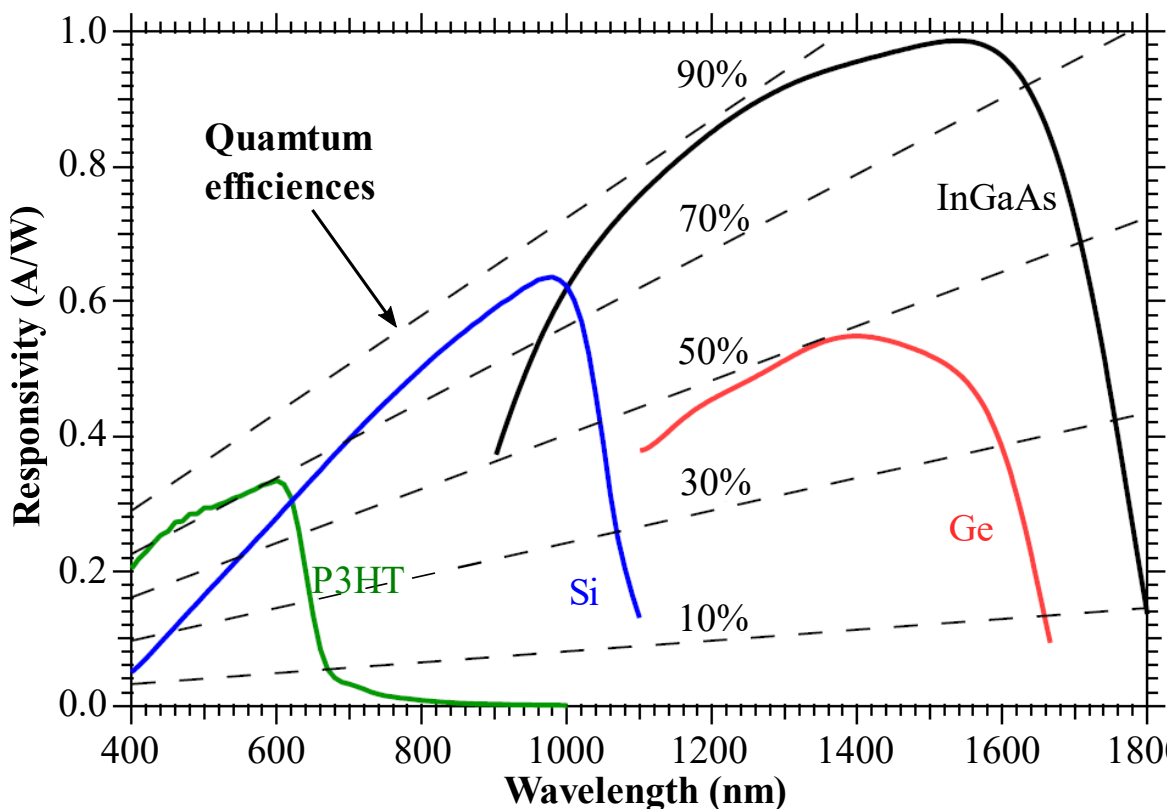


Figure 2-5: Relative response of PDs for different materials.

Table 2.1: Typical parameters of silicon PIN PD and Si APD

Parameter	PIN	APD
Wavelength range (nm)	400-1100	400-1100
Peak (nm)	900	830
Responsivity (A/W)	0.6	77-130
Quantum efficiency (%)	65-90	77
Gain	1	150-250
Rise time (ns)	0.5-1	0.1-2

(ambient-induced) is caused by the fluctuation of generated photons and is given by [1]:

$$\sigma_{shot}^2 = 2\Re q P_r B + 2q I_{bg} B. \quad (2.11)$$

where the parameters I_{bg} and B are the received background noise current and system bandwidth respectively.

Along with the noise caused by ambient light, the Johnson noise linked to the receiver's electronics must also be considered, since this is the most dominant noise source in VLC technology. The thermal noise (Johnson noise) is given as follows [65]:

$$\sigma_{thermal}^2 = \frac{4kTB}{R_L}. \quad (2.12)$$

where k is Boltzmann's constant, R_L is the load resistance, and T indicates the absolute temperature.

On the other hand, the variances of shot noise and the thermal-noise can be described as additive white Gaussian noise (AWGN) [65]. The overall noise variance may thus be expressed as [37]:

$$\sigma_t^2 = \sigma_{shot}^2 + \sigma_{thermal}^2. \quad (2.13)$$

2.3 Challenges in VLC

The literature shows that there are several challenges in VLC, such as bandwidth limitations. Due to the characteristics of commercial LEDs, VLC technology cannot occupy the entire bandwidth, which is ~ 400 terahertz. ISI, diming and LED non-linearity are other challenges [16, 30, 40, 41]. The bandwidth limitation is the essential problem encountered in achieving

high performance in features of visible light communications systems such as data rate, SNB, BER and high capacity. The bandwidth limitation is also a barrier to fulfilling the contemporary demand for fast communication technology which is growing exponentially. To overcome the bandwidth limitation, the research community has already proposed various possible solutions; for instance, implementing a blue filter which reduces received optical power or utilising an equaliser at the transmitter or the receiver, which is increasing the system's computational complexity.

Furthermore, moving from one modulation technique to another is a promising solution, such as non-return to zero time-division multiplexing (NRZ-TDM), wavelength division multiplexing (WDM), and other advanced modulation techniques. However, specific criteria must be taken into account to determine the efficiency of a modulation technique. Firstly, power efficiency (η_p) is the most significant parameter when considering modulation methods appropriate for VLC systems. Bandwidth efficiency (η_B) is also crucial. Although the potential bandwidth of the optical carrier signal may be assumed to be boundless, other components of the system such as LEDs restrict the transmission bandwidth available for distortion-free communication. Also, the reliability of transmission is a significant parameter in a communication system, and so it must be ensured that ISI, noise and distortion in the transmitted signal is mitigated. Other considerations are the computational complexity and implementation costs involved [16, 51]. In addition, the construction of a VLC system with the tens or hundreds of LEDs needed to support wireless communication beyond several Gb/s for many users remains a significant difficulty in practical situations. Furthermore, ISI caused by multipath channels and the non-linearity of the LED are another challenge in VLC systems.

One promising solution to these problems is to adopt an advanced modulation technique, such as orthogonal frequency division multiplexing (OFDM) and carrier-less amplitude and phase modulation (CAP). In the mid-1970s, CAP was invented for the first time in the Bell Laboratories by Falconer et al[66]. CAP is a multi-level and multidimensional modulation scheme, and its operating principle is very similar to that of the QAM technique in that it is capable of sending two streams of data in parallel. However, CAP uses a different method to generate two orthogonal signals, using two FIR filters whose impulse responses form Hilbert pairs[35].

Alternatively, OFDM is an excellent solution to the ISI induced by a dispersive or multipath channel and is a significant paradigm for improvements in spectral efficiency [38, 67]. It also provides a high data rate while requiring minimal hardware complexity with a

simplified equaliser [43]. It is presently used in most modern and emerging broadband wired and wireless communication systems [68], and a number of studies have demonstrated that OFDM is a potentially appropriate method for optical communications [45, 69].

2.4 Carrier-less Amplitude and Phase Modulation (CAP)

CAP, a multilevel and multidimensional modulation technique, was initially developed in the mid-1970s at Bell Labs by Falconer et al. It shares a fundamental operational principle with QAM, as both can transmit two data streams concurrently. However, CAP achieves this by employing two FIR filters with impulse responses forming Hilbert pairs, which simplifies its structure compared to QAM that requires complex oscillators. It is worth noting that CAP has primarily been used in flat fading systems, which are uncommon in VLC (Visible Light Communication) systems due to frequency selective channels resulting from bandwidth limitations [1].

In a flat fading channel, the channel's bandwidth (B_c) is greater than the signal bandwidth (B_s). Conversely, a frequency selective or non-flat fading channel occurs when B_c is smaller than B_s , which is the case in VLC systems. Non-flat fading introduces varying frequency responses for different signal frequency components, leading to increased bit error rate (BER) and lower data rates. In contrast, flat fading channels maintain consistent frequency responses for all signal frequency components, ensuring better transmission quality.

The utilisation of m-CAP provides a viable approach to alleviate the necessity of a flat fading channel, which is a noteworthy solution for limited bandwidth systems like VLC. However, one consideration when implementing m-CAP is that increasing the CAP order, denoted as m , necessitates the incorporation of additional FIR filters. Specifically, each increment in m by one order involves the inclusion of two FIR filters at the transmitter side (one for real data R and another for imaginary data I) as well as two FIR filters at the receiver side. Consequently, this augmentation in m leads to an escalation in the computational complexity of the system [29].

In Figure 2.6 illustrates the concept of m-CAP when alpha $\alpha = 0.2$ is for different CAP orders $m = 1, 2, 4, 8, 10$. It can be noticed that while m is increased the value of each subcarrier's bandwidth is decreased. This contributes towards relaxing the requirement of flat fading channel. Therefore, offers improvement in the BER performance as less attenuation occurs to the subcarriers. However, as mentioned before there is a trade-off between BER system performance and complexity.

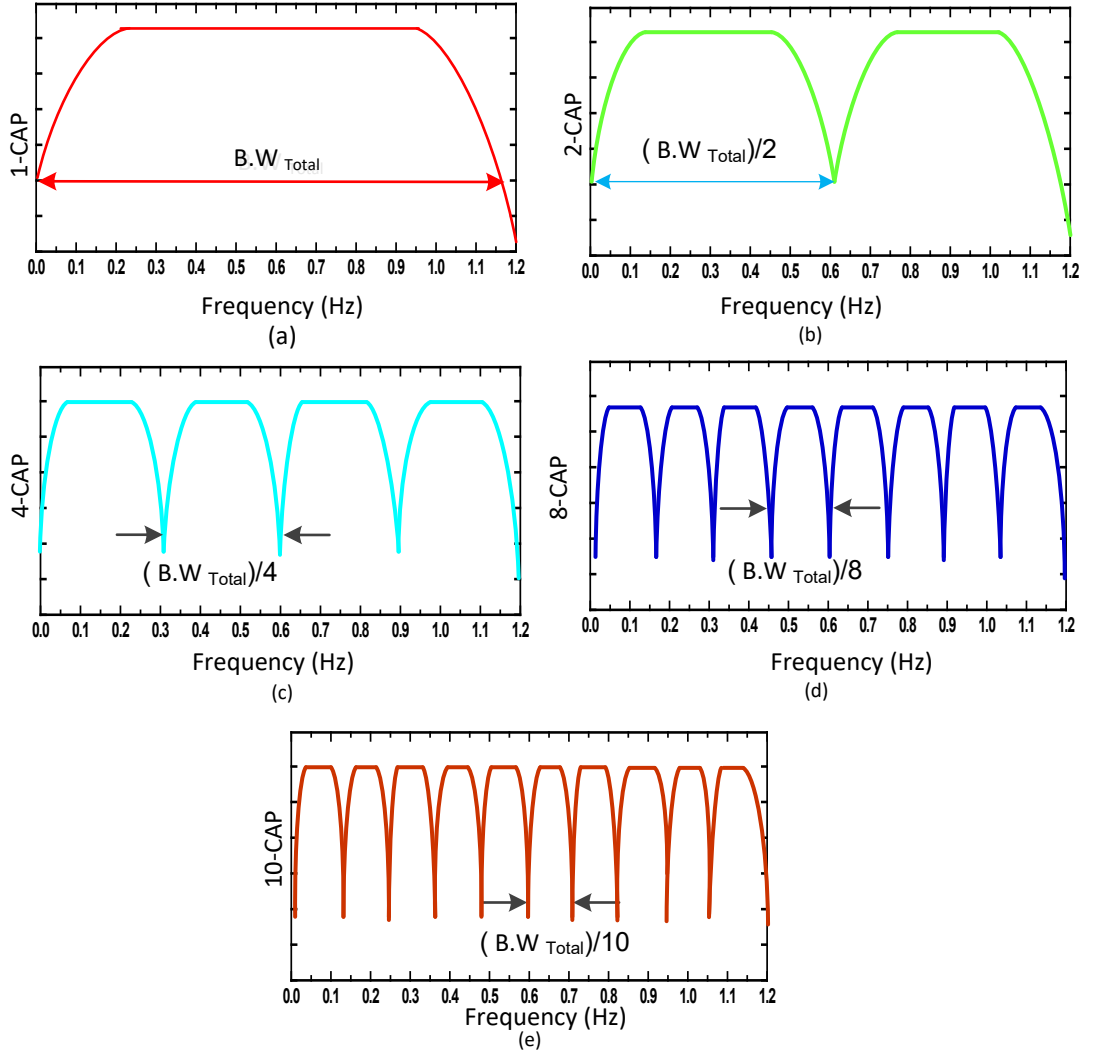


Figure 2-6: The concept of m -CAP demonstrated in terms of the frequency response for $m = 1, 2, 4, 8, 10$.

Figure 2.7 provides an illustration of the m -CAP system's fundamental principle. At the transmitter side, random data streams ($Data_m$) are generated, each with a length of 10^5 , for every m -CAP order up to the desired number of subcarriers ($Data_m$). These data streams are then mapped onto an M_m -QAM constellation, and the constellation diagram for the first subcarrier is depicted as the blue diagram in Figure 2.7. The modulation order, denoted as M , is defined as 2^k , with k representing the number of bits per symbol. In this study, k has been selected as 4 (16-QAM) for the sake of simplicity and without compromising generality.

Following the data mapping process, the data is up-sampled ("UP") by inserting zero bits between the existing bits to align with the system's sampling rate. Subsequently, the data is split into its real (R) and imaginary (I) components, as shown in Figure 2.7. The next step involves passing the data through the real filter $f_I(t)$ and the imaginary filter $f_Q(t)$, which

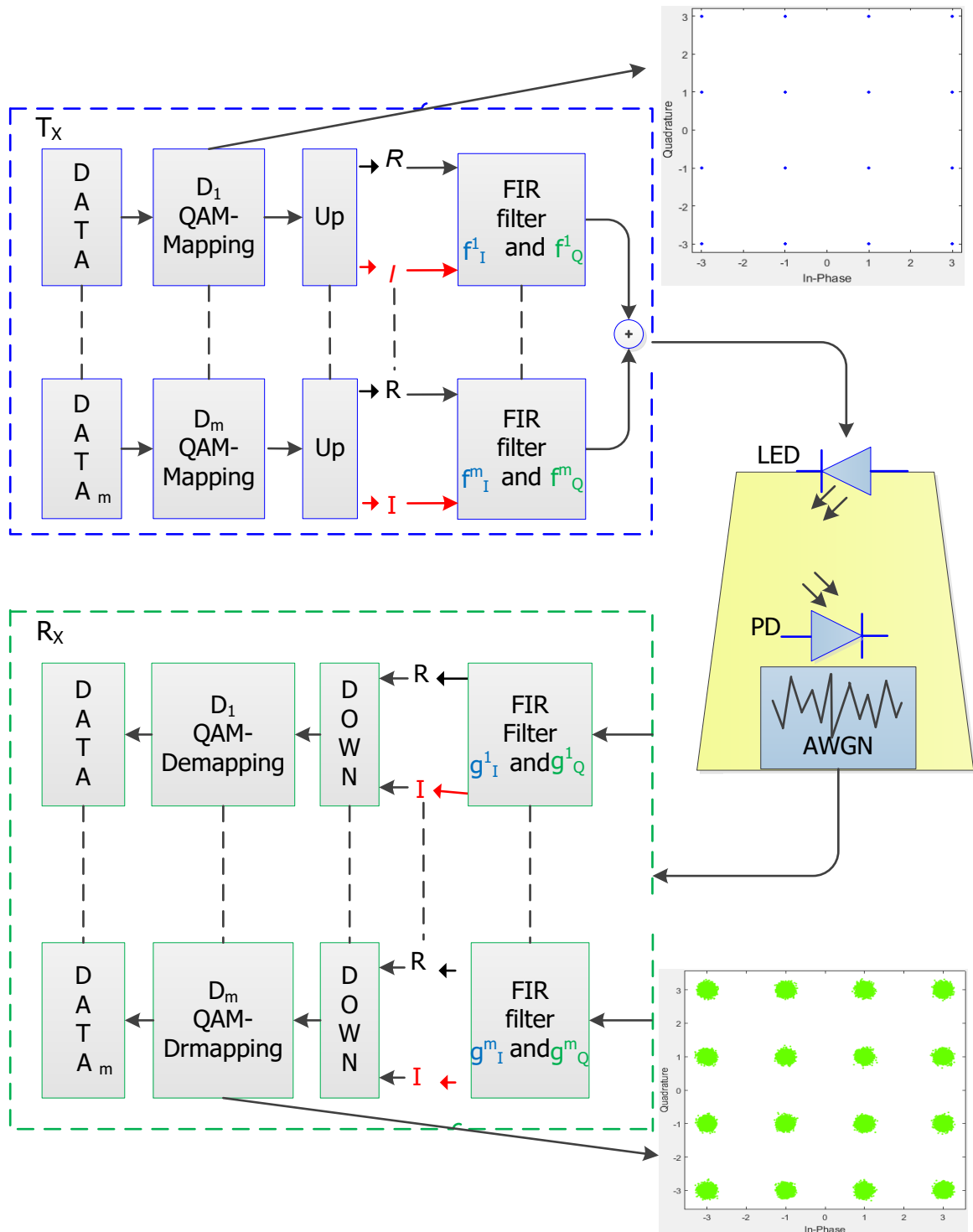


Figure 2-7: Block diagram of m -CAP system.

serve as the Hilbert pairs. The impulse responses of these filters are obtained by convolving the impulse response of the square root raised cosine (SRRC) filter with a cosine or sine wave, resulting in the real and imaginary impulse responses, respectively. It is important to note that the frequency of the cosine and sine waves should be at least twice the pulse width of the SRRC filter. The roll-off factor α of the RRC filter takes on a value between 0 and 1. Figure 2.8 and Figure 2.9 display the time and frequency domains of α , with values set as 0.1, 0.25, 0.5, 0.75,

and 1. From Figure 2.8, it is evident that increasing α reduces the pulse width and diminishes ripples. However, this also leads to an increased pulse width in the frequency domain, resulting in inadequate utilization of the frequency bandwidth, as clearly demonstrated in Figure 2.9. Thus, selecting an appropriate value for α is a crucial parameter when designing the m-CAP system, as the total bandwidth of the system is given by total B.W = $((1 + \alpha) \times \text{baud rate})$. Increasing α necessitates more bandwidth, and the choice of α should be carefully considered. It is important to note that, for simplicity and without sacrificing generality, the system bandwidth is set to unity in this project [70].

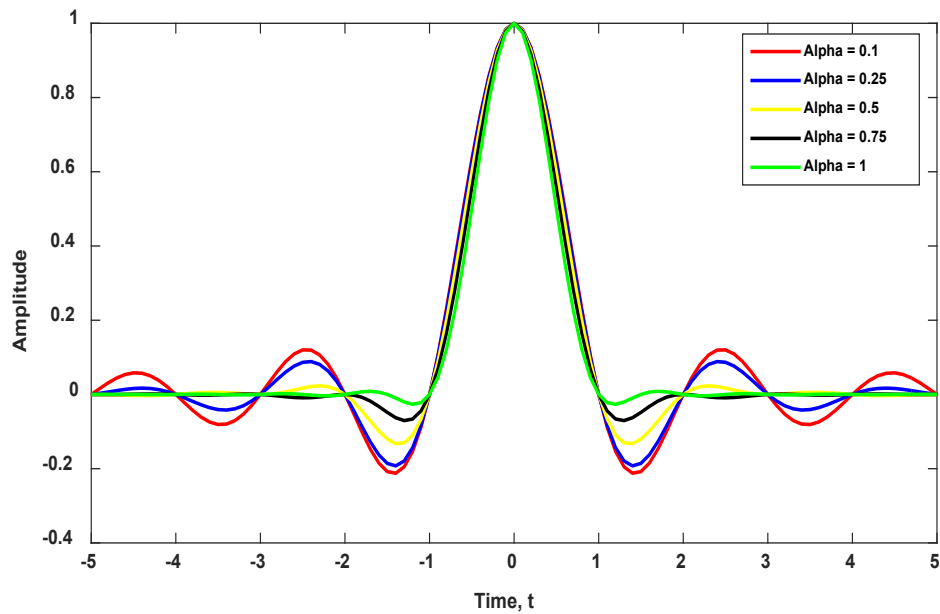


Figure 2-8: Impulse Response of the Raised Cosine Filter [71]

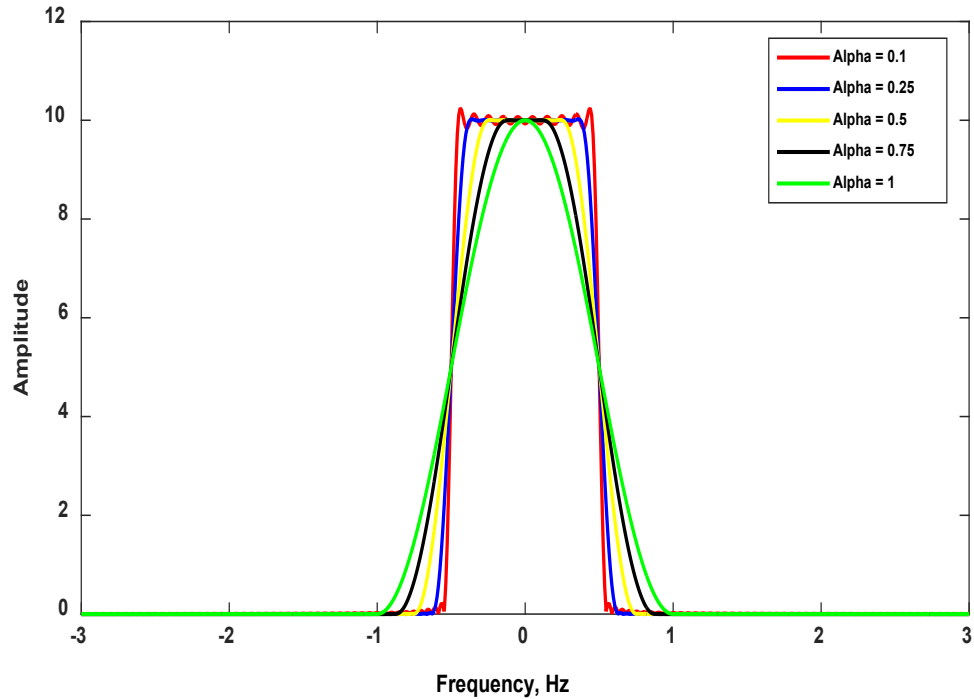


Figure 2-9: Frequency domain representation of raised cosine pulse shaping filters [71].

To summarise, CAP suffers from higher complexity due to the need for complex signal processing techniques to demodulate the signal accurately, making it more challenging to implement. It is susceptible to noise and interference, leading to higher error rates and reduced performance. CAP requires a larger bandwidth compared to other modulation schemes, limiting its spectral efficiency, which can be a constraint in bandwidth-limited environments. It has limited compatibility with existing systems and is not as widely supported as other modulation schemes. Additionally, CAP can experience nonlinear distortion in certain transmission channels, resulting in signal degradation and increased bit error rates.

2.5 Orthogonal Frequency Division Multiplexing (OFDM)

The OFDM modulation system is the cornerstone of this study, and the essential principles underlying the system are introduced in this section.

2.5.1 History of OFDM

Orthogonal frequency division multiplexing (OFDM) is a modulation technique developed over a long period to the novel day OFDM. At the beginning of the 1870s, most researchers turned to frequency division multiplexing FDM, also known as multi-tone [72]. Alexander Graham Bell and his competitors Gray and Edison were in hot pursuit. Bell concentrated on the telephone and his efforts in analogue voice transmission, while others focused on discrete-tone multiplexed telegraphy where Gray had an earlier novelty. In 1910, George Squier, a major in

the U.S. Army Signal Corps, explained for the first time FDM for analogue voice signals with one channel of baseband and passband. This was the most significant utilisation of FDM so far for the analogue telephone [72]. In response to the low throughput of the first FDM system, a system with 5 channels was developed in 1918 by AT&T which did not use the high subcarrier SC frequency and repeaters [72].

At the end of the 1950s, demand increased for a fast communication system with high throughput for military purposes, leading to the modern-day OFDM concept. In the 1960s, Franco and Lachs demonstrated a multi-tone code-multiplexing technique in the frequency domain which had remarkable spectral efficiency and easy coding [73]. The birth of OFDM then followed in 1966 when Robert W. Chang presented a new technique to transmit signals simultaneously over a band-limited system in which inter-symbol interference (ISI) and inter-channel interference (ICI) were prevented. His work was subsequently patented in 1970 [74]. However, high complexity was the main barrier that prevented the wide use of OFDM. In the early 1970s Weinstein and Ebert utilised the discrete Fourier transform (DFT) for the first time for multi-carrier modulation and demodulation. Darlington presented the application of the DFT for the FDM system for the first time in 1971 [73] and ten years later, cyclic extension and equalisation algorithms were proposed by Peled and Ruiz and Hirosaki respectively to overcome orthogonality issue in ISI and ICI. In 1985, Cimini proposed that OFDM technology should be used in mobile communications [73], and in 1987 the technology was also considered for digital audio broadcasting (DAB) systems [75]. A few years later, the success of DAB communication engineers led to the production of a digital video transmission system (DVB) [76]. In August 1991, the potential of utilising OFDM as a modulation technique for digital subcarrier loop (DSL) applications was also suggested [77], followed by the introduction of a multiple-input and multiple-output (MIMO) technique in 1995 [78, 79]. OFDM has been involved in optical communication since 2001 by Rongqing Hui [42]. Moreover, in the last two decades, translation schemes have been rapidly improving. To summarise the history of OFDM, Figure 2-10 illustrates the whole history.

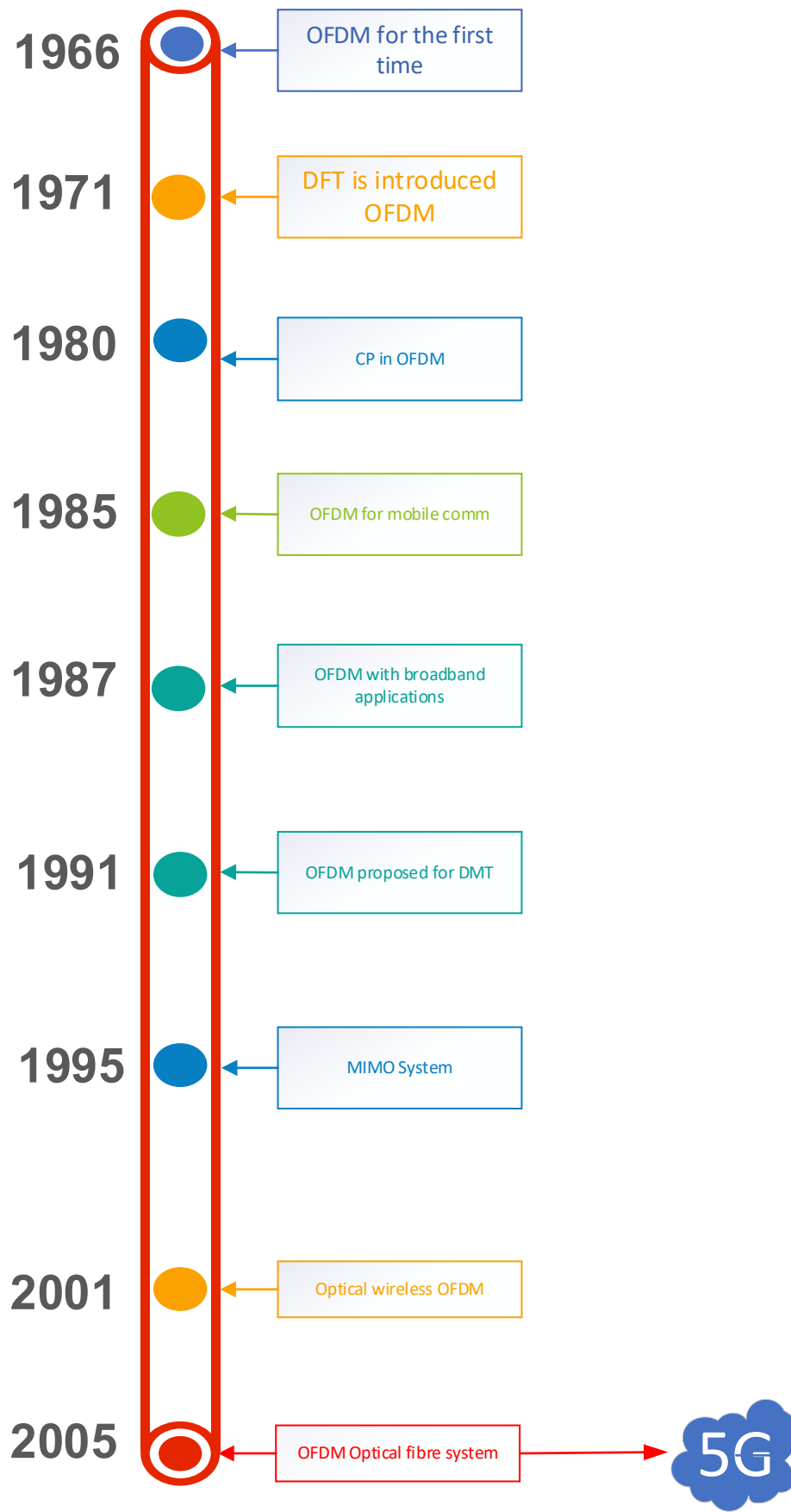


Figure 2-10: The history of OFDM has led to the current system stage.

2.5.2 OFDM in VLC

OFDM has been applied extensively in wired and wireless communication due to its outstanding reputation in resisting ISI without requiring complex equalisers [80]. Moreover, OFDM is almost used ubiquitously in wireless fidelity (WiFi), digital audio broadcasting (DAB), digital video broadcasting (DVB), satellite communication, and 4G (LTE) and 5G new radio (NR) [81, 82]. OFDM has also recently been proposed as a suitable modulation scheme for optical wireless communication, mainly by utilising IM and DD techniques at Tx and Rx respectively [44]. The OFDM scheme is based on multi-carrier modulation (MCM) where the high data rate series is transmitted by dividing it into parallel symbols streams with lower rates and then modulating them individually into different subcarriers (SCs) [83]. By adding a guard band between each adjacent channel, inter-channel interference will therefore be avoided.

Moreover, all SCs in OFDM are orthogonal, which means that if one subcarrier is at high amplitude, the subcarriers before and after are at zero peaks. Also, OFDM has much higher bandwidth efficiency compared to frequency division multiplexing (FDM). Figure 2-12 shows the frequency domain of OFDM and FDM, showing that the effect of ISI caused by the multipath propagation has been reduced due to increased symbol duration; put simply, the period of the symbol has become longer than the channel delay. Figure 2-13 shows the depiction of OFDM with four subcarriers in the time domain. As is evident, each subcarrier in the frequency domain is represented in the time domain by an integer number of cycles [84].

In addition, the OFDM technique basically changes a non-flat fading channel into flat fading by transmitting several series of SCs, where flat fading means that the bandwidth of a channel B_c is greater than the signal bandwidth B_s . Also, when B_c is less than B_s it is known as a frequency selective or non-flat fading channel, which is the case in VLC system, as shown in Figure 2-11.

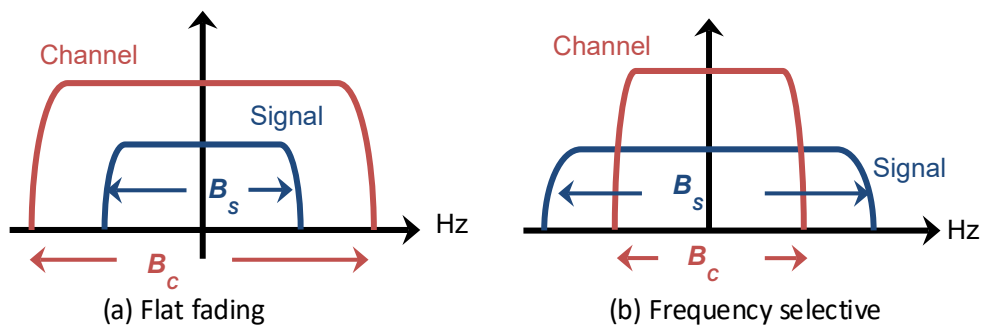
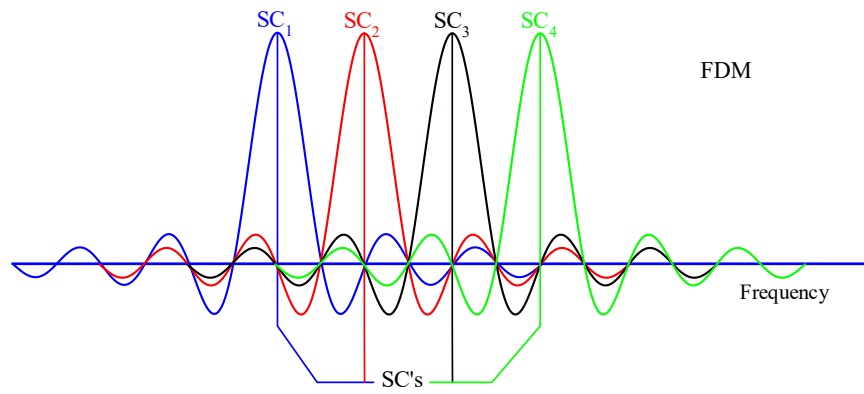
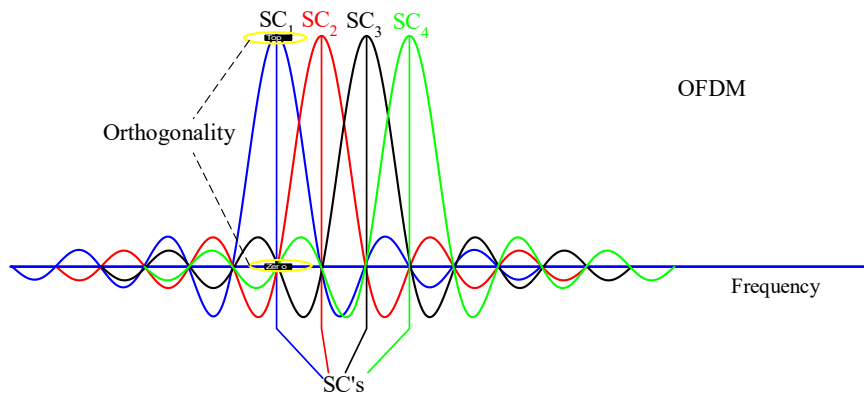


Figure 2-11: (a) Flat fading channel (b) Frequency selective



(a) FDM



(b) 4 SC's in one OFDM symbol in frequency domain

Figure 2-12: Frequency spectrums of FDM and OFDM systems with four SCs.

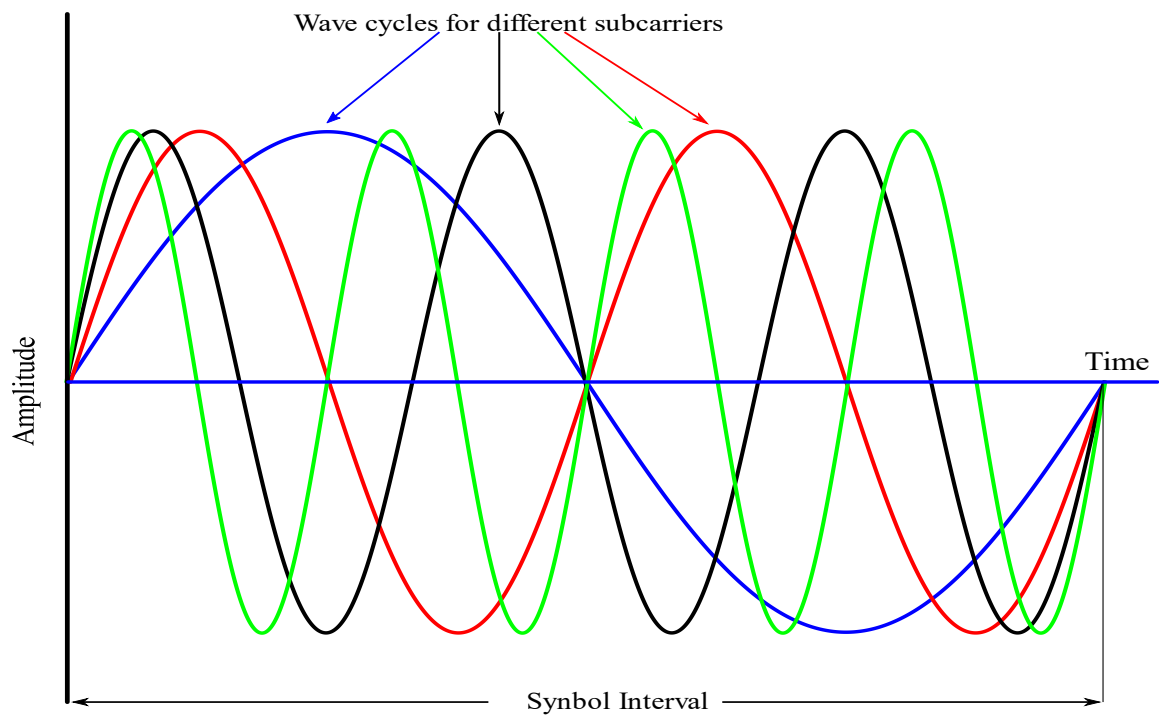


Figure 2-13: OFDM symbol in time domain with four SCs

In other words, in non-flat fading, the signal frequency components will experience different frequency responses, resulting in degradation in the BER and, therefore, lower data rates. Whereas having a flat fading channel means that the signal frequency components will experience the same frequency response.

Changing from the frequency domain to the time domain is accomplished by utilising IFFT. However, the size of IFFT on the Tx side should be chosen carefully, because large IFFT reduces the detrimental effect of multipath propagation but at great computational cost. Therefore, a trade-off between high performance and computational complexity costs must be considered [85]. In addition, the ISI effect can be reduced in OFDM systems by adding a cyclic prefix (CP) to the transmitted symbol. In order to reduce the impact of ISI, the CP interval must be greater than or equal to the maximum propagation way delay, and the next section explains the CP in more detail. Most recently, researchers have proposed replacing the CP with zero padding (ZP) [86, 87]. In the case of the CP, the tail of the transmitted symbol is pasted into the beginning of the transmitted symbol and, vice versa, copying the front of the transmitted symbol and attaching it to the end of the transmitted symbol. Put simply, the transmitted OFDM symbols are thus cyclically extended whereas in ZP zeroes are attached at the end of the transmitted OFDM symbol so that its length is greater than or equal to the time delay of the system [86]. The FFT is then applied to the OFDM symbols at the Rx, allowing the sending signal to be reconstructed [88]. Figure 2.8 illustrates OFDM with four subcarriers in the time domain. Here, within the symbol interval T_s , each subcarrier has precisely an integer number of cycles, and there is an exactly one cycle difference between neighbouring subcarriers [89].

2.5.3 Cyclic prefix (CP)

In nineteen eighty, [90] introduced the cyclic prefix to reduce the complexity of the equalisation and ISI in OFDM system. A cyclic prefix (CP) is regarded as a crucial component of the OFDM system since it prevents and eradicates both intersymbol interference (ISI) and intercarrier interference (ICI). The length N_{cp} of the CP should be longer than the channel delay spread T_{max} [45].

$$N_{cp} \geq T_{max}. \quad (2.14)$$

Although the CP compensates for the effect of the multipath propagation, it consumes a significant amount of spectrum and power. Therefore, the length of a CP utilised in DCO-

OFDM needs to be chosen according to the instantaneous parameters of the channel [91], which thereby improves overall system performance. The concept of CP is illustrated in Figure 2.14, showing a copy of the last part of the OFDM symbol appended to the beginning of the OFDM symbol, so that this end part of the output of IFFT is also attached to the start of the output [1, 45].

To understand the concept of the CP, the frequency selective channel can be modelled as $y(n)$, which is a model for a frequency selective channel.

$$y(n) = h(0)x(n) + h(1)x(n - 1) + h(2)x(n - 2) + \dots + h(L - 1)x(n - L + 1). \quad (2.15)$$

It can be seen from Equation 2.15 that the output of $y(n)$ has L channel taps. Also, the output of $y(n)$ depends not only in input symbol $x(n)$ but also depends on $x(n - 1)$, $x(n - 2)$ and $x(n - L + 1)$ from the previous symbol. Therefore, this channel has ISI in the time domain, which is the same as being frequency selective in the frequency domain, whereas $x(n)$ is the transmitted symbol and $h(L)$ the channel tap.

Consider two consecutive OFDM symbols.

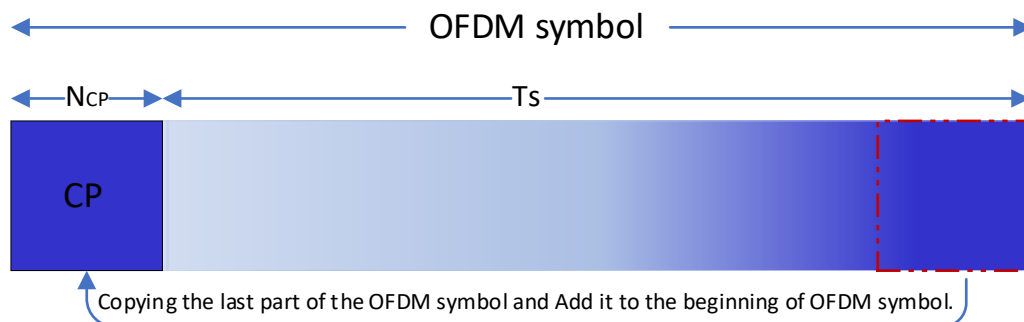
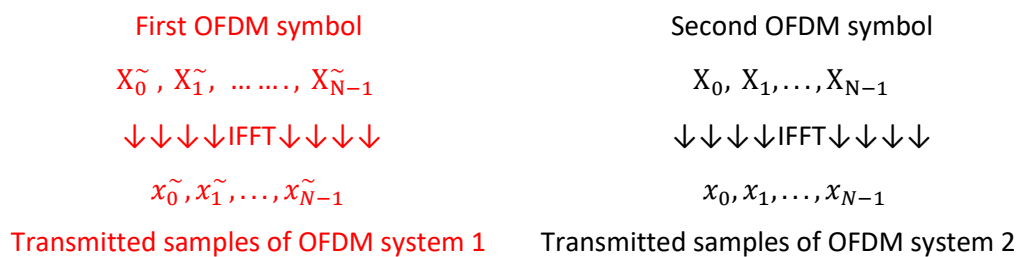


Figure 2-14: Cyclic prefix extension.



The output for x_0 is $y(0)$

$$y(0) = h(0)x(0) + h(1)x^{\sim}(N-1) + h(2)x^{\sim}(N-2) + \dots + h(L-1)x^{\sim}(N-L+1). \quad (2.16)$$

Equation 2.16 shows that there is inter-block interference IBI from the previous OFDM symbol x^{\sim} . Therefore, CP has been used to avoid IBI or ICI. With the prefix of $N_{CP} \cong L-1$ samples from the tail of the OFDM symbol, then the total number of samples transmitted is $N+N_{CP}$. Now consider one OFDM symbol and the addition of CP [92]:

$$\begin{array}{c} X_0, X_1, \dots, X_{N-1} \\ \downarrow \downarrow \downarrow \downarrow \text{IFFT} \downarrow \downarrow \downarrow \downarrow \\ x_1, x_2, \dots, x_{N-1} \\ \downarrow \downarrow \downarrow \downarrow \text{CP} \downarrow \downarrow \downarrow \downarrow \\ x_{N-L}, \dots, x_{N-2}, x_{N-1}, x_0, x_1, \dots, x_{N-1} \end{array}$$

Now write $y(0)$ can be written:

$$y(0) = h(0)x(0) + h(1)x(N-1) + h(2)x(N-2) + \dots + h(L-1)x(N-L+1). \quad (2.17)$$

To simplify the concept of the CP, it can be assumed that $N=4$ and the channel tap is 2. Then: $y = x_3, x_0, x_1, x_2, x_3$. Therefore,

$$y(0) = h(0)x(0) + h(1)x(3). \quad (2.18)$$

$$y(1) = h(0)x(1) + h(1)x(0). \quad (2.19)$$

$$y(2) = h(0)x(2) + h(1)x(1). \quad (2.20)$$

$$y(3) = h(0)x(3) + h(1)x(2). \quad (2.21)$$

From Equations 2.18 - 2.21, there is no IBI. Also, a matrix of a channel output y can be written as:

$$\begin{bmatrix} y_0 \\ y_1 \\ y_2 \\ y_3 \end{bmatrix} = \begin{bmatrix} h_0 & 0 & 0 & h_1 \\ h_1 & h_0 & 0 & 0 \\ 0 & h_1 & h_0 & 0 \\ 0 & 0 & h_1 & h_0 \end{bmatrix} \times \begin{bmatrix} x_0 \\ x_1 \\ x_2 \\ x_3 \end{bmatrix}. \quad (2.22)$$

From Equation 2.22, it is clearly seen that the channel taps h circular shift over the OFDM symbol x in the time domain. As can be seen h_1 in the first row and last column have moved to the second row in the first column, and h_0 which was in the first row and the first column has moved to the second row and column and kept moving to the right. Adding the CP leads to conversion from linear to circular convolution and removes IBI in the time domain. Therefore, the output or the receiving signal y is equal to

$$y = h \circledast x + v. \quad (2.23)$$

where \circledast denotes the convolution operation and v is the noise. Applying FFT to Equation 2.23

$$FFT(y) = FFT(h \circledast x + v). \quad (2.24)$$

Because the FFT operator is linear, then Equation 2.24 becomes

$$FFT(y) = FFT(h \circledast x) + FFT(v). \quad (2.25)$$

Furthermore, because the circular convolution property in the time domain is equal to multiplication in the frequency domain, $FFT(\circledast) = \times$, then Equation 2.25 can be written as

$$FFT(y) = FFT(h) \times FFT(x) + FFT(v). \quad (2.26)$$

Therefore, the PC in the OFDM system has two advantages: firstly, ISI is avoided when the CP's length exceeds the maximum channel delay; and secondly it inhibits IBI or ICI by converting the multipath fading channel into flat fading subchannels. On the other hand, utilising the CP in the OFDM modulation is not purely positive [86].

In VLC technology, the transmitted electrical power will change into the optical domain by IM through the LED, which needs a real and positive signal. On the other hand, the output of IFFT could be imaginary and negative, which is an input to LED. In order to achieve the real OFDM signal, half of the spectrum bandwidth is paid. The real signal will be achieved by inserting Hermitian symmetry (HS) into the transmitted data as the input of IFFT. Moreover, a real OFDM signal could be obtained from a real transform such as a discrete cosine transform

(DCT). However, the problem of negative signal can be solved by adding a DC bias, which is usually added to a VLC system [44]. In the literature it has been shown that several techniques can produce positive OFDM signals with regard to IM/DD modulation:

- DC-biased optical OFDM (DCO-OFDM) comes at the cost of reducing power efficiency.
- Asymmetrically clipping optical OFDM (ACO-OFDM) comes at the cost of reducing spectral efficiency.

Another technique based on the above techniques is known as asymmetrically clipped DC-biased optical OFDM (ADO-OFDM). This newer scheme combines the concepts of DCO-OFDM and ACO-OFDM by simultaneously applying DCO-OFDM and ACO-OFDM to the even and odd SCs respectively [44]. It has been claimed that, in consequence, “optimal values are found for several configurations and it is shown that in several cases ADO-OFDM requires less optical power than existing schemes (DCO-OFDM) and (ACO-OFDM)” [46].

2.5.4 DC biased optical OFDM (DCO-OFDM)

DCO-OFDM has been described as one of the earlier forms of optical OFDM, where a sufficient amount of DC bias is applied to the bipolar signal to produce a positive unipolar signal [37]. Figure 2.11 illustrates the DC-biased optical OFDM (DCO-OFDM) system. As can be seen, the design is like that of the DCO-OFDM system. However, there are two additional main blocks HS and DC-biased to allow the IM/DD modulation technique. As mentioned, the HS process occurs at the input of IFFT and the DC is biased before the electrical to optical E/O. The LED, in this case, is used at Tx instead of the conventional RF antenna [93].

Figure 2-15 shows an incoming bitstream d mapped into M-quadrature amplitude modulation M-QAM, where M is the constellation order. Then, a serial-to-parallel (S/P)

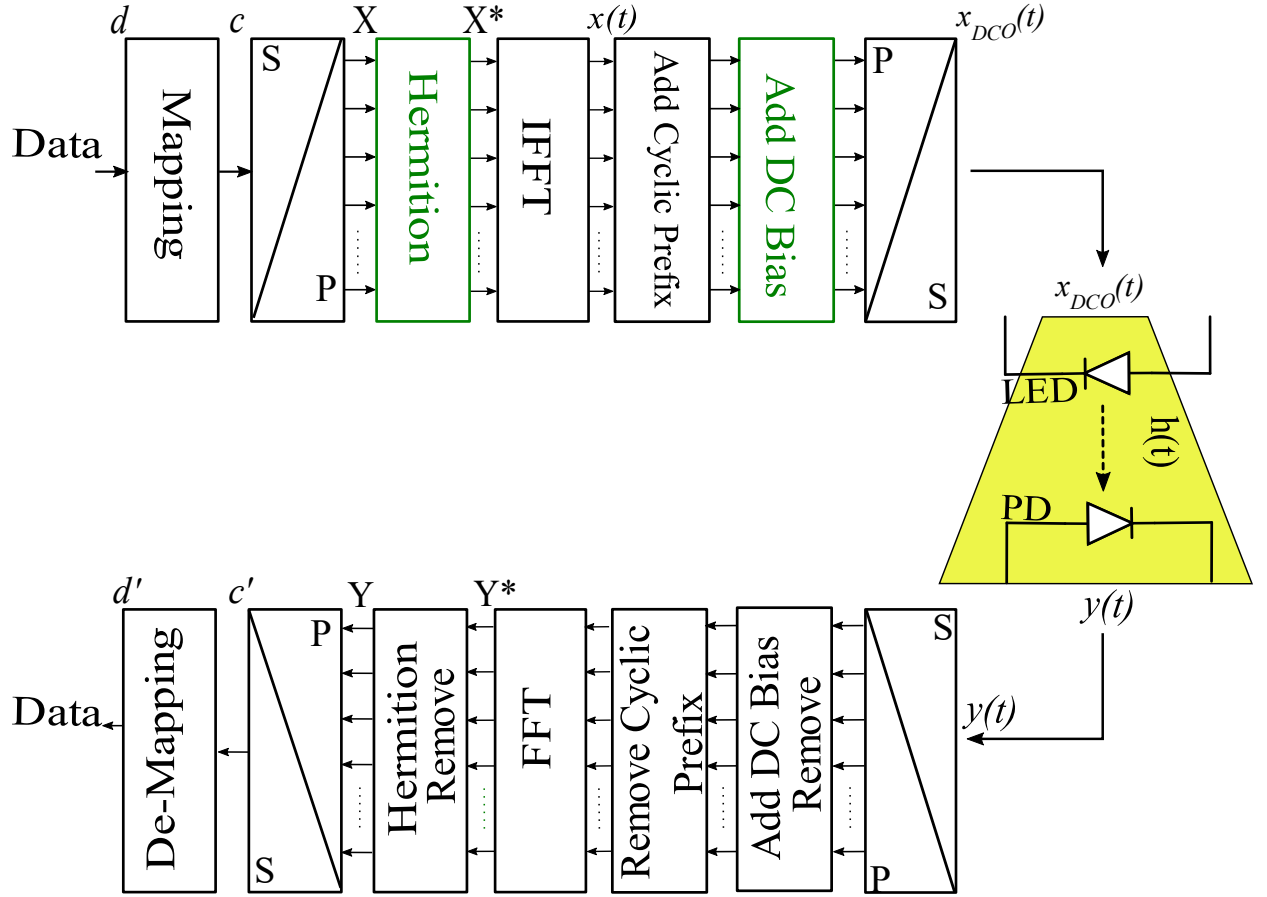


Figure 2-15: Block diagram of the DCO-OFDM.

converter is used to divide this stream of symbols c into several parallel subcarriers N , which are denoted as X . These symbols are fed to Hermitian symmetry (HS) to generate a real output of IFFT to meet the IM condition. This means that, if there are N subcarriers overall, only $\frac{N}{2}$ will be used for data transmission and the other half will be flipped as complex conjugate counterparts of the previous ones according to the requirements of Hermitian symmetry. Figure 2-16 provides a visualisation of the phenomena using the Hermitian Symmetry criterion [28]. Mathematically, HS is given as follows [46]:

$$X_k \begin{cases} 0 & k = 0 \\ x_k & 0 < k < N/2 \\ 0 & k = N/2 \\ x_k^* & k > N/2 \end{cases} \quad (2.27)$$

Consequently, the input to the IFFT is as follows:

$$X^* = [0, X_1, X_2, \dots, X_{N/2-1}, 0, X_{N/2-1}^*, \dots, X_2^*, X_1^*]^T \quad (2.28)$$

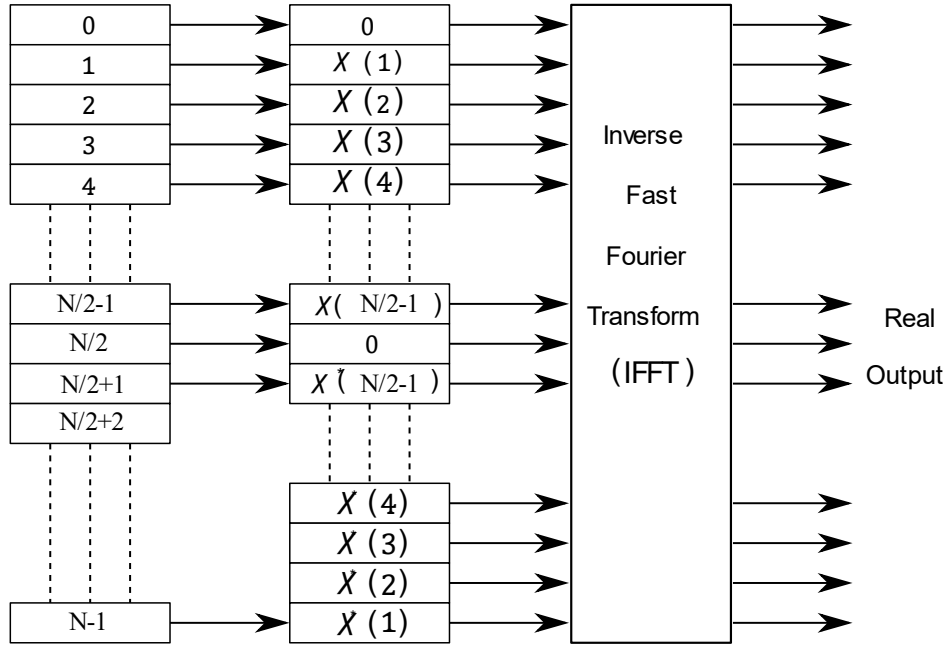


Figure 2-16: Hermitian Symmetry (HS) of DCO-OFDM

The following equation provides the output of IFFT that is more prevalent [47].

$$x(t) = \frac{1}{\sqrt{N}} \sum_{k=0}^{N-1} X(k) e^{\frac{j2\pi tk}{N}}. \quad (2.29)$$

where $x(t)$ and $X(k)$ are a time sample of OFDM and the data symbols obtained from a modulation constellation, and N is the total number of subcarriers. Consequently, Equation 2.29 may be resolved by including the HS to produce the time domain signal as:

$$x(t) = \frac{1}{\sqrt{N}} \left[X(0) e^{\frac{j2\pi t(0)}{N}} + \sum_{k=1}^{\left(\frac{N}{2}-1\right)} X(k) e^{\frac{j2\pi tk}{N}} + X\left(\frac{N}{2}\right) e^{\frac{j2\pi t\frac{N}{2}}{N}} + \sum_{k=\frac{N}{2}+1}^{N-1} X(k) e^{\frac{j2\pi tk}{N}} \right]. \quad (2.30)$$

When Equation 2.27 is added to Equation 2.30, the latter may be written as follows:

$$x(t) = \frac{1}{\sqrt{N}} \left[\sum_{k=1}^{\left(\frac{N}{2}-1\right)} X(k) e^{\frac{j2\pi tk}{N}} + \sum_{k=\frac{N}{2}+1}^{N-1} X(k) e^{j2\pi tk} \right]. \quad (2.31)$$

In order to surpass the effects of intersymbol and inter-carrier interference from becoming a problem in the optical wireless communication channel, a cyclic prefix (CP) is often added to the OFDM signal. The cyclic prefix (CP) must be longer than the channel maximum delay spread to reduce the ISI or 25% of the subcarrier's size [37, 47]. In most cases, this cyclic prefix added signal, denoted by the notation $x_{cp}[t]$, is real, although it is not always positive. Therefore, a specific amount of DC bias needs to be supplied to $x_{cp}[t]$ so as to convert it into a positive (unipolar) signal. Although OFDM has several benefits, it is susceptible to having a high peak-to-average power ratio (PAPR) because it superimposes many subcarriers. Consequently, adding a high level of DC bias causes the ratio of optical power per bit to signal noise power to become high, making the DCO-OFDM technique inefficient in terms of optical energy [46]. Therefore, the best location for the DC bias point would be in the middle of the linear range between the voltage at turn-on and that at saturation power. Outside of that linear range, clipping distortion of the OFDM signal will occur [94]. Moreover, this could lead to the operation of the LEDs outside of the linear region. Consequently, a DC bias level, denoted by B_{DC} , which is proportional to the power of $x_{cp}[t]$ must be used in order to avoid excess DC bias while also reducing the optical power needed [46, 95]. B_{DC} is determined according to the standard deviation of $x_{cp}[t]$ [46]

$$B_{DC} = \mu \sqrt{E\{x_{cp}^2[n]\}}, \quad (2.32)$$

where μ is a constant of proportionality and $E\{\ \}$ is a statistical expectation.

However, Armstrong [61] defined the DC B_{DC} as $10 \log_{10}(\mu^2 + 1) \text{ dB}$, where any remaining negative peak after the addition of DC is clipped at zero. Then, $x_{DC}(t) = x_{cp}(t) + B_{DC}$ is transmitted through the LED. In the ideal scenario, the strength of optical power that comes out of the LED is directly proportional to the amount of electrical current that goes into the LED. After that, a flat channel is used to send the LED output signal.

At the receiver, a photodiode converts the received signal from an optical signal into an electrical signal (O/E). The bottom of Figure 2-15 shows inverse operations at the receiver, including removing the DC bias and cyclic prefix and applying FFT to transform the time-domain signal into a frequency domain signal. Finally, the HS is removed, a parallel-to-serial (P/S) converter is applied, and the proper demodulation techniques are used to recover the transmitted data successfully. To provide simulation findings here in a manner that is

2.5.5 Asymmetrically clipping optical OFDM (ACO-OFDM)

ACO-OFDM methodology may be used to produce a signal with a positive value in order to significantly overcome the problem of power inefficiency in DCO-OFDM. A unipolar signal is created primarily without the need to include DC bias. By assigning zero to the even subcarriers in ACO-OFDM, only the odd subcarriers contain data symbols, and this ensures that the transmitted OFDM signal satisfies the non-negativity condition [16, 46]. Figure 2-18 shows that the ACO-OFDM transmitter is similar to a DCO-OFDM transmitter where data d has been converted by S/P after it has been mapped to only the odd SCs. Thus, the clipping will occur only in the even subcarriers since the IFFT input carries data in odd subcarriers [45]. In this case, the even subcarriers are given a value of zero, while the odd subcarriers are modulated and given Hermitian symmetry assignments. As a consequence, the resulting signal may be shown as [96]:

$$X(n) \begin{cases} X(n) & n \text{ is odd} \\ 0 & n \text{ is even} \end{cases} . \quad (2.33)$$

Therefore, the IFFT input is supplied as in Equation 2.34 in order to produce a real-time domain signal. However, only 25% of the N subcarriers are intended to carry data owing to the Hermitian symmetry requirement as shown in Figure 2-19.

$$X = \left[0, X_1, 0, X_3, 0, X_5, \dots, X_{N/2-1}, 0, X_{N/2-1}^*, 0, \dots, X_5^*, 0, X_3^*, 0, X_1^* \right]^T . \quad (2.34)$$

The CP is then added to the IFFT output $x(t)$ before a parallel-to-serial (P/S) converter. After that $x(t)$ is clipped to zero to meet the condition of IM/DD because a negative signal could not be transmitted through the LED. The $x_{ACO}(t)$ is transmitted through a flat AWGN channel, except that only the odd subcarriers in ACO-OFDM are demodulated since only they contain the data symbols, while the processing in the receiver is comparable to that of a DCO-OFDM receiver.

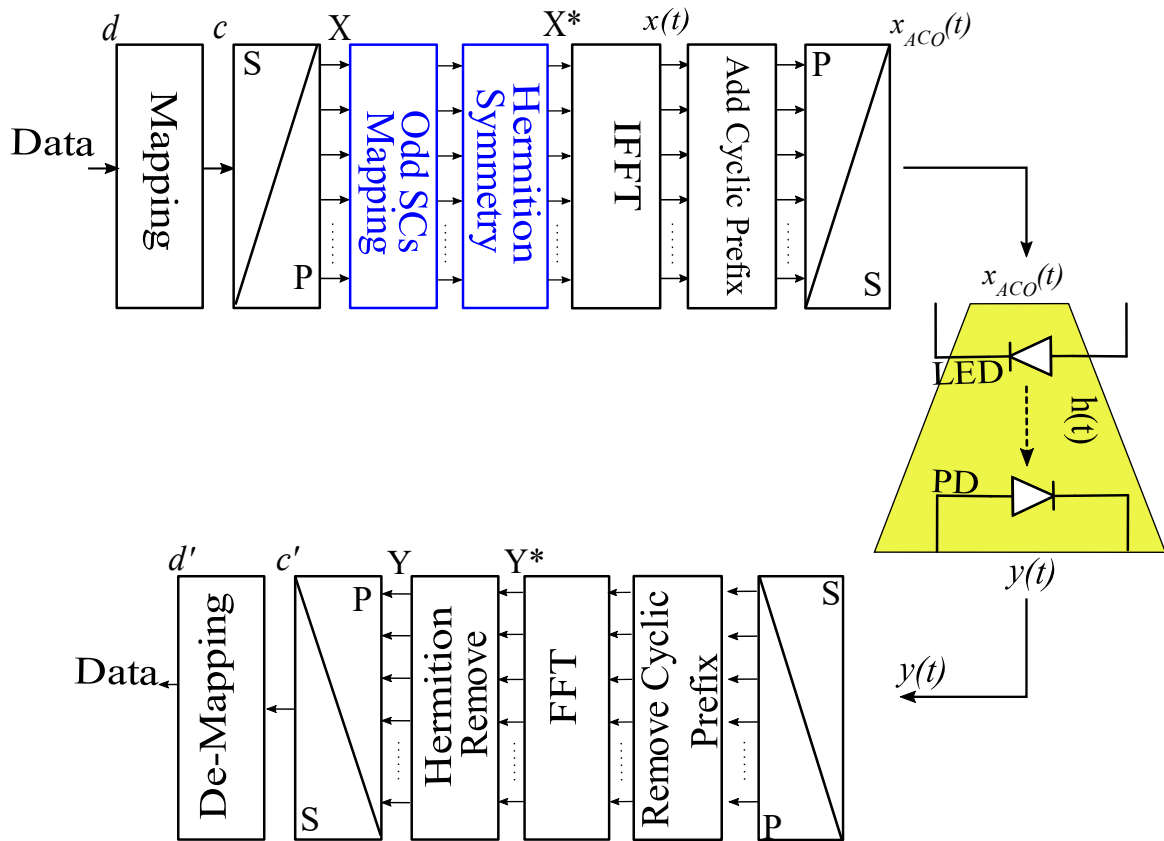


Figure 2-17: Block diagram of the ACO-OFDM.

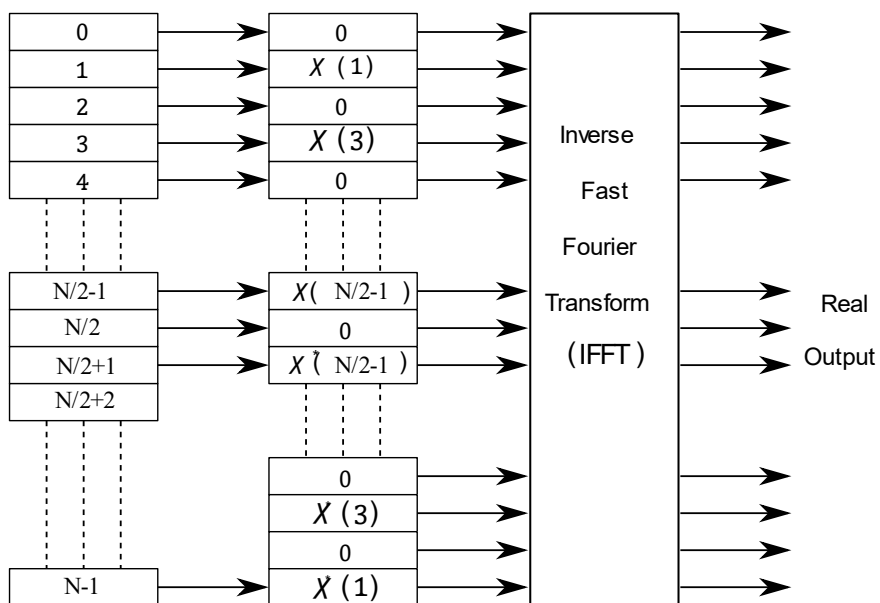


Figure 2-18: Hermitian Symmetry (HS) of ACO-OFDM.

2.6 Advantages and disadvantages of OFDM

As mentioned, the OFDM system has several advantages, such as resistance to ISI and improving the spectrum bandwidth. However, the drawback of OFDM technique is more important.

2.6.1 Drawbacks of OFDM Systems.

Although DCO-OFDM modulation has been considered to be a successful modulation technique for wired and wireless communication systems in several applications, it has several areas that need to be developed as follows:

- Peak-to-average power ratio (PAPR)

A high PAPR is considered to be the main barrier to achieving high performance in OFDM systems [45]. The PAPR has dual importance, in that: firstly, it should be as low as is achievable in order to reduce the system's dynamic range and prevent the non-linearity issue in optoelectronic devices; and, secondly, to fulfil eye safety regulations. Therefore, attention must be paid to determining the optimal PAPR ratio. High PAPR leads OFDM to suffer from the influence of non-linear distortion [97], and so the PAPR is generally calculated by dividing its highest transmitted power by its average transmission [47]:

$$PAPR = \frac{\max_{0 \leq n \leq N-1} |x^2[n]|}{E[x^2[n]]}. \quad (2.35)$$

Multi-carrier modulation (MCM) is based on orthogonal frequency division multiplexing (OFDM), such as OFDM with direct current biasing (DCO-OFDM) and asymmetrically clipped optical OFDM with multi-level quadratic amplitude modulation (M-QAM). Consequently, in all these techniques signals have a high peak-to-average power ratio (PAPR) and are nonlinearly transmitted by the optical front end [98]. The non-linear distortion of the signal causes a reduction in the system's performance, including an increase in BER or SNR [16].

- Inter carrier interference (ICI)

Due to the SCs being close to each other, the carrier frequency offset (CFO) is more likely to be present in the OFDM system, which leads to failing the orthogonality condition resulting in the introduction of ICI. Tackling the abovementioned issues requires additional complexity for the OFDM system, which could significantly affect progress in improving the next generation of communications.

2.7 Conclusion

The concept of VLC is presented in this chapter along with its history. Also, the development of mobile communication networks is covered, and then problems experienced with VLC systems are introduced. Since an OFDM modulation scheme forms the basis of this project the history of OFDM is explained and detailed discussions are provided of its advantages and disadvantages. The advantages include the reduction of ISI by splitting the available bandwidth into several sub-bands and transforming the selective fading channel into a flat fading channel. The chapter also covers problems with OFDM, such as offset and PAPR.

Chapter 3

C-transform

The C-transform (CT) is a unitary transform that combines the effect of two transforms: the Walsh-Hadamard transform (WHT) and discrete cosine transform (DCT). Rathore and Kaur [99] have presented a novel transform for image processing that computes the discrete cosine transform DCT via the WHT. Their original idea was to apply the two transforms separately. However, in order to reduce complexity, combining them in one transform named the C-transform [100] was then used to build the OFDM system. This chapter provides an in-depth discussion of this transform, analyses its structure and computational complexity, and compares it to the DCT-OFDM and DCO-OFDM. Therefore, if it is to be deemed a suitable candidate for employment in specialised communication systems, the new transform must be efficient in terms of complexity and speed.

3.1 Discrete Cosine Transform (DCT)

The DCT-based OFDM system has been shown to be a viable substitute for the traditional OFDM system [43]. However, a set of complex exponential functions is not the only orthogonal basis on which the MCM approach may be constructed. One set of cosine functions may be used as an orthogonal foundation for implementing the MCM system, and this system can then be constructed using a discrete cosine transform (DCT). The commonly used DCT is given as follows [101, 102]:

$$DCT_{N \times N}(r, c) = \begin{cases} \frac{1}{\sqrt{N}} & r = 0, \\ \sqrt{\frac{2}{N}} \cos \left[\frac{\pi(2c + 1)r}{2N} \right] & 1 \leq r \leq N - 1 \end{cases} \quad (3.1)$$

where r ($0 \leq r \leq N-1$) and c ($0 \leq c \leq N-1$) are the row and the column of the DCT matrix respectively.

Therefore, a DCT matrix of size eight can be presented as:

$$DCT_{8 \times 8} = \begin{bmatrix} 0.35 & 0.35 & 0.35 & 0.35 & 0.35 & 0.35 & 0.35 & 0.35 \\ 0.5 & 0.41 & 0.28 & 0.1 & -0.1 & -0.28 & -0.42 & -0.5 \\ 0.46 & 0.19 & -0.19 & -0.46 & -0.46 & -0.19 & 0.19 & 0.46 \\ 0.41 & -0.1 & -0.5 & -0.28 & 0.28 & 0.5 & 0.1 & -0.42 \\ 0.35 & -0.35 & -0.35 & 0.35 & 0.35 & -0.35 & -0.35 & 0.35 \\ 0.28 & -0.5 & 0.1 & 0.42 & -0.41 & -0.1 & 0.5 & -0.28 \\ 0.19 & -0.46 & 0.46 & -0.19 & -0.19 & 0.46 & -0.46 & 0.19 \\ 0.1 & -0.28 & 0.42 & -0.5 & 0.5 & -0.41 & 0.28 & -0.1 \end{bmatrix} \quad (3.2)$$

3.2 Walsh-Hadamard Transform (WHT)

In 1923, Walsh [103] completed an incomplete set of Rademacher functions, resulting in the complete orthonormal set of rectangular functions which are commonly referred to as Walsh functions. The collection of Walsh functions has been divided into three categories: (i) sequence or Walsh ordering, (ii) dyadic or Paley ordering; and (iii) natural or Hadamard ordering. These groupings are distinguished by the sequence in which individual functions appear in the three forms of orderings. Details of the Walsh and Hadamard order are discussed below.

The idea of using the WHT function in well-formulated applications such as non-linear problems did not emerge until the early 1960s [85]. The WHT has since been used to solve various issues in engineering, physics, and other physical sciences. Furthermore, because it can effectively be computed using just additions and subtractions of ± 1 , the WHT has gained popularity in various digital signal processing applications [104, 105]. As a result, its hardware implementation is likewise more straightforward, and it has also been used in the medical field and in the geological as well as biological sciences [104].

Rearranging the rows of a Hadamard matrix (H) into a sequence order yields the WHT [106]. A lower order H matrix can be used to create the $N \times N$ Hadamard matrix as follows:

$$H_N = \otimes^n H_2. \quad (3.3)$$

where $H_2 = \begin{bmatrix} 1 & 1 \\ 1 & -1 \end{bmatrix}$ is a Hadamard matrix of 2-point, $n = \log_2 N$ and \otimes is the presented Kronecker product. An illustration of the concept of the Kronecker product of two-dimensional square matrices can be given as

$$\begin{aligned} \begin{bmatrix} x_{11} & x_{12} \\ x_{21} & x_{22} \end{bmatrix} \otimes \begin{bmatrix} y_{11} & y_{12} \\ y_{21} & y_{22} \end{bmatrix} &= \begin{bmatrix} x_{11} \begin{bmatrix} y_{11} & y_{12} \\ y_{21} & y_{22} \end{bmatrix} & x_{12} \begin{bmatrix} y_{11} & y_{12} \\ y_{21} & y_{22} \end{bmatrix} \\ x_{21} \begin{bmatrix} y_{11} & y_{12} \\ y_{21} & y_{22} \end{bmatrix} & x_{22} \begin{bmatrix} y_{11} & y_{12} \\ y_{21} & y_{22} \end{bmatrix} \end{bmatrix} \\ &= \begin{bmatrix} x_{11}y_{11} & x_{11}y_{12} & x_{12}y_{11} & x_{12}y_{12} \\ x_{11}y_{21} & x_{11}y_{22} & x_{12}y_{21} & x_{12}y_{22} \\ x_{21}y_{11} & x_{21}y_{12} & x_{22}y_{11} & x_{22}y_{12} \\ x_{21}y_{21} & x_{21}y_{22} & x_{22}y_{21} & x_{22}y_{22} \end{bmatrix}. \end{aligned} \quad (3.4)$$

Therefore, based on an assumption that $N=4$, and applying Equation 3.3, $n=2$ and H_4 can be as follows:

$$\begin{aligned} H_{4 \times 4} = H_2 \otimes H_2 &= \begin{bmatrix} 1 & 1 \\ 1 & -1 \end{bmatrix} \otimes \begin{bmatrix} 1 & 1 \\ 1 & -1 \end{bmatrix} = \begin{bmatrix} 1 \begin{bmatrix} 1 & 1 \\ 1 & -1 \end{bmatrix} & 1 \begin{bmatrix} 1 & 1 \\ 1 & -1 \end{bmatrix} \\ 1 \begin{bmatrix} 1 & 1 \\ 1 & -1 \end{bmatrix} & -1 \begin{bmatrix} 1 & 1 \\ 1 & -1 \end{bmatrix} \end{bmatrix} \\ &= \begin{bmatrix} 1 & 1 & 1 & 1 \\ 1 & -1 & 1 & -1 \\ 1 & 1 & -1 & -1 \\ 1 & -1 & -1 & 1 \end{bmatrix} \begin{bmatrix} S_{ch}(0) \\ S_{ch}(3) \\ S_{ch}(1) \\ S_{ch}(2) \end{bmatrix}. \end{aligned} \quad (3.5)$$

where (-) is represented by -1 and S_{ch} is the number of sign-changes in the row. Rearranging the rows of $H_{4 \times 4}$ can generate $W_{4 \times 4}$. The successive rows in Equation 3.5 have ordered 0,3,1 and 2 sign changes, which is a Hadamard ordering; if the rows are changed in sequence order, the WHT can be written as [103]

$$WHT_{4 \times 4} = \begin{bmatrix} 1 & 1 & 1 & 1 \\ 1 & 1 & -1 & -1 \\ 1 & -1 & -1 & 1 \\ 1 & -1 & 1 & -1 \end{bmatrix} \begin{bmatrix} S_{ch}(0) \\ S_{ch}(1) \\ S_{ch}(2) \\ S_{ch}(3) \end{bmatrix}. \quad (3.6)$$

Alternatively, the WHT matrix may be defined as:

$$WHT_{x,u} = (-1)^{\sum_{i=0}^{n-1} x_i u_i} \quad (3.7)$$

where $n = \log_2(N)$ and $x_i * u_i$, which is the i^{th} product operation of bit by bit for the binary number representing the integer numbers x , u , and $n-1$ is the number of binary digits in each index. To clarify Equation 3.7, let us assume that $W(6,5)$ where $x = 6$ and $u = 5$ and x is the sixth row while u is the 5th column in $W_{8 \times 8}$, which are presented in binary as 110 and 101 respectively. Applying, these numbers in Equation 3.7, would result in:

$$g(x, u) = \sum_i^{n-1} x_i u_i$$

$$g(6,5) = \sum_{j=0}^{3-1} 6_j * 5_j$$

$$g(6,5) = b_0(6) * b_0(5) + b_1(6) * b_1(5) + b_2(6) * b_2(5)$$

$$g(6,5) = 0 * 1 + 1 * 0 + 1 * 1 = 1$$

$$W(6,5) = (-1)^1 = -1$$

Moreover, a Hadamard matrix in Equation 3.3 is defined as a function of a lower-order matrix as in any orthogonal transform [106]:

$$H_{N \times N} = \begin{bmatrix} H_{N/2} & H_{N/2} \\ H_{N/2} & -H_{N/2} \end{bmatrix} \quad (3.8)$$

The following example illustrates creating a Walsh matrix (8x8) by rearranging the rows of a Hadamard matrix (8x8):

$$H_{8 \times 8} = \begin{bmatrix} 1 & 1 & 1 & 1 & 1 & 1 & 1 & 1 \\ 1 & -1 & 1 & -1 & 1 & -1 & 1 & -1 \\ 1 & 1 & -1 & -1 & 1 & 1 & -1 & -1 \\ 1 & -1 & -1 & 1 & 1 & -1 & -1 & 1 \\ 1 & 1 & 1 & 1 & -1 & -1 & -1 & -1 \\ 1 & -1 & 1 & -1 & -1 & 1 & -1 & 1 \\ 1 & 1 & -1 & -1 & -1 & -1 & 1 & 1 \\ 1 & -1 & -1 & 1 & -1 & 1 & 1 & -1 \end{bmatrix} \begin{matrix} S_{ch}(0) \\ S_{ch}(7) \\ S_{ch}(3) \\ S_{ch}(4) \\ S_{ch}(1) \\ S_{ch}(6) \\ S_{ch}(2) \\ S_{ch}(5) \end{matrix} \quad (3.9)$$

$$W_{8 \times 8} = \begin{bmatrix} 1 & 1 & 1 & 1 & 1 & 1 & 1 & 1 \\ 1 & 1 & 1 & 1 & -1 & -1 & -1 & -1 \\ 1 & 1 & -1 & -1 & -1 & -1 & 1 & 1 \\ 1 & 1 & -1 & -1 & 1 & 1 & -1 & -1 \\ 1 & -1 & -1 & 1 & 1 & -1 & -1 & 1 \\ 1 & -1 & -1 & 1 & -1 & 1 & 1 & -1 \\ 1 & -1 & 1 & -1 & -1 & 1 & -1 & 1 \\ 1 & -1 & 1 & -1 & 1 & -1 & 1 & -1 \end{bmatrix} \begin{matrix} S_{ch}(0) \\ S_{ch}(1) \\ S_{ch}(2) \\ S_{ch}(3) \\ S_{ch}(4) \\ S_{ch}(5) \\ S_{ch}(6) \\ S_{ch}(7) \end{matrix} \quad (3.10)$$

where $H_{8 \times 8}$ is a Hadamard ordering and $W_{8 \times 8}$ is a Walsh ordering, and $S_{ch}(7)$ illustrates that in this row the sign has changed seven times.

Also, $S_{ch}(0)$ indicates that the signs of the matrix element remain identical. Hadamard ordering could be found by using the bit reversal (BR) of binary number A, then Gray code (G) to binary conversion, as illustrated in Table 3.1. Moreover, Figure 3.1 shows the discrete Walsh

Table 3.1: Relation between the Walsh-ordered and Hadamard-ordered Walsh functions

No	A	Bit revers of A	Gray code of bit revers	Hadamard order
0	000	000	000	0
1	001	100	111	7
2	010	010	011	3
3	011	110	100	4
4	100	001	001	1
5	101	101	110	6
6	110	011	010	2
7	111	111	101	5

function of: (a) Hadamard ordered 8 points; and (b) Walsh-ordered 8 points.

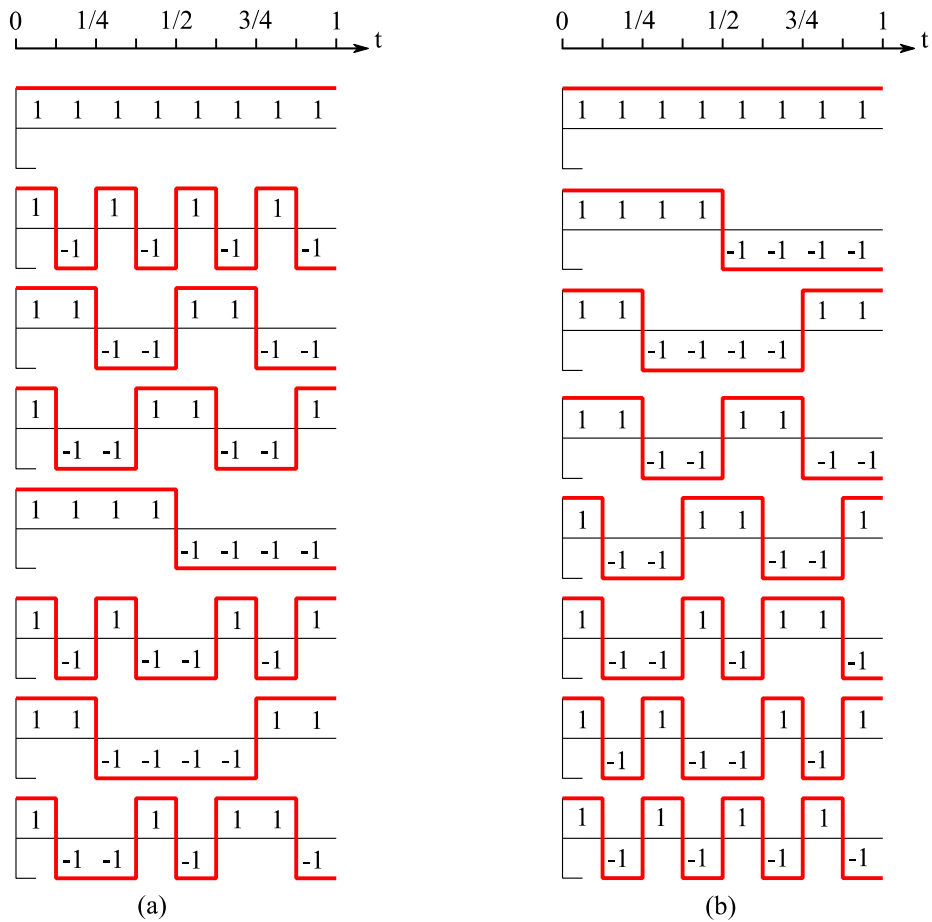


Figure 3-1: Discrete Walsh functions, $N = 8$ (a) Hadamard-ordered; (b) Walsh-ordered

As a result, combining the WHT with other transforms has piqued the attention of many researchers and has shown to be a potential contender for next generation of wireless communication systems such as DFT. The so-called (WHT-OFDM) system is introduced using orthogonal frequency division multiplexing [107]. The fast Walsh-Hadamard-Fourier transform method is also described, which combines the computation of the Walsh-Hadamard transform with the discrete Fourier transform [108].

3.3 C-transform matrix

As mentioned above, DCT and WHT are compressed into one transform, resulting in the CT in a certain way. Therefore, the CT can be presented as:

$$CT_{8 \times 8} = \frac{1}{\sqrt{N}} \left[[(DCT_{8 \times 8})^\wedge] \left[\{(WHT_{8 \times 8})^\wedge\}^T \right] \right]. \quad (3.11)$$

where $(.)^\wedge$ denotes the bit-reversed order and $(.)^T$ signifies the transpose. For clarity and without a loss of generality, a matrix 8×8 of the C-transform is shown as follows:

$$CT_{8 \times 8} = \begin{bmatrix} \mathbf{1} & 0 & 0 & 0 & 0 & 0 & 0 & 0 \\ 0 & \mathbf{1} & 0 & 0 & 0 & 0 & 0 & 0 \\ 0 & 0 & \mathbf{0.92} & \mathbf{0.38} & 0 & 0 & 0 & 0 \\ 0 & 0 & \mathbf{-0.38} & \mathbf{0.92} & 0 & 0 & 0 & 0 \\ 0 & 0 & 0 & 0 & \mathbf{0.91} & \mathbf{-0.07} & \mathbf{0.37} & \mathbf{0.18} \\ 0 & 0 & 0 & 0 & \mathbf{0.21} & \mathbf{0.77} & \mathbf{-0.51} & \mathbf{0.32} \\ 0 & 0 & 0 & 0 & \mathbf{-0.32} & \mathbf{0.51} & \mathbf{0.77} & \mathbf{0.21} \\ 0 & 0 & 0 & 0 & \mathbf{-0.18} & \mathbf{-0.37} & \mathbf{-0.07} & \mathbf{0.91} \end{bmatrix}. \quad (3.12)$$

Given that CT is a real orthonormal matrix, its inverse ICT is the same as its transpose

$$ICT = CT^T. \quad (3.13)$$

Also, for inverse C-transform, matrix 8×8 , $N = 8$, is given as:

$$ICT = \begin{bmatrix} 1 & 0 & 0 & 0 & 0 & 0 & 0 & 0 \\ 0 & 1 & 0 & 0 & 0 & 0 & 0 & 0 \\ 0 & 0 & 0.92 & -0.38 & 0 & 0 & 0 & 0 \\ 0 & 0 & 0.38 & 0.92 & 0 & 0 & 0 & 0 \\ 0 & 0 & 0 & 0 & 0.91 & 0.21 & -0.32 & -0.18 \\ 0 & 0 & 0 & 0 & -0.07 & 0.77 & 0.51 & -0.37 \\ 0 & 0 & 0 & 0 & 0.37 & -0.51 & 0.77 & -0.07 \\ 0 & 0 & 0 & 0 & 0.18 & 0.32 & 0.21 & 0.91 \end{bmatrix}. \quad (3.14)$$

where:

$$ICT * CT = I. \quad (3.15)$$

where I is the identity matrix.

Therefore, the C -transform has two significant features: the first is orthogonality, since it is the product of two orthogonal matrices; and, secondly, it has the block diagonal structure (BDS) which reduces the number of addition and multiplication operations [100, 109]. The result of having BDS is that $> 2/3$ of the matrix is zero, which leads to reduced numbers of real additions and multiplications. Moreover, the N -class matrix C -transform differs from the $N/2$ C -transform matrix only at the bottom of the diagonal block structure, as can be seen in Figure 3.2.

3.4 Computational Complexity

One important consideration in determining if a transform is appropriate for usage in real communication systems is its computational complexity. This section assesses in further detail the proposed CT's computational cost compared to the DCT, DCT-WHT, and FFT.

3.4.1 DCT Computational

The numbers of real additions R_A^{DCT} and multiplications R_M^{DCT} and total real operations C_{Total}^{DCT} are presented in Equations 3.16, 3.17 and 3.18 respectively [110].

$$R_A^{DCT} = N \log_2 N. \quad (3.16)$$

$$R_M^{DCT} = \frac{N}{2} \log_2 N. \quad (3.17)$$

$$C_{Total}^{DCT} = \frac{3}{2} N \log_2 N. \quad (3.18)$$

It is important to note that the complexity above should be computed twice when a complex constellation is employed, one of which for the real and the other for the imaginary components of the signal. The total computational complexity is then given as:

$$C_{Total}^{DCT} = 3N \log_2 N. \quad (3.19)$$

3.4.2 WHT+DCT Computational Complexity

The fast implementation of the WHT followed by the DCT has the following areas of arithmetic complexity. That of the WHT only requires real additions and no multiplications at all, as follows:

$$R_A^{WHT} = N \log_2 N. \quad (3.20)$$

Also, the previous section has presented the numbers of real additions and multiplications and the total real operations for the DCT. Therefore, the entire process of real additions and multiplication for this combination of WHT-DCT will be as follows:

$$R_A^{WHT-DCT} = R_A^{WHT} + R_A^{DCT}. \quad (3.21)$$

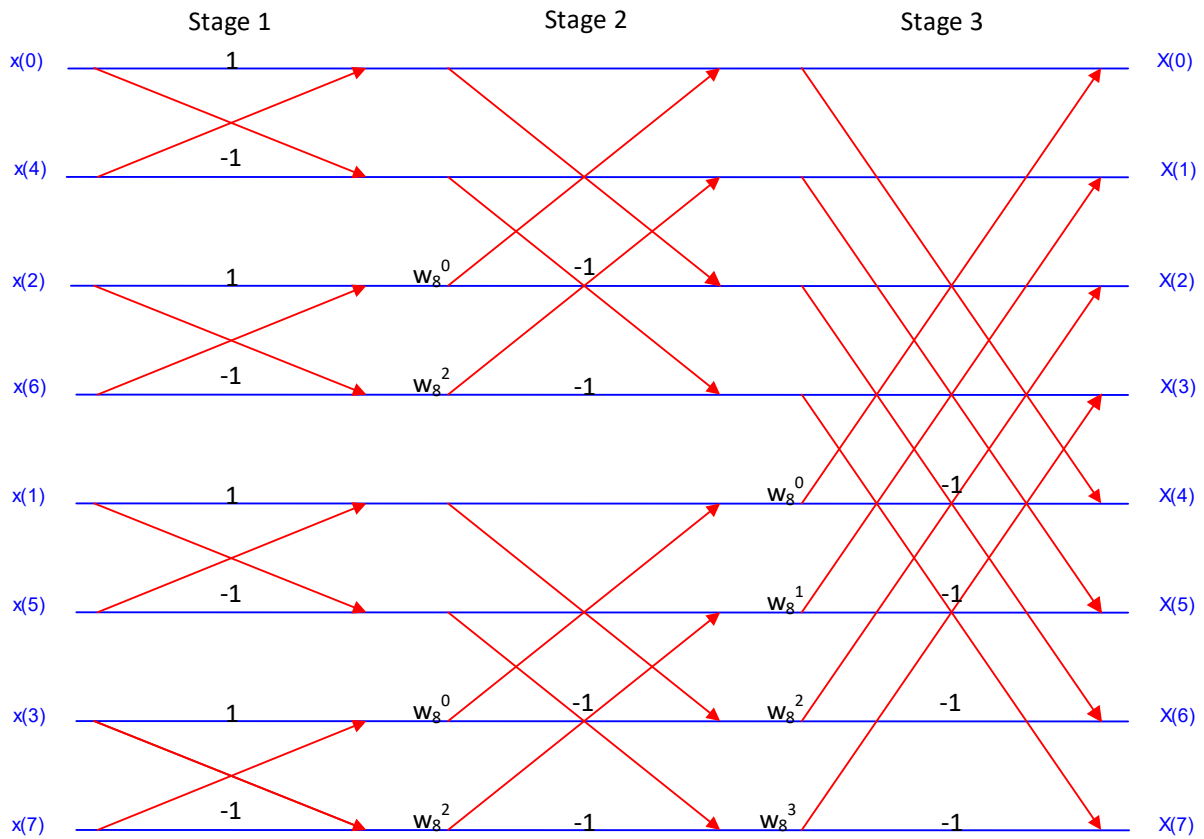
$$R_A^{WHT-DCT} = N \log_2 N + N \log_2 N = 2 N \log_2 N. \quad (3.22)$$

$$R_M^{WHT-DCT} = \frac{N}{2} \log_2 N. \quad (3.23)$$

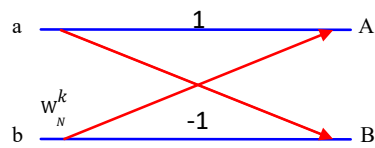
$$C_{Total}^{WHT-DCT} = R_A^{WHT-DCT} + R_M^{WHT-DCT} = 2.5 * N \log_2 N. \quad (3.24)$$

3.4.3 IFFT Computational Complexity

It is important to note that our actual comparison is with the DCT transform; however, an additional comparison with the IFFT transform is included to provide more context. According to the literature [111], an IDFT matrix needs $N(N-1)$, N^2 complex addition and multiplication operations for direct implementation. On the other hand, there are $\log_2 N$ stages and $\frac{N}{2}$ butterflies per stage according to the fast implementation shown in the structure of IFFT flowcharts in Figure 3-3 [99].



(a) 8-point 2-radix FFT butterfly flowchart



(b) DIT FFT butterfly

Figure 3-3: (a) 8-point 2-radix FFT butterfly flowchart; (b) DIT FFT butterfly.

where $w_N^k = e^{jk\theta}$ is the Twiddle factor.

As shown in Figure 3.3b, the individual butterfly is viewed in more detail as:

$$A = a + W_N^k b$$

$$B = a - W_N^k b$$

For any FFT/IFFT implementation, the total number of butterflies $Bu_{N_0}^{IFFT}$ needed to implement a size $N \times N$ matrix is:

$$Bu_{N_0}^{IFFT} = \frac{N}{2} \log_2 N. \tag{3.25}$$

There are two complex additions and one multiplication needed for a butterfly. Therefore, the overall computational complexity C_{Total}^{FFT} , the number of complex additions C_A^{IFFT} and multiplications C_M^{IFFT} are as follows:

$$C_A^{IFFT} = 2\left(\frac{N}{2} \log_2 N\right) = N \log_2 N. \quad (3.26)$$

$$C_M^{IFFT} = \frac{N}{2} \log_2 N. \quad (3.27)$$

According to previous studies [100, 112], one complex addition causes two real additions, and one complex multiplication causes three real multiplications and additions. Thus, the overall computational complexity in terms of real additions, R_A^{IFFT} , real multiplications, R_M^{IFFT} , and the total number of operations, C_{Total}^{IFFT} , is as follows:

$$R_A^{IFFT} = 2[N \log_2 N]. \quad (3.28)$$

$$R_M^{IFFT} = 3[N \log_2 N]. \quad (3.29)$$

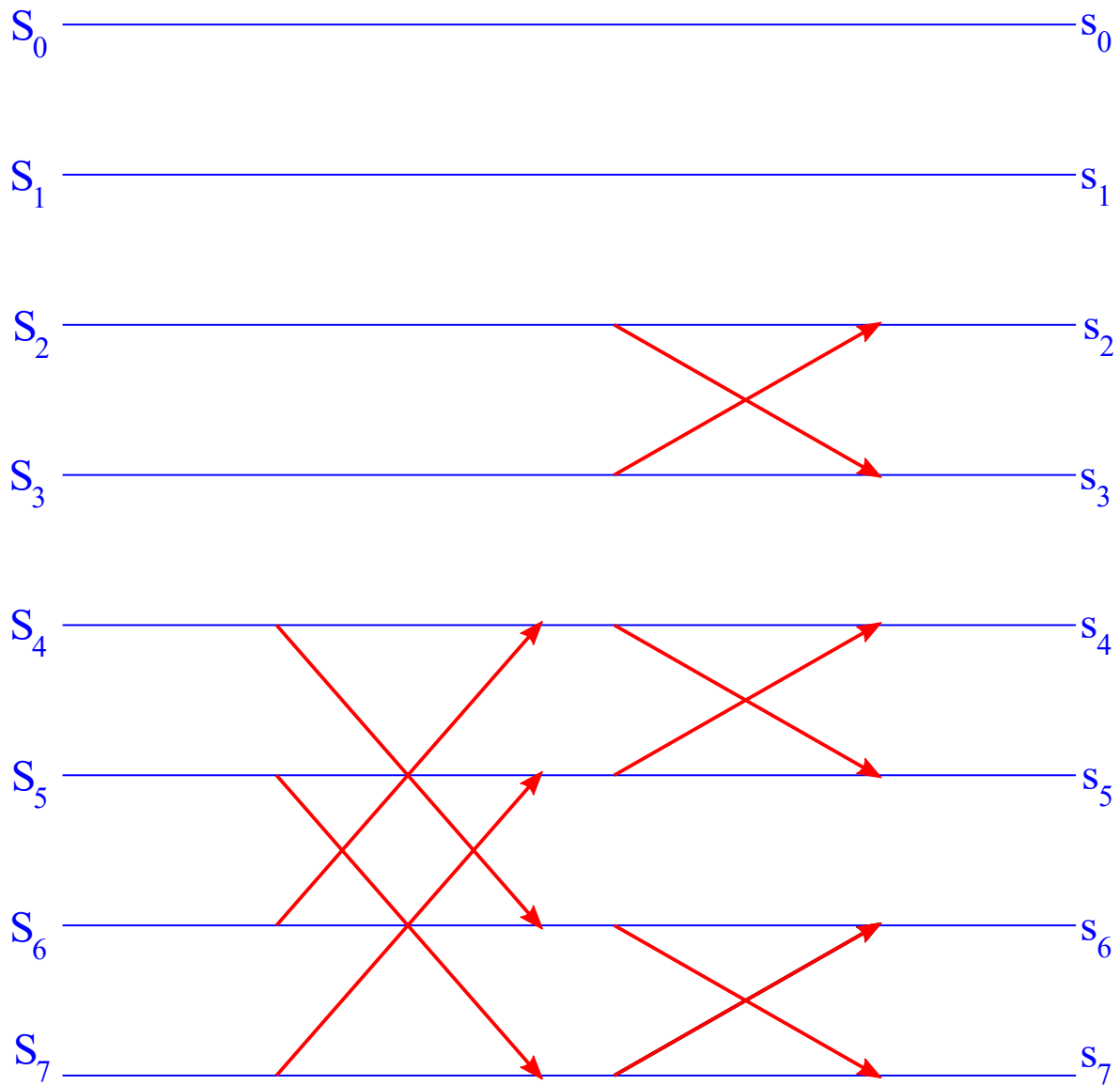
$$C_{Total}^{IFFT} = 5N \log_2 N. \quad (3.30)$$

3.4.4 CT Computational Complexity

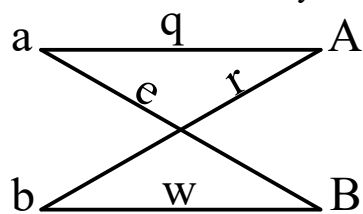
As mentioned, one of the significant features of the CT is that it has a sparse block diagonal structure, with approximately 67% of its matrix being zero. That will reduce its computation to $N^{2/3}$ and $N(N - 1)$ for real multiplication and real summation respectively [113]. Figure 3.4 depicts the BDS transform butterfly flow graph [114].

The total number of butterflies in the C-transform is equal to:

$$Bu_{No}^{C-transform} = \frac{1}{2} N \log_2 N - N + 1. \quad (3.31)$$



(a) The BDS transform butterfly.



(b) One butterfly structure.

Figure 3-4: (a) BDS transform butterfly; (b) one butterfly structure.

The individual butterfly is more thoroughly examined as shown in Figure 3.4b.

$$A = aq + br$$

$$B = bw + ae$$

Moreover, each butterfly has four multiplication and two real summations. Therefore the real multiplications $R_M^{C-transform}$ and real additions $R_A^{C-transform}$ can be calculated as [100]

$$R_M^{C-transform} = 4 Bu_{No}^{C-transform}.$$

$$R_M^{C-transform} = 4 Bu_{No}^{C-transform}.$$

$$R_M^{C-transform} = 2N \log_2 N - 4N + 4. \quad (3.32)$$

$$R_A^{C-transform} = 2 Bu_{No}^{C-transform}.$$

$$R_A^{C-transform} = 2 \left[\frac{1}{2} N \log_2 N - N + 1 \right].$$

$$R_A^{C-transform} = N \log_2 N - 2N + 2. \quad (3.33)$$

Consequently, the total computational complexity of the CT will be as follows [100]

$$C_{Total}^{C-transform} = R_M^{C-transform} + R_A^{C-transform}.$$

$$C_{Total}^{C-transform} = \frac{6}{2} N \log_2 N - 6N + 6. \quad (3.34)$$

Note that, when using complex signs, the C transformation's arithmetic operations will be double Equation 3.34. Finally, the most significant parameter used to assess computational complexity is the computational complexity reduction ratio (CCRR), which is calculated as [115]:

$$CCRR = \left(1 - \frac{C - transform}{comparing\ transform}\right) \times 100\% . \quad (3.35)$$

The real additions R_A and multiplications R_M and computational complexity for CT, DCT, DCT-WHT and FFT under different lengths of the transform N are shown in Table 3.2. It is evident that the C-transform is superior in terms of additions, and in terms of multiplications is better than the FFT. In addition, Figure 3.5 illustrates the number of additions as a function of transform length N and as can be seen, CT has the fewest additions.

Also, Table 3.3 presents the total computational complexity of the real operation of the CT compared with DCT, DCT-WHT and FFT. It is clear that the CT has the lowest computational complexity compared with the DCT-WHT and FFT. However, the computational complexity of the CT is higher than that of the DCT when $N > 16$.

Table 3.2: Real additions R_A and multiplications R_M in computational complexity for CT, DCT, DCT-WHT and FFT under different lengths of the transform N

N	C-transform		DCT		DCT-WHT		FFT	
	R_M	R_A	R_M	R_A	R_M	R_A	R_M	R_A
4	4	2	4	8	4	16	16	24
8	20	10	12	24	12	48	48	72
16	68	34	32	64	32	128	128	192
32	196	98	80	160	80	320	320	480
64	516	258	192	384	192	768	768	1152
128	1284	642	448	896	448	1792	1792	2688
256	3076	1538	1024	2048	1024	4096	4096	6144
512	7172	3586	2304	4608	2304	9216	9216	13824
1024	16388	8194	5120	10240	5120	20480	20480	30720

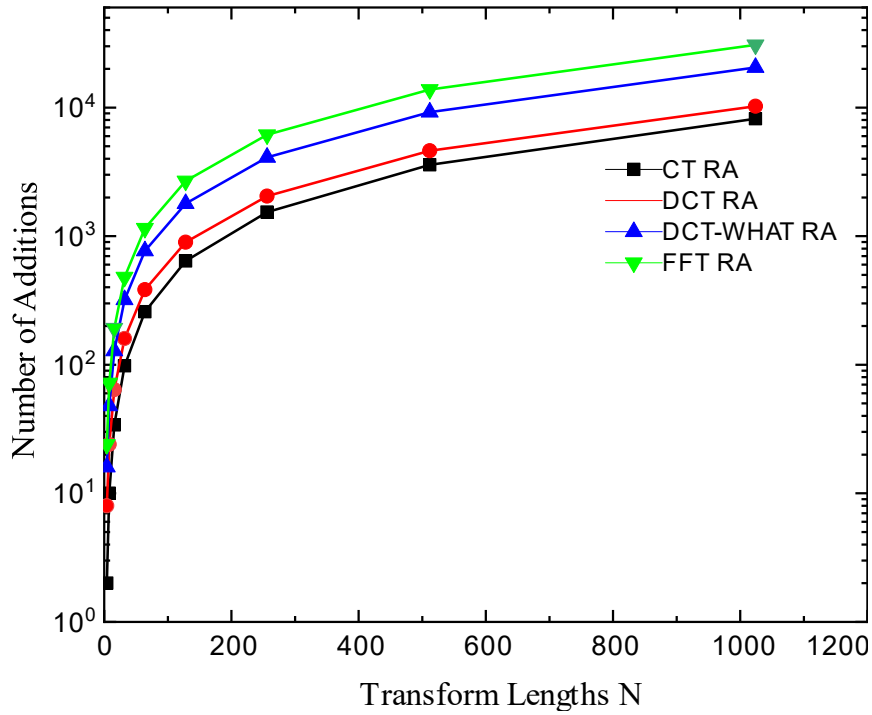


Figure 3-5: Computational cost number.

Table 3.3: Total computational complexity for CT, DCT, DCT-WHT and FFT under different lengths of the transform N

N	$C_{Total}^{C-transform}$	C_{Total}^{DCT}	$C_{Total}^{WHT-DCT}$	C_{Total}^{FFT}
4	6	12	20	40
8	30	36	60	120
16	102	96	160	320
32	294	240	400	800
64	774	576	960	1920
128	1926	1344	2240	4480
256	4614	3072	5120	10240
512	10758	6912	11520	23040
1024	24582	15360	25600	51200

For further comparison, the CCRR is given in Table 3.4, which presents the reduction in terms of computational complexity between the transforms and CCRR1, CCRR2 and CCRR3 denote the CCRR of the CT over the DCT, CT over DCT-WHT and CT over FFT respectively. The average computational complexity reduction in CT over FFT is almost 60% in general and 30% in CT over DCT-WHT. However, CCRR is slightly higher when N is greater than 16 in CT over DCT because CT combines two transfers.

Table 3.4: The computational complexity reduction ratio for CT, DCT, DCT-WHT and FFT under different lengths of the transform N

N	C_{Total}^{CT}	C_{Total}^{DCT}	CCRR1%	$C_{Total}^{WHT-DCT}$	CCRR2%	C_{Total}^{FFT}	CCRR3%
4	6	12	50.0	20	70.0	40	85.0
8	30	36	16.7	60	50.0	120	75.0
16	102	96	-6.3	160	36.3	320	68.1
32	294	240	-22.5	400	26.5	800	63.3
64	774	576	-34.4	960	19.4	1920	59.7
128	1926	1344	-43.3	2240	14.0	4480	57.0
256	4614	3072	-50.2	5120	9.9	10240	54.9
512	10758	6912	-55.6	11520	6.6	23040	53.3
1024	24582	15360	-60.0	25600	4.0	51200	52.0

3.5 Conclusion

The crucial idea of the C-transform, which will be utilised throughout the rest of this thesis, has been covered in this chapter. The discrete cosine transform (DCT) and Walsh-Hadamard transform (WHT), which are two well-known transforms that may be utilised effectively for communication systems, were highlighted in a discussion of fast transforms. Meanwhile, the C-transform combines the DCT and WHT into a single rapid orthonormal unitary transform. In addition, this chapter emphasises how the C transform's computational complexity is reduced when utilised in combination with the DCT, WHT, and FFT transforms as distinct cascaded transforms. This chapter serves as a foundation for the systems proposed in this study. In the following chapters 4, 5, and 6, the C-transform is used to address more challenging issues such as peak-to-average-power ratio (PAPR), the non-linear effect of the LED, multipath dispersion mitigation in the C-OFDM system, and complexity reductions.

Chapter 4

Performance Comparison of C-OFDM, DCO-OFDM and F-OFDM in terms of PAPR Reduction

This chapter details a comparison of three distinct orthogonal frequency division multiplexing (OFDM) formats for visible light communication in terms of peak-to-average power ratio and computational complexity. The formats under investigation include fast OFDM, standard DC-biased OFDM, and C-transform-based OFDM (C-OFDM) which combines a discrete cosine transform with a Walsh-Hadamard matrix. We look at how these systems perform when broadcast across channels with band limitations and additive white Gaussian noise.

4.1 Introduction

White light emitting diodes (LEDs) in the current solid-state lighting (SSL) infrastructure are being explored for visible light communications (VLCs) as a potential solution for future broadband networks. VLC systems offer advantages such as non-interference with radio frequency (RF) systems, no health concerns, energy efficiency, and suitability for sensitive environments like hospitals and aeroplanes. However, VLCs face bandwidth limitations due to the low-pass nature of LEDs. To overcome this, advanced modulation techniques like OFDM have been proposed. OFDM provides bandwidth efficiency and robustness against interference but suffers from a high peak-to-average power ratio (PAPR). Various PAPR reduction strategies have been suggested, but some are not directly applicable in the optical domain. Recently, the C-transform-based OFDM (C-OFDM) has been proposed to reduce PAPR significantly while maintaining BER performance, showing promise for VLC applications.

4.2 Fast OFDM

Although the set of complex exponential functions is not the only orthogonal basis that could be utilised to construct MCM technique, one set of cosine functions could be utilised as an orthogonal basis to implement the MCM system. This system could be created using a discrete cosine transform (DCT) [116]. However, F-OFDM excludes complex modulation and allows real one-dimensional modulation formats such as pulse amplitude modulation (PAM), which is an advantage in OWC utilising the IM/DD technique. However, while the signal generated by F-OFDM is still a real signal, it is not yet positive; whereas conventional OFDM generated complex signals using complex two-dimensional modulation formats such as QPSK and 16QAM [117, 118]. The commonly cited IDCT is given as follows [116]:

$$x(t) = \sqrt{\frac{2}{N}} \sum_{n=0}^{N-1} \psi_n X_n \cos \left[\frac{n\pi t}{N} \right]. \quad (4.1)$$

where X_n are the data symbols obtained from a modulation constellation, $x(t)$ is the time sample of OFDM, and ψ_n is the normalisation factor which is determined by:

$$\psi_n = \begin{cases} \frac{1}{\sqrt{2}}, & n = 0 \\ 1, & 0 < n < N - 1 \end{cases}. \quad (4.2)$$

Similarly, the IFFT is [36]

$$x(t) = \frac{1}{\sqrt{N}} \sum_{n=0}^{N-1} X_n e^{\frac{j2\pi nt}{N}}. \quad (4.3)$$

The frequency spacing between two adjacent subcarriers Δf is the difference between F-OFDM and OFDM where values of Δf are $1/(2T)$ and $1/T$ respectively [116]. Figure 4.1 illustrates the concept of F-OFDM, and it can be seen that there is a difference in frequency separation between neighbouring subcarriers for OFDM (top of Figure 4.1) and F-OFDM (bottom of Figure 4.1). It should be noted in Figure 4.1 that F-OFDM can support twice as many subcarriers as OFDM, while maintaining the existence of the orthogonality by limiting

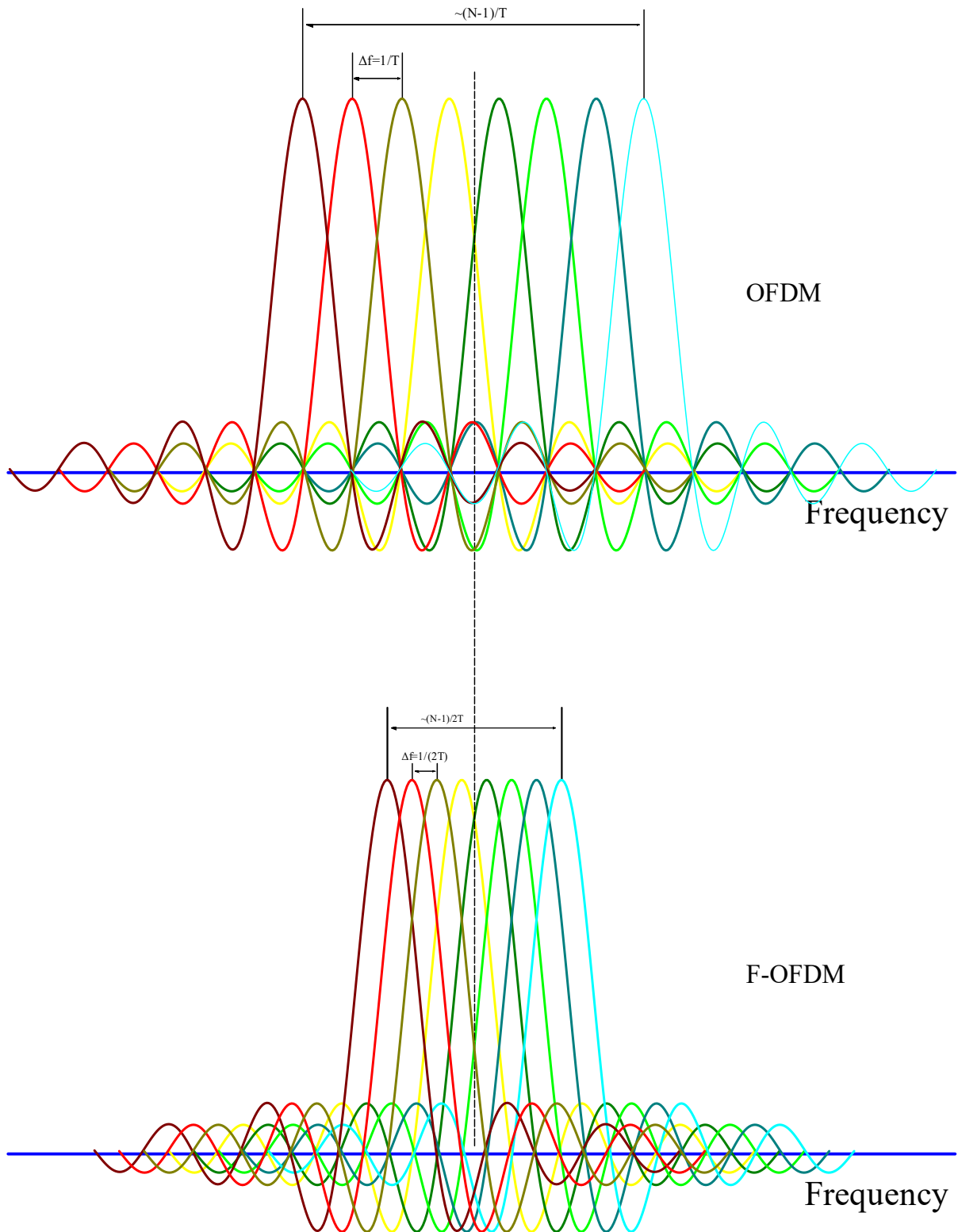


Figure 4-1: Subcarrier separation for OFDM (top) and F-OFDM (bottom),

modulation to one-dimensional formats such as BPSK or PAM. This allows the subcarrier spacing to be $1 / (2T)$, which is half the space required for OFDM at $1 / T$ [119-121]. A schematic block diagram for the F-OFDM is illustrated in Figure 4.2. There are several differences between the F-OFDM technique and the conventional OFDM system, such as the

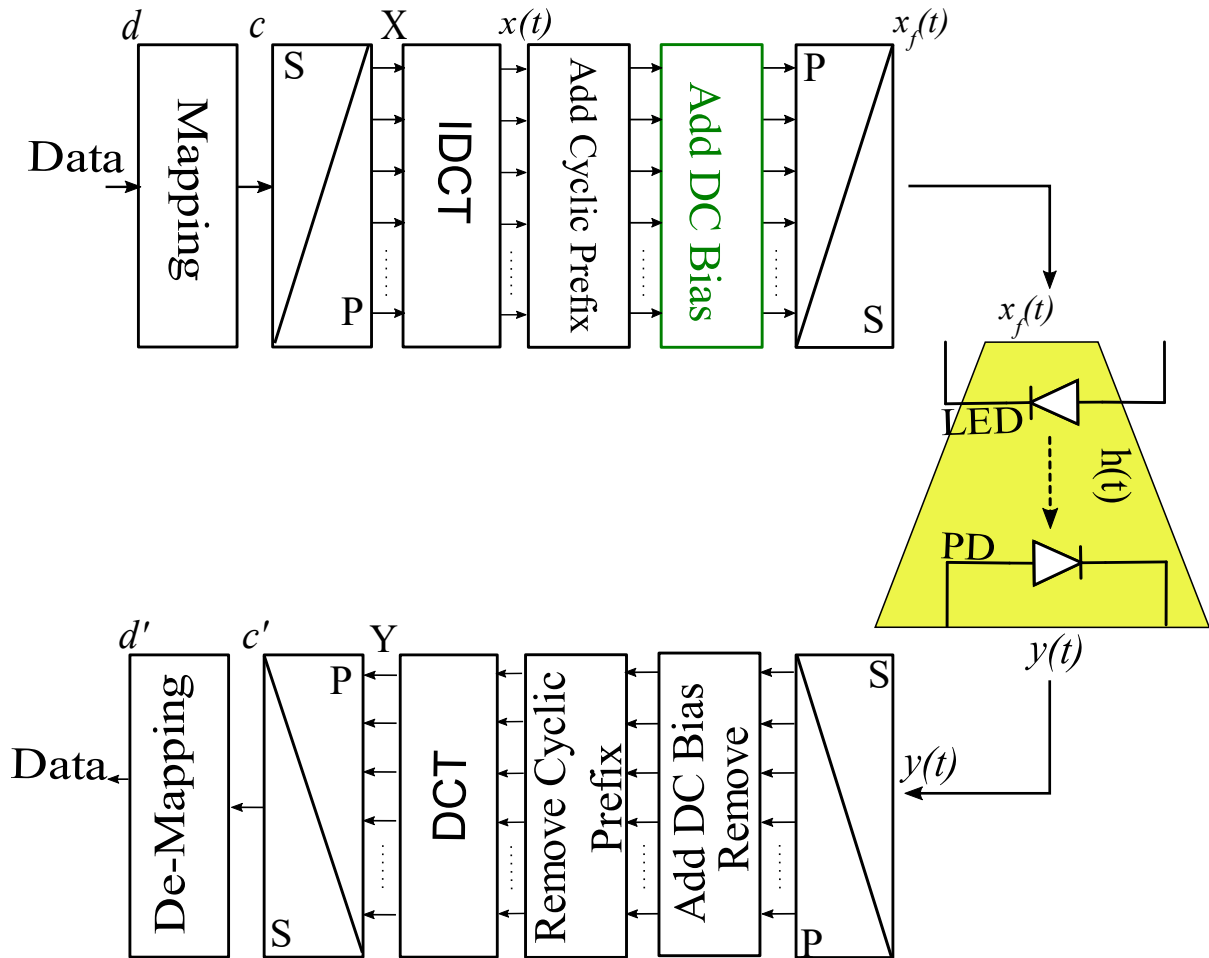


Figure 4-2: F-OFDM system.

fact that PAM, which is a 1-dimensional constellation and an IDCT, is used to generate the time domain signal for F-OFDM. In contrast, QAM, the 2-dimensional constellation and an IFFT, is used to create the time domain signal for OFDM.

4.3 PAPR Performance of OFDM Systems

As mentioned earlier, adding a large number of SCs in OFDM creates samples with extremely high peak values relative to the OFDM average power. The PAPR is the standard measure for this phenomenon, which Haas defines for discrete-time signals as [47]:

$$PAPR = \frac{\max_{0 \leq n \leq N-1} |x[n]|^2}{E[|x[n]|^2]} \quad (4.4)$$

In the case of the F-OFDM and typical OFDM the discrete-time signals are as follows:

$$x^{OFDM}(t) = \frac{1}{\sqrt{N}} \sum_{n=0}^{N-1} X_n e^{\frac{j2\pi nt}{N}}. \quad (4.5)$$

$$x^{F-OFDM}(t) = \sqrt{\frac{2}{N}} \sum_{n=0}^{N-1} \psi_n X_n \cos\left[\frac{n\pi t}{N}\right]. \quad (4.6)$$

Then $\max_{0 \leq n \leq N-1} |x[n]|^2 \leq N |X_n|_{max}^2$ and $E[|x[n]|^2] = E[|X_n|^2]$, $0 \leq n \leq N-1$. Therefore, their PAPR can be written as follows [100, 122]:

$$PAPR \leq N \frac{|X_n|_{max}^2}{E[|X_n|^2]}. \quad (4.7)$$

More specifically, the addition of N data symbols is required for each output sample of size N generated by either the IDCT or IFFT operations. On the other hand, the proposed C-OFDM system does not operate in this manner. This is because each N output sample from the ICT operation includes less than or equal to the total of half of the data symbols (N) since the C-transform has a block diagonal structure. As a result, the PAPR for the C-OFDM technique scenario may be as follows [100]:

$$PAPR^{C-OFDM} \leq \frac{N}{2} \frac{|X_n|_{max}^2}{E[|X_n|]}. \quad (4.8)$$

Therefore, the worst-case scenario for PAPR in the traditional OFDM and F-OFDM schemes is of the order of N; however, in the new optical C-OFDM it is N/2.

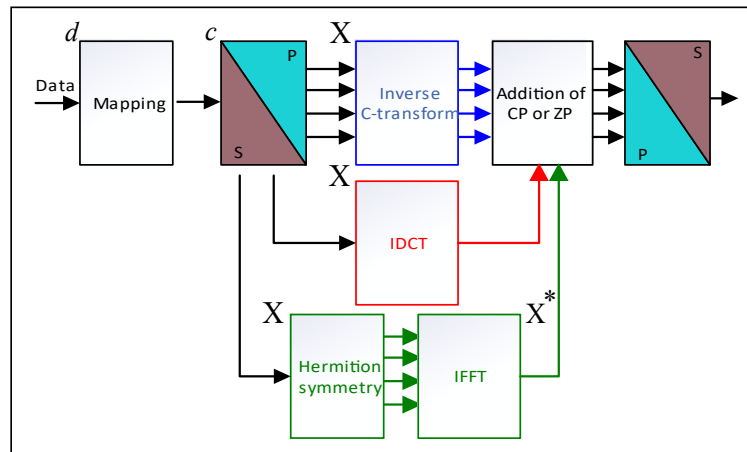
4.4 VLC Applications of the Proposed Schemes.

In this section, the proposed C-OFDM system performance in terms of PAPR and BER is examined as an example of a VLC system, together with that of F-OFDM and the traditional OFDM systems.

4.4.1 Test Set-up

On the transmitter side, block diagrams for each of the OFDM systems tested are presented in Figure 4.3. Data d is mapped onto the modulation alphabet, which must be purely real for DCT and C-transform-based OFDM systems. Therefore, we modulate C-OFDM and fast-OFDM

Transmitter



Receiver

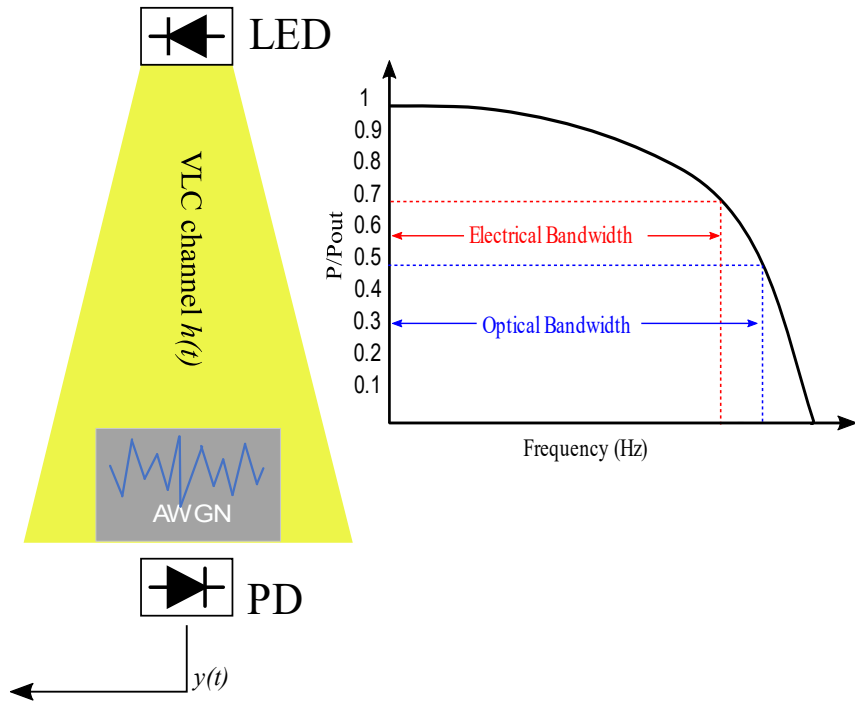
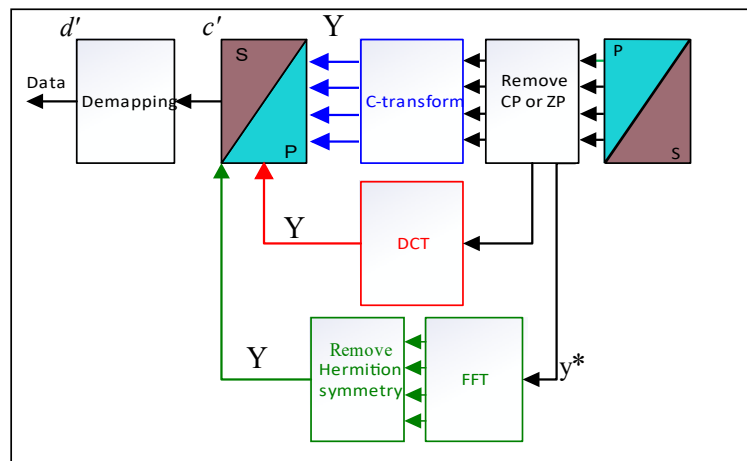


Figure 4-3: System block diagram

(F-OFDM) with pulse amplitude modulation (PAM) and conventional OFDM with quadrature amplitude modulation (QAM). The number of bits-per-symbol is set at $k_{PAM} = \frac{k_{QAM}}{2}$ so as to maintain spectral efficiency taking Hermitian symmetry requirements into account plus the fact that the DCT transform separates subcarriers by $d_f = \frac{1}{2T}$ [43, 119]. The data c is then passed through a serial-to-parallel converter for every system before either: (a) the inverse C-transform in the case of C-OFDM in blue; or (b) transformation by the IDCT is applied in the case of fast OFDM (FOFDM) in red; and, finally, (c) Hermitian symmetry generation and transformation via IFFT for the case of OFDM in green given as follows [28]:

$$S_m \begin{cases} 0 & m = 0 \\ X_m & 0 < m < N/2 \\ 0 & m = N/2 \\ X_m^* & N/2 < m < N - 1 \end{cases} . \quad (4.9)$$

where S_m is the Hermitian symmetric output, X_m is the m^{th} parallel data stream and N is the number of subcarriers. Next, CP is added to the signal before parallelisation and transmission by the LED.

In the literature, the LED can be represented as a first order low-pass filter response as follows [2]:

$$HS(f) = \frac{1}{\sqrt{1 + \left(\frac{f}{f_c}\right)^2}} . \quad (4.10)$$

where HS is the LED model, f is the frequency range of the signal and f_c is the cut-off frequency. This model is adopted in the present study.

At the receiver, AWGN is added to the received data $x(t)$ before serial-to-parallel conversion and the removal of CP. Then the data is injected into either the forward C transform (C-OFDM), the DCT (F-OFDM), or the FFT (DCO-OFDM). One more step for FFT-OFDM is the removal of Hermitian symmetry. Finally, the data c' is de-mapped from the modulation alphabet. Interestingly, the C-OFDM scheme is robust against frequency selectivity due to its structure, where the WHT distributes the data over all the subcarriers in the same manner as an interleave. Thus, the performance penalties associated with deep notches in the channel response are avoided, as can similarly be observed in direct sequence spread spectrum systems.

4.4.1.1 Proposed System Theory

The outline of the C-transform is discussed in this section. Firstly, the input data is mapped onto modulation symbols $X = [X_0, X_1, X_2, \dots, X_{N-1}]$. The output of the inverse C-transform can be expressed in two steps. The first step is the Walsh-Hadamard transform H_m shown below [109]:

$$H_m = \frac{1}{\sqrt{N}} \sum_{m=0}^{N-1} X_m (-1)^{g(i,n)}. \quad (4.11)$$

where $g(i, n)$ is defined as:

$$g(i, n) = \sum_{j=0}^{N-1} m_j * n_j. \quad (4.12)$$

where $i_j * n_j$ is the j^{th} product operation of bit-by-bit for the binary number which represents the integer numbers i and n , and $N-1$ is the number of binary digits in each index. In matrix terms, H_m could be represented as follows:

$$H_m = W^{\wedge T} X_m. \quad (4.13)$$

Then the output H_m is passed through IDCT in Equation 4.1, given as:

$$C_m = DCT^{\wedge} * H_m. \quad (4.14)$$

where $(.)^{\wedge}$ denotes the bit-reversed order and $(.)^T$ signifies the transpose.

4.5 Simulation Results and Discussion

The results are considered in relation to performance in terms of complexity, BER and PAPR, comparing C-OFDM against conventional and fast OFDM. It is worth mentioning that the signal bandwidth of the proposed scheme is half of that of conventional OFDM due to the subcarrier spacing being reduced by half by the DCT.

4.5.1 PAPR Reduction

The high PAPR is one of the significant disadvantages of the OFDM technique and it is caused by the periodic constructive superposition of the SCs. The PAPR can cause a degradation in

BER due to SNR limitations, reducing the performance of OFDM systems. However, several techniques have been applied to reduce the effect of the PAPR in OFDM systems, albeit with a high cost in terms of complexity and reduced data rates and/or increased BER. The PAPR is given in Equation 4.4.

It was found through simulation that C-OFDM had the lowest PAPR for a variable number of subcarriers ($N = 16$, and 64), for 16-QAM and 4 PAM modulations, compared to conventional OFDM and DCT-OFDM. The Complementary Cumulative Distribution Function (CCDF) has been used in determining the probability that a given OFDM time-domain symbol's PAPR will be greater than a present threshold $PAPR_0$ as follows:

$$CCDF = Pr = (PAPR > PAPR_0). \quad (4.15)$$

In Figure 4.4 the CCDF has been plotted in order to gain knowledge of and an intuitive understanding of the PAPR statistics.

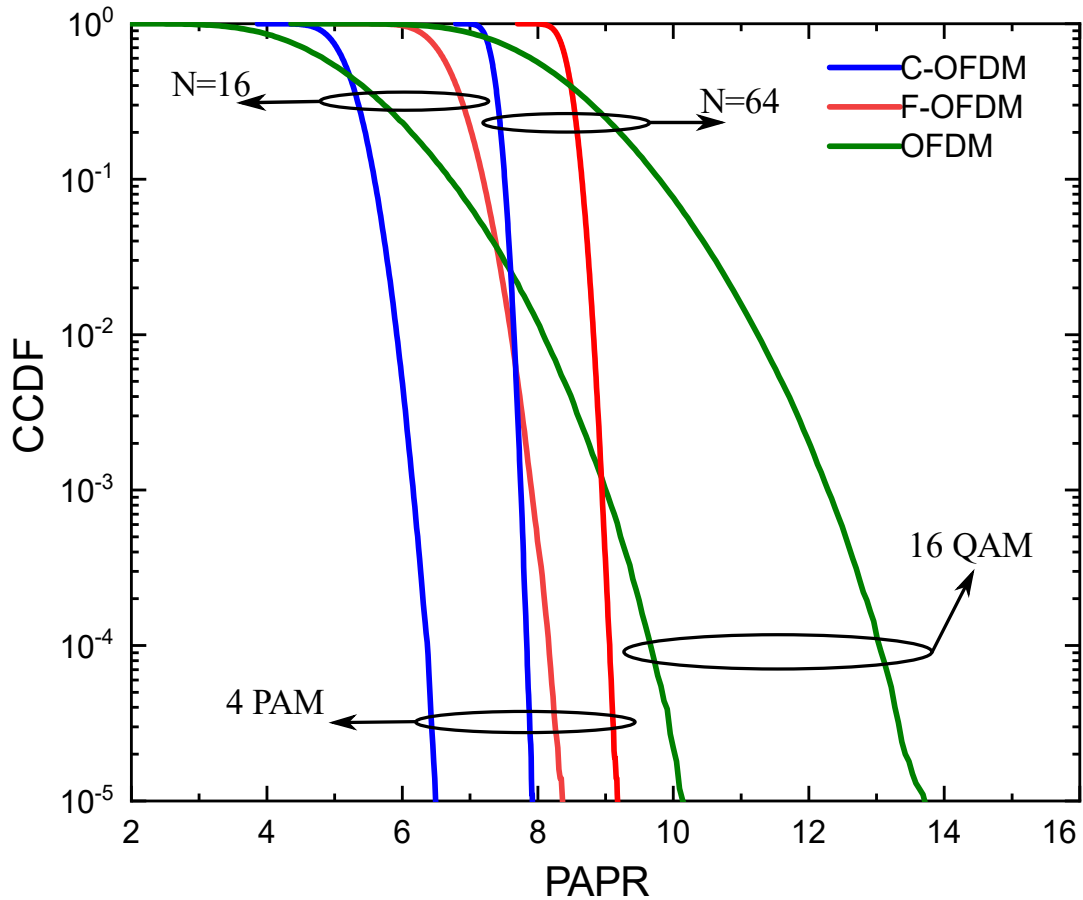


Figure 4-4: PAPR performance of the proposed system, F-OFDM, and OFDM.

Simulation results shown in Figure 4.4 for the C-OFDM, F-OFDM and OFDM systems indicate that C-OFDM achieves the lowest PAPR for values of N of 16 and 64. Two reductions of $\cong 2$ dB and 5dB PAPR are performed relative to F-OFDM and OFDM. This is because BDS reduces the likelihood of the constructive superposition of the input samples. Also, Figure 4.4 shows that the F-OFDM system achieved about 2 dB improvement at CCDF 10^{-5} . Also, Figure 4.5 indicates that the PAPR for C-OFDM is lower compared to F-OFDM and OFDM across the range of SCs. The reason for the increase in the PAPR with greater numbers of subcarriers is that the superposition principle increases the alignment and addition of cosine and sine at the output of the transforms. Whereas C-OFDM and F-OFDM have less PAPR than OFDM for the entire range of subcarriers since only the cosine signal is involved in the power signal.

Furthermore, the C-transform plays a more significant part in reducing the PAPR compared to F-OFDM due to its specific features. A signal with less PAPR is clearly useful for communication systems because of the limitations caused by the transmitters' non-linearity.

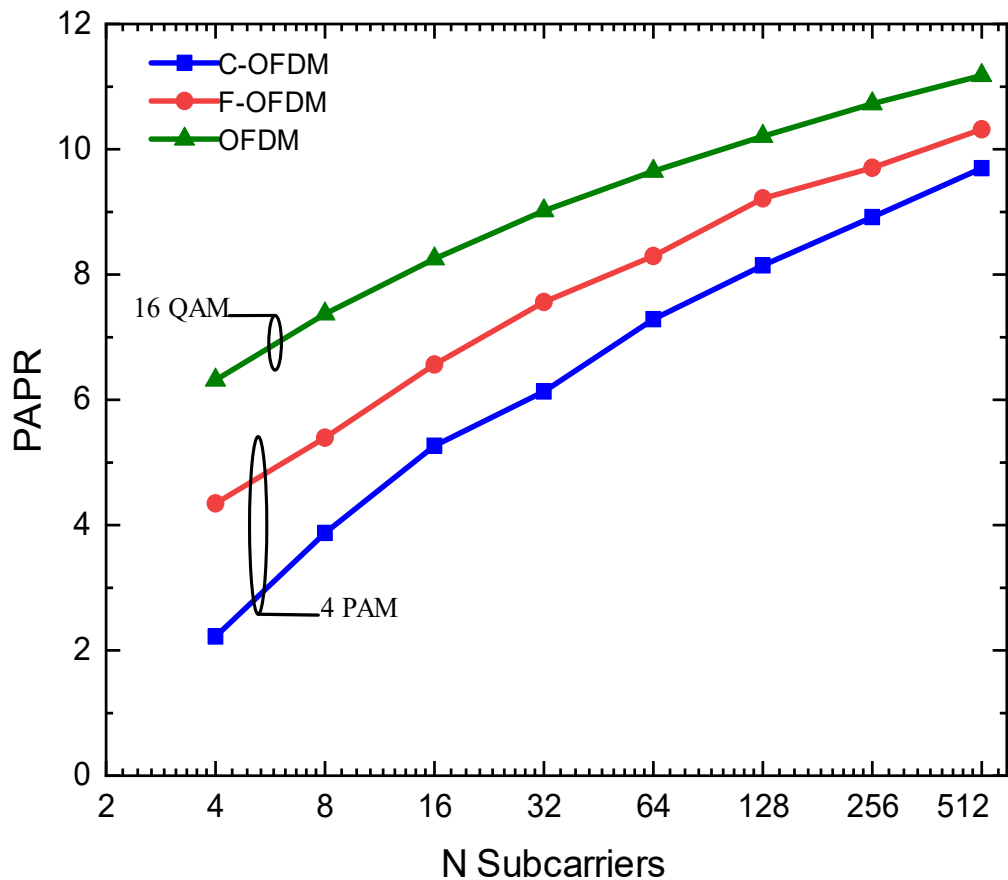


Figure 4-5: Measured PAPR for C-OFDM, F-OFDM and OFDM.

4.5.2 BER Performance

In this section a comparative study of BER performance as a function of E_b/N_0 for the proposed C-OFDM, F-OFDM and conventional OFDM is carried out over AWGN and bandwidth limitation channels.

4.5.2.1 BER Performance over AWGN Channel

Figure 4.6 shows the BER performance of C-OFDM, F-OFDM and conventional OFDM systems on the AWGN channel. It is noticeable that all three OFDM techniques, C-OFDM, F-OFDM and typical OFDM, have identical BER performance for M-PAM and M-QAM. The BER performance of the proposed method satisfies Shannon's theory when an AWGN channel is considered, as expected. This is because the WHT does not affect the AWGN noise power as it is already evenly distributed among all subchannels. Additionally, the WHT has not affected the signal strength since it is a unit transformation.

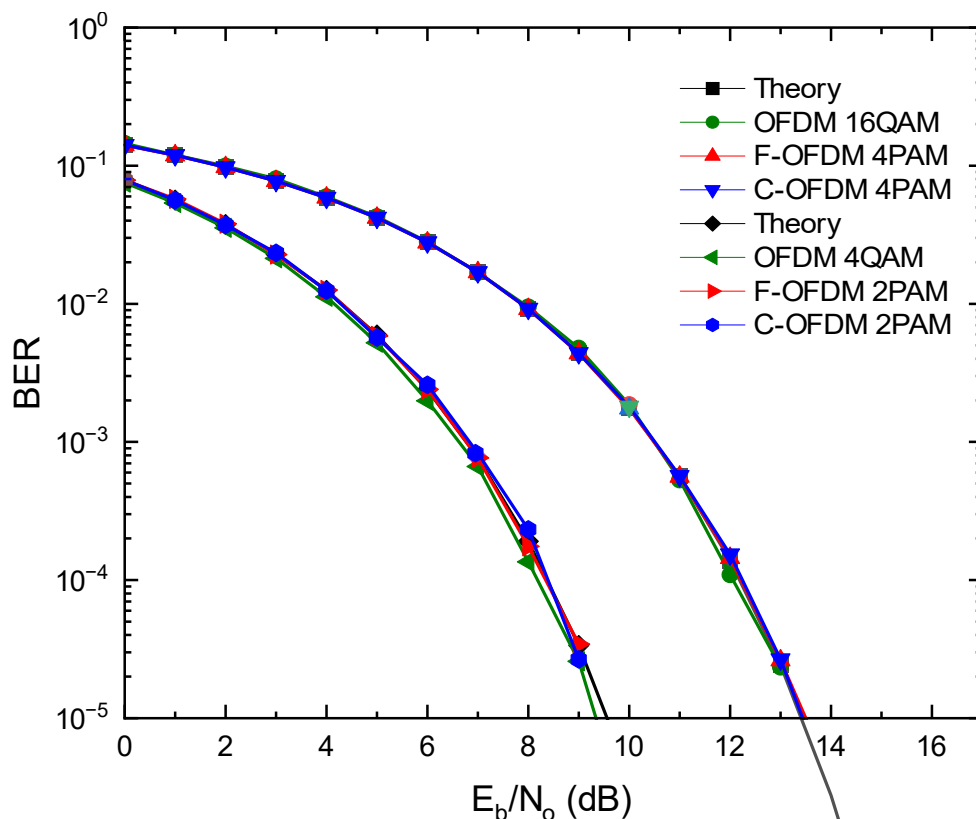


Figure 4-6: BER performance as a function of E_b/N_0 for C-OFDM, F-OFDM with 2-PAM, and OFDM with 4-QAM across AWGN channel.

4.5.2.2 BER Performance under the Influence of the Bandwidth Limitation of the LED.

However, it is unclear how the system will perform under the influence of the bandwidth limitation of the LED. Therefore, we set the bandwidth of the LED f_c to be equivalent to half the conventional OFDM signal bandwidth B in order to understand its performance. BER performance over the optical channel is illustrated in Figure 4.7 and Figure 4.8 the values of the BER performance of C-OFDM, FOFDM with 2-PAM and conventional OFDM with 4-QAM are under the same condition of band-limitation.

The proposed C-OFDM system offers an improvement of several dBs E_b/N_o for $f_c=1B$ and $0.5B$. Figure 4.8 shows the BER performance of the proposed system, F-OFDM with 4-PAM, and OFDM with 16-QAM, each of which have rather similar graphs.

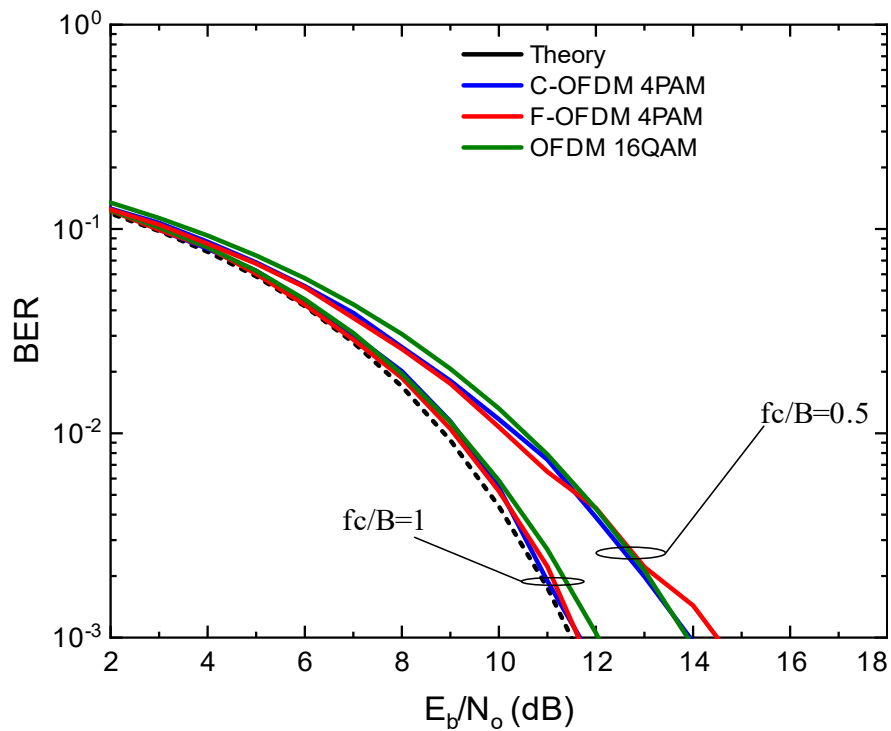


Figure 4-7: BER performance as a function of E_b/N_o for C-OFDM, F-OFDM with 2-PAM and OFDM with 16-QAM

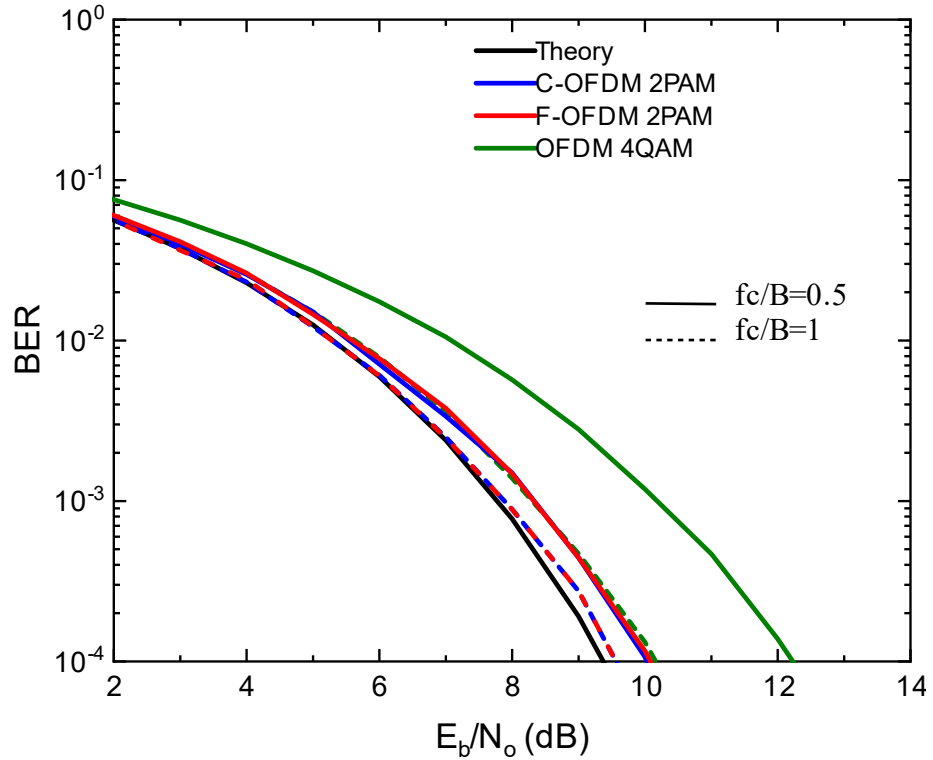


Figure 4-8: BER performance as a function of E_b/N_o for C-OFDM, F-OFDM with 2-PAM and OFDM with 4-QAM

4.5.3 Computational Complexity

In Figure 4-9 and Figure 4-10 computational complexity and CCRR are illustrated. As in the previous subsection, the computational complexity of the C-OFDM system is reduced compared to the FFT. When N is low, the reduction ratio is approximately 75%, which falls to around 50% when N is increased, as reflected by the CCRR on the right-hand axis. A noticeable reduction of between 52-75% can be observed as the number of subcarriers increases. In other words, using the C-transform reduces computational complexity compared to conventional OFDM. Figure 4.9, also shows that the C-OFDM has slightly higher computational complexity when $N > 32$ relative to FOFDM, where CCRR is F-OFDM: C-OFDM at $N \geq 16$.

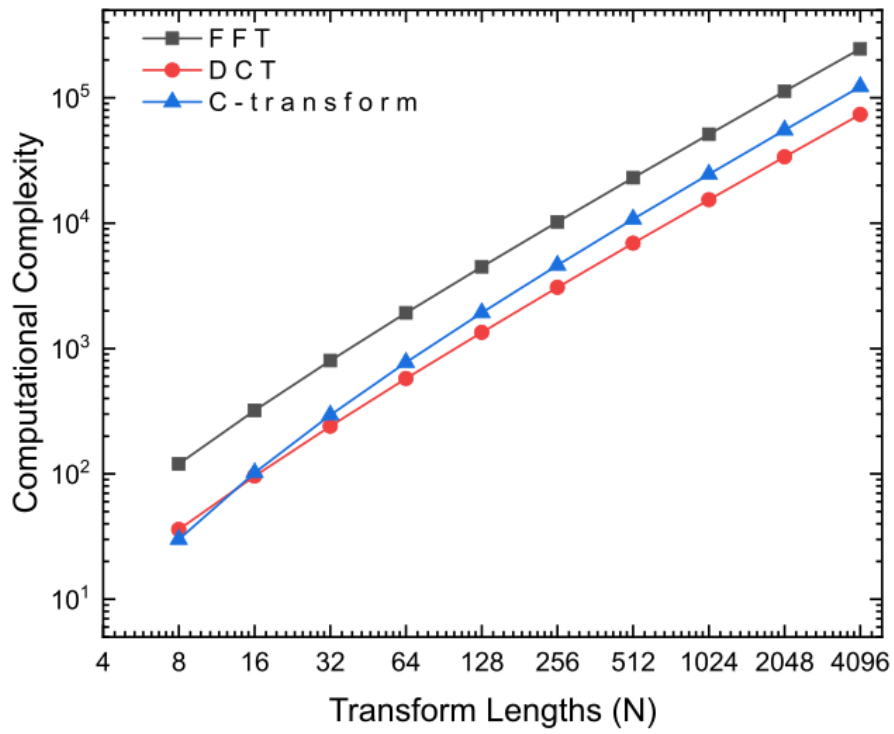


Figure 4-9: Computational complexity comparison of CT, DCT and FFT

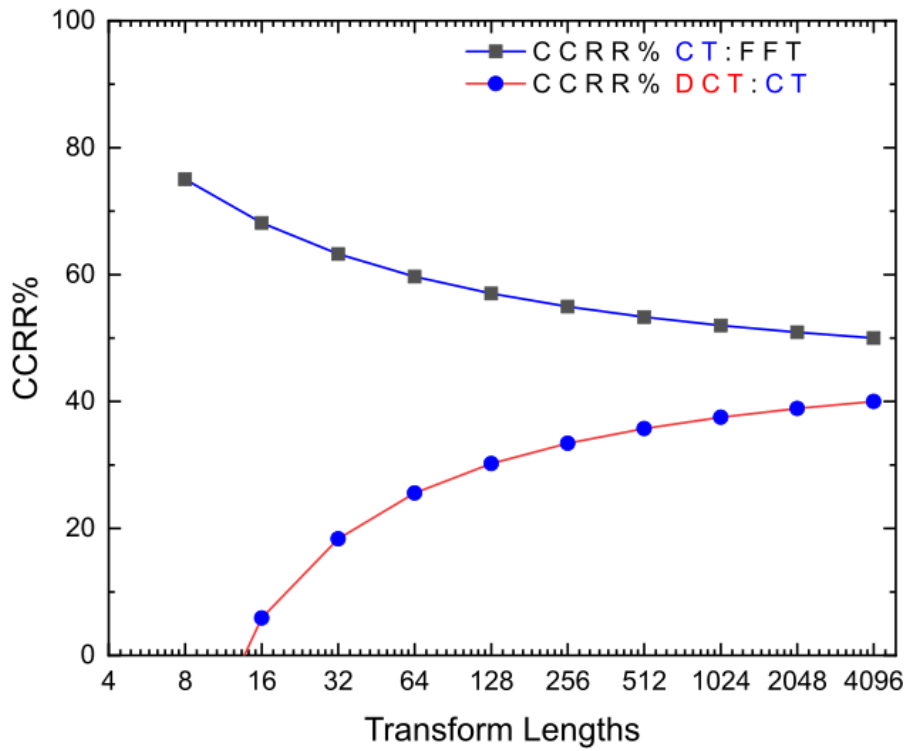


Figure 4-10: CCRR shows when N is low, the reduction ratio is approximately 75%, which falls to around 50% when N is increased comparing to FFT,

4.6 Conclusion

In this chapter, a novel OFDM scheme has been proposed using the C-transform, which is a combination of a DCT with a Walsh transform that leads to a block diagonal matrix. The performance of the proposed CT is investigated by comparing it with conventional and fast-OFDM variants in terms of PAPR, BER and computational complexity. The theoretical analysis of the CT indicates reduced computational complexity compared with typical OFDM. The computational complexity of the C-OFDM system is reduced by 52-75% in comparison to the FFT. Moreover, the BER over the AWGN channel has the same curve compared with that of conventional OFDM for 4- and 16-QAM.

The decrease in PAPR of the proposed C-OFDM that was discussed in this chapter is another benefit. According to simulation results, the PAPR of the transmitted signal in the case of the C-OFDM system is about 2 dB lower than that of the DCT-OFDM and $\cong 5$ dB lower than that of the DFT-OFDM systems at 10^{-4} of CCDF. This is because the C transform's block diagonal structure allows for maximal signal superposition and an addition requirement of $N/2$ rather than N as would be in the case of the DCT-OFDM and OFDM systems.

Chapter 5

LED Non-linearity Effect on VLC Utilising C-OFDM

The electro-optic output of light-emitting diodes commonly used in visible light communication systems is generally nonlinear in nature. This is particularly problematic when using advanced modulation formats such as orthogonal frequency-division multiplexing (OFDM) which have a high peak-to-average power ratio due to clipping and distortion. This chapter incorporates into the system architecture the so-called C-transform, which utilises a Walsh–Hadamard matrix in conjunction with a discrete cosine transform to deterministically spread the information and reduce the peak-to-average power ratio (PAPR). Several bias points along the electro-optic transfer function were selected for comparison purposes, and the new transform was compared with more traditional formulations of OFDM.

5.1 Introduction

Nevertheless, the light-emitting diodes (LEDs) used in VLC have two key challenges. Firstly, the intrinsic low-pass nature of LEDs leads to bandwidth limitations. This has traditionally been the fundamental challenge associated with VLC [1, 25]. This challenge has mainly been overcome by using advanced modulation formats such as OFDM to deliver higher spectral efficiency [28, 34]. Digital signal processing algorithms, including equalisers and artificial neural network-based classifiers, have also pushed data rates into the Gb/s regions [32, 33]. The second major LED-based challenge relates to the non-linearity in the electro-optic transfer function (see Figure 5.1), which causes issues because the signals are intensity-modulated onto the optical power [123]. Figure 5.1 depicts the linear region with a DC bias point around 350 mA to ensure the system is working in the linear area. The solid red line in Figure 5.1 shows the measurement curve between the injected current and the output optical

power of LED. Also, the dashed lines are different linearised fitting functions of the LED. The relationship between the optical power output and the forward current is non-linear because of the way LEDs are built. Therefore, linearising the non-linear area of the LED and using PAPR reduction methods are two ways to overcome the non-linearities of LEDs.

Predistortion has been proposed as one method for linearising the relationship between the output optical power and the forward current [122]. On the other hand, this method needs a precise model to construct pre-distortion and linearisation across the LED dynamic range. Elgala claimed that a proposed pre-distorter model is valid for all LEDs [123]; however, it has been reported that a “polynomial model is employed to describe the non-linear transfer function of the optical sources from which a predistortion function can be designed to linearise the non-linear region. The problem encountered while using the predistortion technique is that the non-linear transfer function of the optical sources can change due to many reasons, one of which is the temperature of the transmitter” [94], where a percentage of the energy from LED is lost as heat. Consequently, the device’s temperature is raised, which alters the non-linear relationship

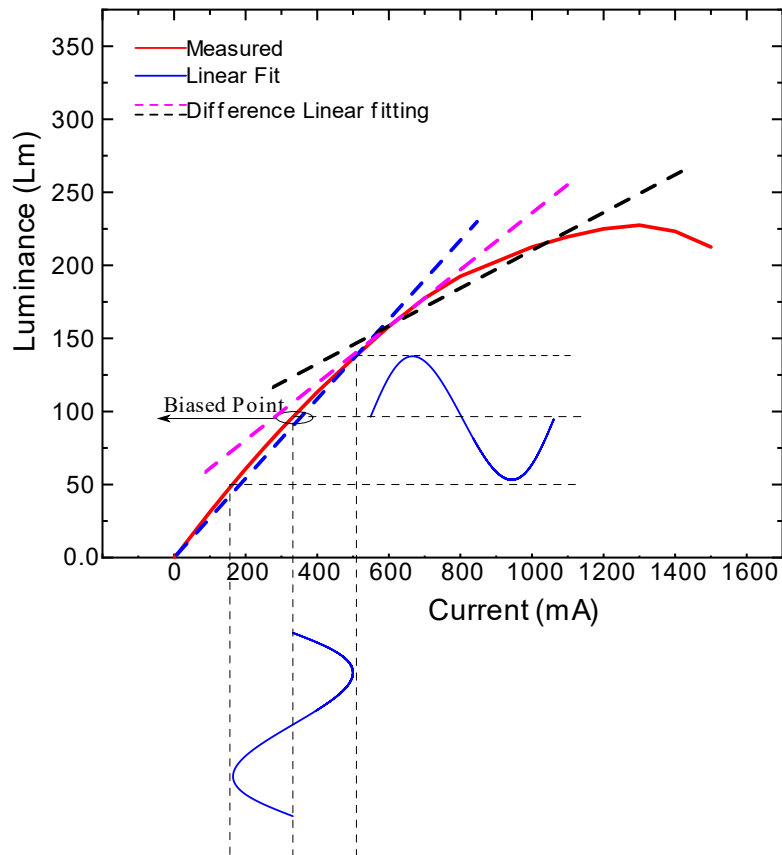


Figure 5-1: Non-linear LED transfer function[2].

between optical power output and forward current. Therefore, the predistortion function is insufficient to preserve the device's linearity. As a result, this situation necessitates the use of dynamic feedback to change the LEDs' instantaneous non-linear transfer function [37].

PAPR reduction is another way to overcome the non-linearity issue of LEDs. Clipping, coding, selected mapping (SLM), the partial transmit sequence (PTS), tone reservation (TR), tone injection (TI) and other techniques may be applied to solve the PAPR issue in conventional radio frequency (RF) communication systems, as summarised elsewhere [122, 124]. In the RF domain, power amplifiers introduce a nonlinear distortion. Furthermore, DC-biased OFDM requires a high bias to avoid low-end clipping, which significantly degrades the system's power efficiency. Consequently, reducing the PAPR in the VLC OFDM technique is even more important. In asymmetrically clipped OFDM, subcarrier mapping is utilised to guarantee positive OFDM signals. Therefore, traditional PAPR reduction approaches may not be suitable [125]. A pilot-assisted PAPR reduction technique has been proposed [126, 127] which achieves better PAPR efficiency than SLM. However, depending on the density of pilot symbols, the pilot-assisted approach causes some loss in data rates. Meanwhile a significant PAPR reduction was achieved via a proposed exponential nonlinear commanding algorithm [128] and this technique reduced PAPR significantly although it also entailed a high bit-error rate (BER).

The relationship between the current, optical power and forward voltage is illustrated in Figure 5.2. The green dashed curve shows the relationship between the LED's current and voltage from 2.4 V to 3 V on the right-hand side. Thus, the amplitude of signals transmitted below 2.4 V and above 3 V will be clipped. The LEDs have a turn-on voltage (TOV) which is the minimal threshold value and marks the beginning of the current flow and light emission, as seen in Figure 5.2. The LED is in a cut-off area at voltages below the TOV, meaning that there is no current flow. Above the TOV, however, the LED has current flow, and the voltage grows exponentially with optical power. LEDs produce light in a linear relationship to the driving current, but the efficiency of electrical-to-optical (E/O) conversion is reduced due to thermal factors. It is crucial to consider these factors, since they may cause a decline in the LED's optical power which finally reaches a steady-state value. Therefore, it is necessary to appropriately control the DC and AC currents in order to prevent the deterioration of output illumination or, in the worst possible case, the complete failure of the LED chip [129]. Therefore, the clipping of lower and upper peaks below and above the TOV is required for the time domain signal before LED modulation so as to avoid overheating it. Moreover, the solid red curve in Figure 5.2 demonstrates the linearised forward current, I , and the luminance

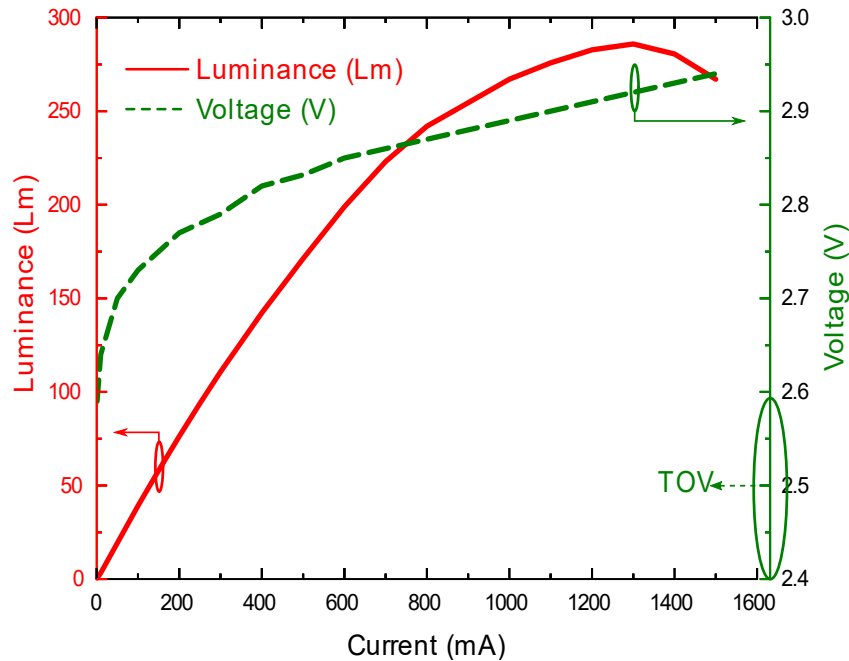


Figure 5-2: The measured L-I-V curves of the LED.

relationship on the left-hand side.

Figure 5.3 illustrates all of the measurement data for the LED as follows. Figure 5.3 (a) demonstrates the LED's voltage, V_{LED} , with the forward current, I_{LED} , using the range from 2.55 V to 2.95 V to obtain the equivalent amounts of the forward current, and Figure 5.3 (b) uses a current range from 0 to 1.6 A to derive the corresponding values of voltage. Similarly, Figure 5.3 (c) explains the connection between the optical power output of the LED and the LED voltage in the range from 2.55 V to 2.95 V, and Figure 5.3 (d) depicts the non-linearity of the forward current, I_{LED} Ma, for the range from 0 mA to 1.6 mA.

As a result, due to the non-linear properties of LEDs, the optical time domain signal transmitted in OFDM could be limited to a particular range. Due to the solid dynamic power excursion caused by the high PAPR of optical OFDM signals, the energy efficiency of both transmitting and receiving sides is negatively impacted. As a result, the LED transmitter clips the optical OFDM signal with a high PAPR, leading to significant distortion in the transmitted signal. This scenario is highly undesirable since it considerably worsens the system's overall performance and raises distortion levels in the time-domain signal which is sent. Thus, different OFDM schemes were tested, namely: conventional DC-biased OFDM, F-OFDM and C-OFDM. To compare these systems, the DC bias and peak-to-peak AC signal amplitude were varied to

understand the impact of the electro-optic non-linearity of the LED on the BER performance of the optical OFDM architectures whilst also considering the PAPR.

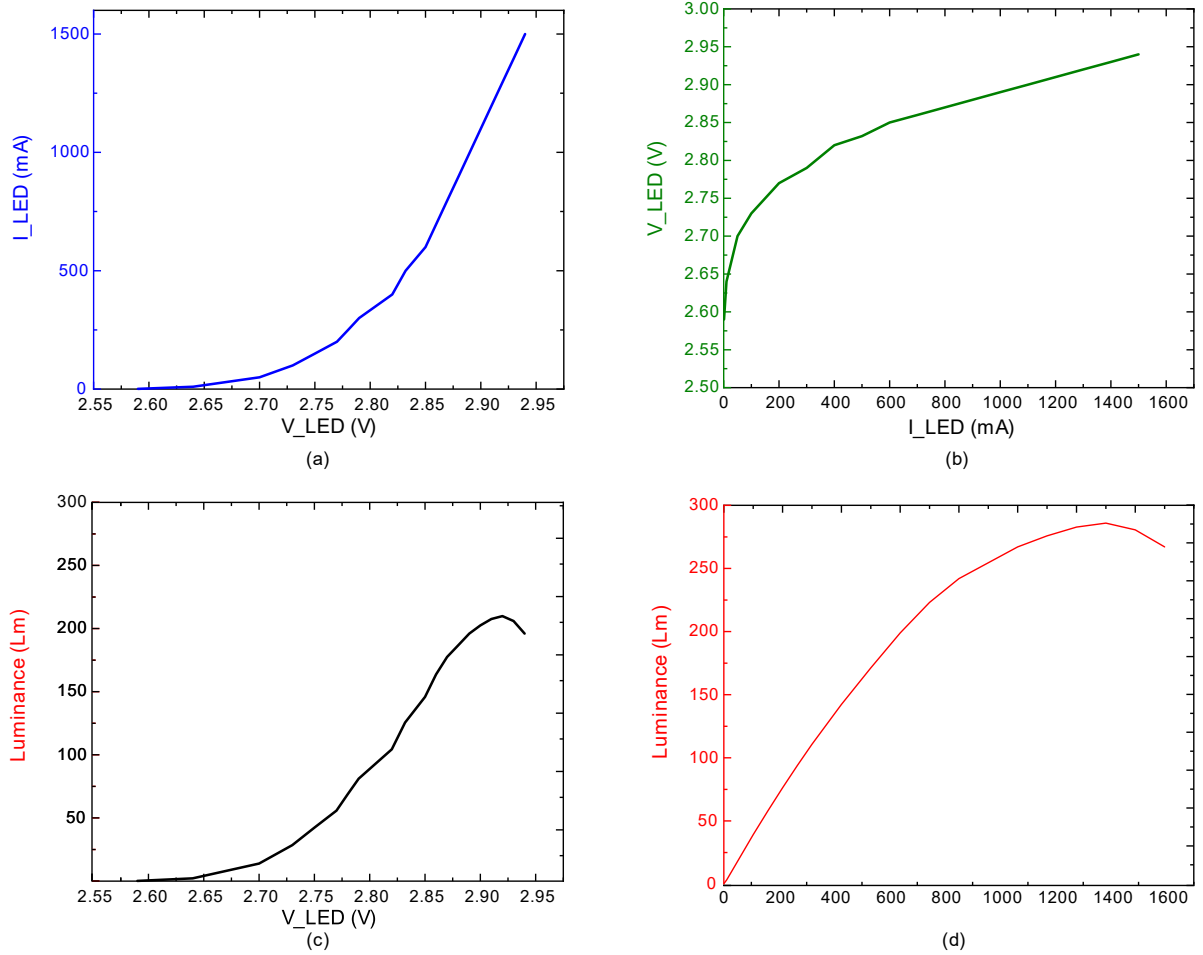


Figure 5-3: LED measurement data (a) V-I curve; (b) I-V curve; (c) V-L curve; (d) I-L curve.

5.2 OFDM Systems Model

A schematic block diagram of each OFDM system tested is shown in Figure 5.4. Firstly, the architectures were very similar, and the C-OFDM (blue) and F-OFDM (red) variations were slightly different from the conventional OFDM approach (green). The first step generates data (d) for each SC up to the SC number required (N). An independent data stream (d) was mapped onto the modulation alphabet for all systems explicitly selected for the format involved. For the F-OFDM and C-OFDM systems, a real-valued modulation format such as a pulse amplitude modulation (PAM) had to be considered because the cosine transform accepted a real input only and produced a real output. Quadrature amplitude modulation (QAM) could be utilised for the conventional OFDM system. The number of bits-per-symbol was set to $k_{PAM} = M_{QAM}/2$ in order to preserve the equivalent bit rate where $k = \log_2(M)$. Moreover, the DCT transform was spacing the subcarriers by $df = 1/(2T)$, although in IFFT the spacing between the subcarriers was $1/T$ [28, 43, 120]. Furthermore, all the subcarriers N carried the information using PAM in terms of C-OFDM and fast OFDM. On the other hand, in OFDM, $N/2$ subcarriers carried information, and $N/2$ was conjugated to obtain the real output of IFFT using QAM. It is worth mentioning that a fair comparison was performed with F-OFDM, while results for the OFDM were added for reference.

For each scheme, the data were subsequently passed through a serial-to-parallel converter (c) before the first scheme, the inverse C-transform in the case of C-OFDM or, in the second scheme IDCT was applied in the case of F-OFDM (X). Finally, Hermitian symmetry (HS) generation and transformation through IFFT in the OFDM case formulated the IFFT (X^*) output as a real-time-domain signal. HS was considered as an additional stage compared to C-OFDM and F-OFDM. The concept of HS has been explained in chapter two (sections 2.4.4 and 2.4.5). The final steps on the transmitted side are addition (by zero padding or CP) to the transmitted time domain data $x(t)$ with the effect of LED nonlinearity and parallel-to-serial conversion.

On the receiver side, prior to serial-to-parallel conversion and zero padding or CP elimination, AWGN was added to the received data $y(t)$ at the receiver. These data were subsequently injected into the forward C transform (C-OFDM), DCT (F-OFDM) or FFT (conventional OFDM) respectively. The elimination of Hermitian symmetry was an extra step in relation to FFT-OFDM. Finally, the modulation alphabet was de-mapped from the results.

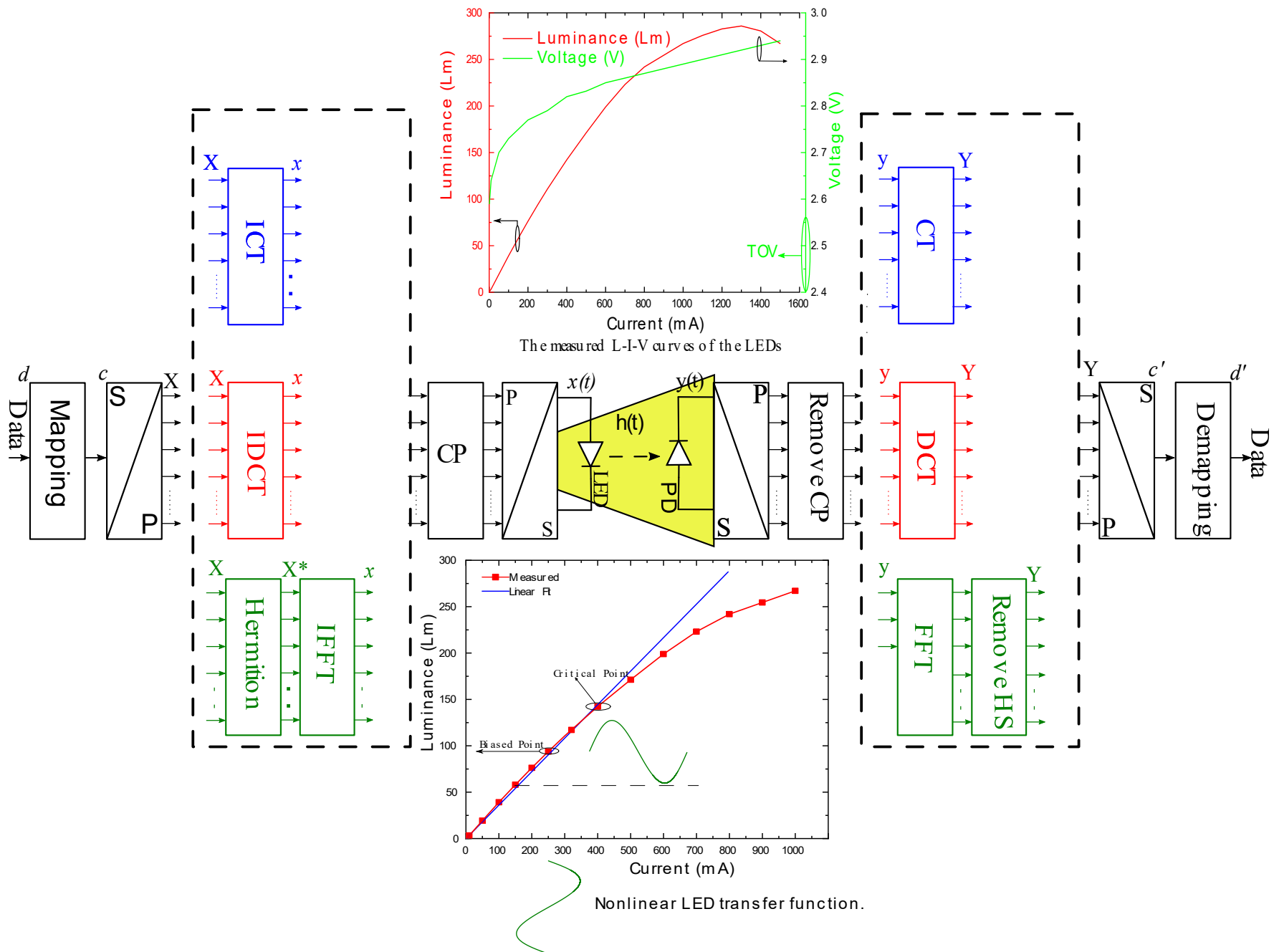


Figure 5-4: Block diagram of the OFDM schemes tested.

In this investigation, several bias points were selected along with the LED electro-optic transfer function and the AC level chosen was varied. By running the LED in a quasi-linear segment for its characteristics around the bias point selected and AC value, the BERs of the F-OFDM and C-OFDM signal were monitored to examine the distortion levels. Consequently, this resulted in a better understanding of the optimal bias conditions.

5.3 Simulation Results and Discussion

The effectiveness of the proposed technique for non-linear distortion of LED in additive white Gaussian noise channels is assessed using simulation in this section. The performance of the optical OFDM system was significantly impacted by LED non-linearity. The DC bias point was one of the critical characteristics that the distortion it led to depended on. This section considers the results regarding BER performance and the power penalty. The main comparison between C-OFDM and F-OFDM is discussed, since both use real transforms. However, the additional comparison with conventional OFDM provides greater clarification.

5.3.1 BER Performance

Figure 5.5 demonstrates the BER performance of conventional 4-QAM OFDM under the operating conditions of 200 AC and different bias points. The solid black curve represents the theoretical curve for BER performance in all the following figures. From Figure 5.5, it can be observed that the BER managed to meet the designated BER target of 10^{-4} at $E_b/N_o \sim 20$ dB when the bias point was 100 mA. However, when the DC bias point is more than 100 mA the BER target was not achieved. Moreover, Figure 5.6 illustrates the BER performance of 2-PAM F-OFDM. It shows a slight improvement and the BER target was met at $E_b/N_o < 10$ dB when the DC bias was equal to 500 mA or less. Nevertheless, the 2PAM fast OFDM failed to meet the BER 10^{-4} target when the DC bias was greater than 500 mA. On the other hand, Figure 5.7 illustrates the BER performance of 2-PAM C-OFDM under the same operating conditions of the DC bias point. An improvement in the BER is shown in this figure when using C-OFDM. An improvement in the BER could be observed in contrast to the OFDM, F-OFDM and C-OFDM results in Figure 5.5 and Figure 5.6 respectively.

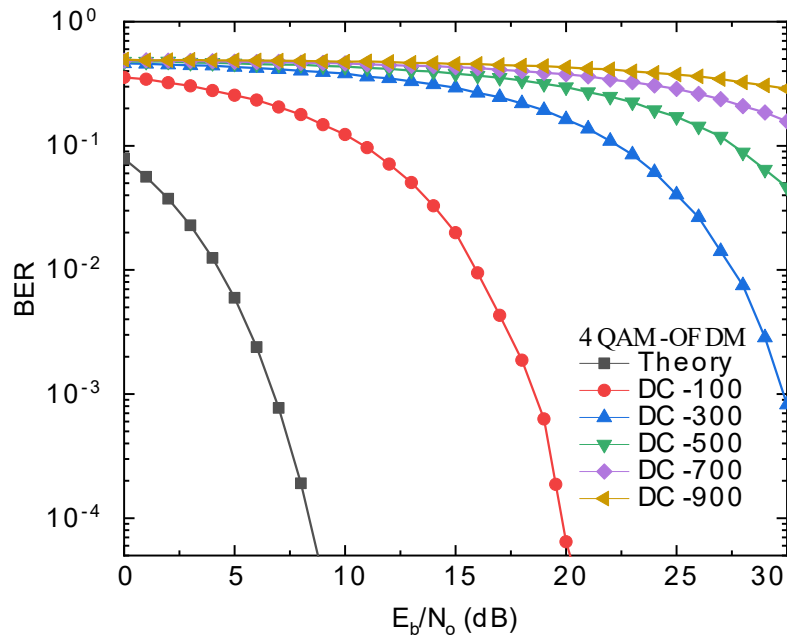


Figure 5-5: BER performance as a function of E_b/N_0 for OFDM with 4-QAM and 200 AC.

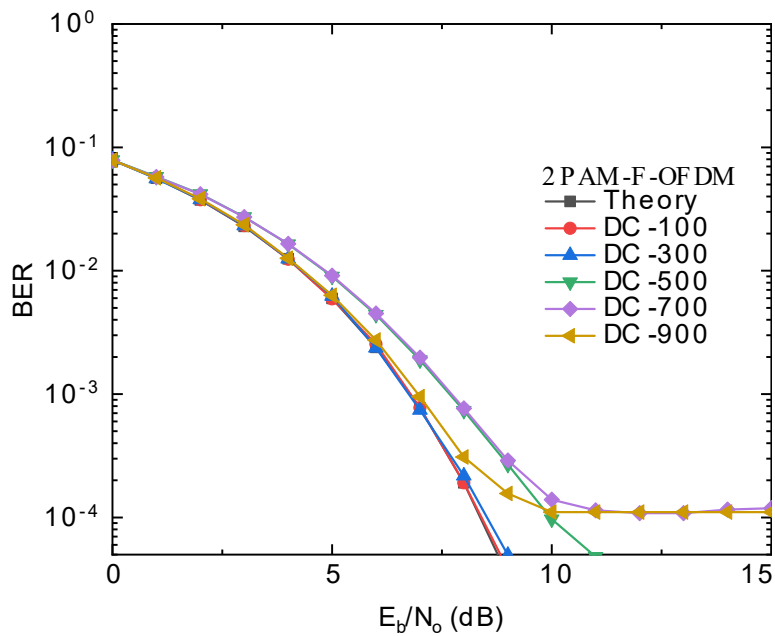


Figure 5-6: BER performance as a function of E_b/N_0 for F-OFDM with 2-PAM and 200 AC.

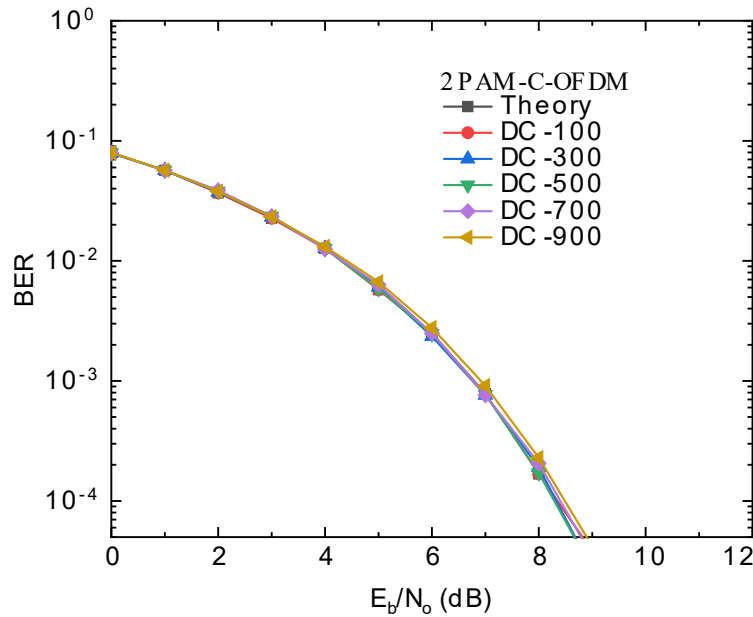


Figure 5-7: BER performance as a function of E_b/N_0 for C-OFDM with 2-PAM and 200 AC

The 16-QAM OFDM BER performance is depicted in Figure 5.8, which shows that the BER target was not achieved at the low E_b/N_0 value. Approximately 25 dB of energy was consumed to reach the BER target when the DC bias point was 100 mA. After increasing the DC bias point to greater than 100 mA, it was hard to achieve the BER target. Figure 5.9 shows the BER performance as a function of E_b/N_0 for F-OFDM with 4-PAM and 200 AC. In this figure, it can be noted that, for most of the different bias point values, the BER target was not achieved. However, at the BER target of 10^{-4} the BER curves between 100 and 300 DC bias could be achieved at E_b/N_0 values of 14 and 16 respectively. The BER performance of 4-PAM C-OFDM is presented in Figure 5.10, showing a significant improvement where all the BER curves managed to meet the BER target at the lowest E_b/N_0 in contrast to the results in Figure 5.9.

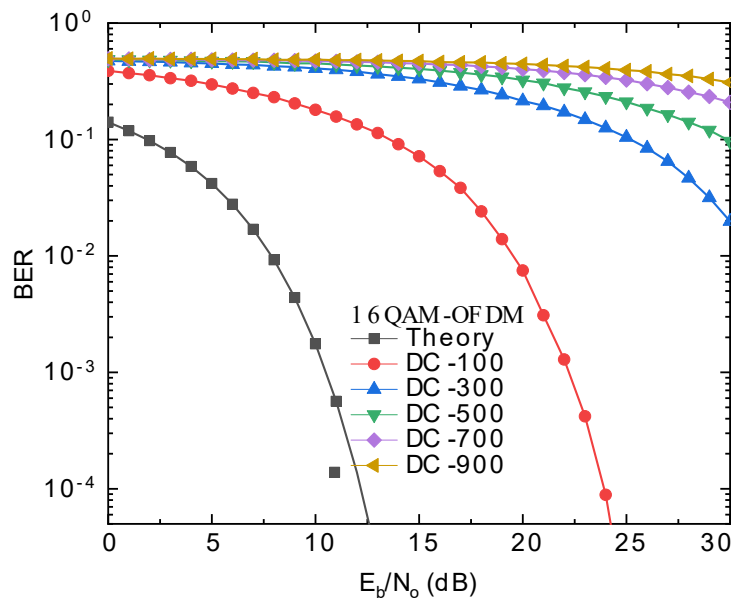


Figure 5-8: BER performance as a function of E_b/N_0 for OFDM with 16-QAM and 200 AC.

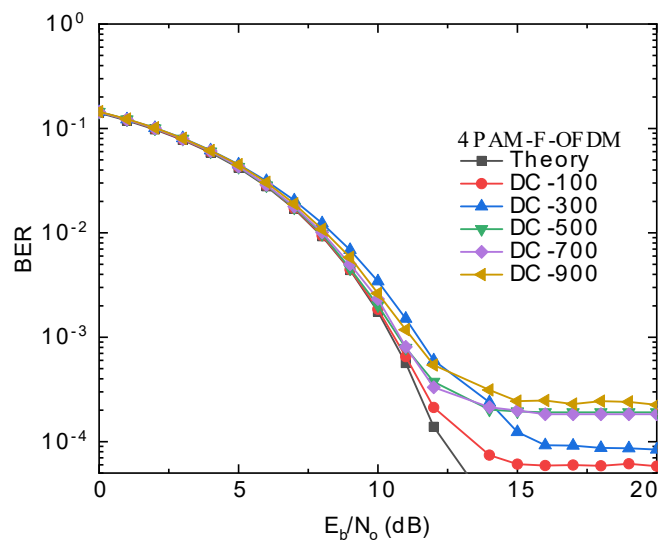


Figure 5-9: BER performance as a function of E_b/N_0 for F-OFDM with 4-PAM and 200 AC.

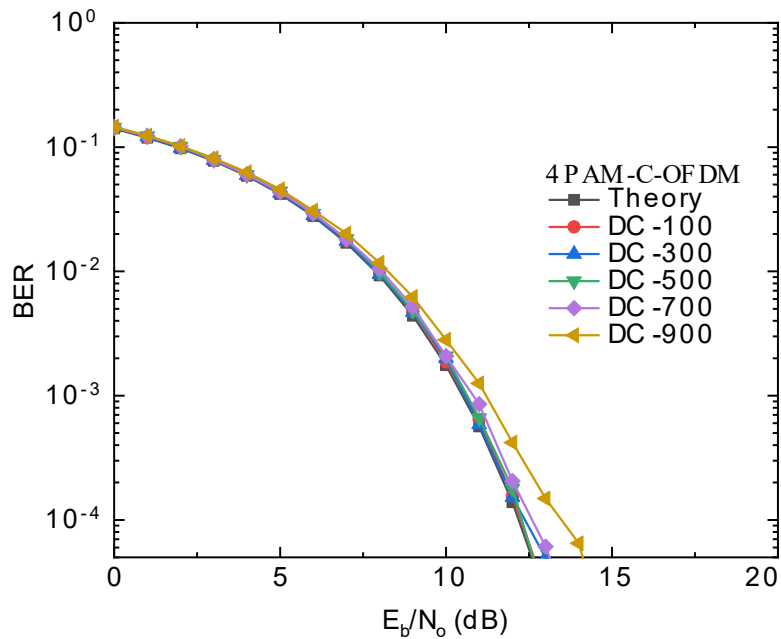


Figure 5-10: BER performance as a function of E_b/N_0 for C-OFDM with 4-PAM and 200 AC.

It is clear that, for all the bias points, the C-OFDM's BER performance was better than that of conventional OFDM and F-OFDM. Furthermore, Figure 5.7 and Figure 5.10 show the BER performance of the proposed systems with 2-PAM and 4-PAM respectively, and both show improved BER performance in contrast to typical OFDM and F-OFDM. Finally, the AC level has been changed to 600 mA along with a DC bias change from 200 to 900 mA. It can be seen from Figure 5.11, Figure 5.12, Figure 5.13 for the conventional, fast and proposed OFDM systems that an improvement of $\cong 10$ dB was achieved at the first bias point compared to conventional OFDM and C-OFDM. At DC bias values of 300 and 500, an improvement of ~ 4 dB and 9 dB was also achieved when compared with C-OFDM and F-OFDM respectively, in Figure 5.12 and Figure 5.13. However, the BER did not reach the target using F-OFDM with the 600 DC level and an AC bias point greater than 500 mA.

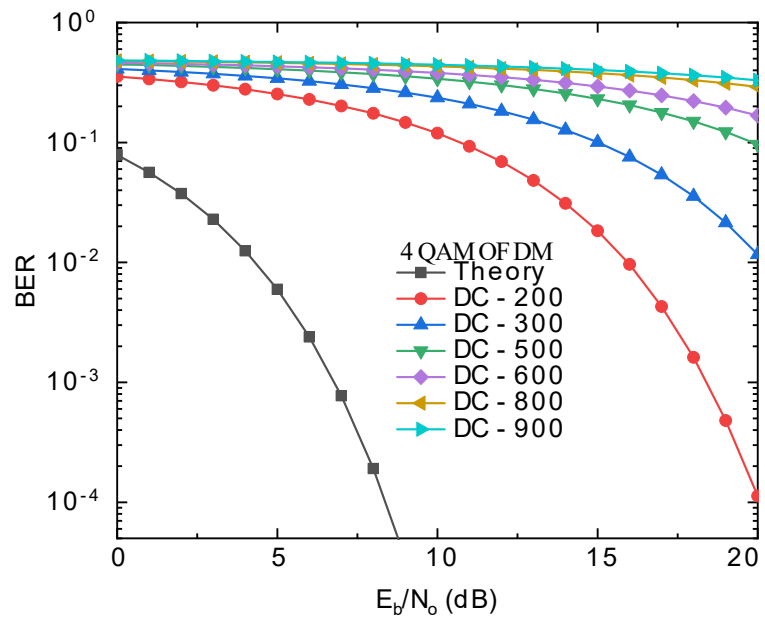


Figure 5-11: BER performance as a function of E_b/N_o for OFDM with 4-QAM and 600 AC.

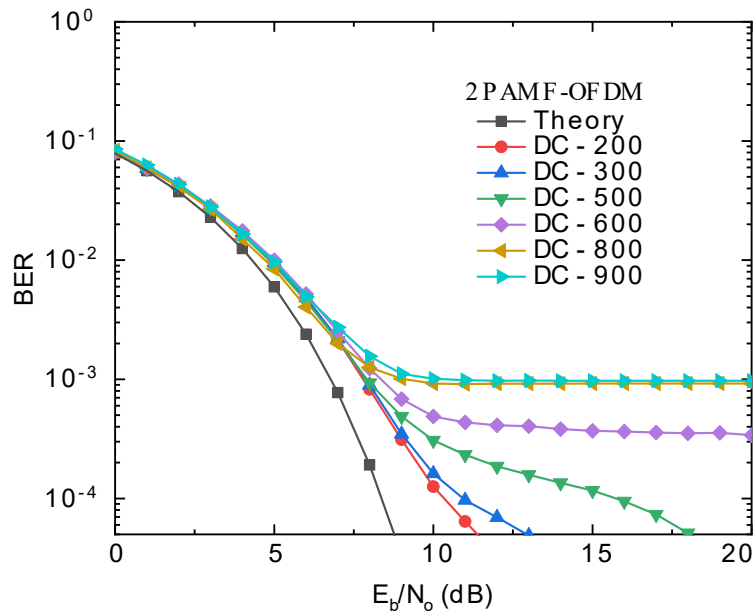


Figure 5-12: BER performance as a function of E_b/N_o for F-OFDM with 2-PAM and 600 AC.

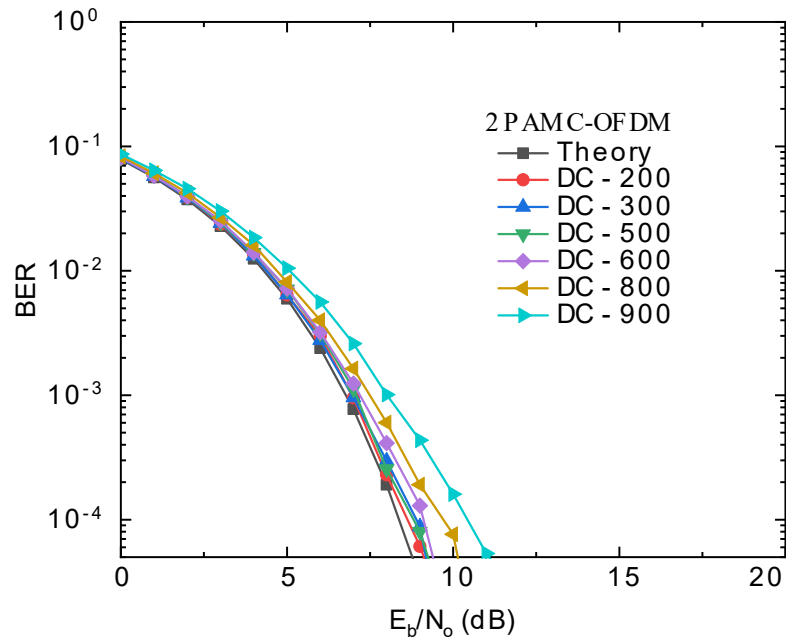


Figure 5-13: BER performance as a function of E_b/N_o for C-OFDM with 2-PAM and 600 AC.

In general, in this section, the change in the performance of the BER can be explained as a function of E_b/N_o when several bias points changed, along with the DC level. As can be observed in Figure 5.7Figure 5.10Figure 5.13, the BER target was achieved with the lowest power penalty for E_b/N_o in comparison with Figure 5.5Figure 5.6Figure 5.8Figure 5.9Figure 5.11Figure 5.12. Moreover, a remarkable improvement was achieved when comparing the power penalty for conventional OFDM, F-OFDM and C-OFDM under the same bias point conditions and DC levels. All of these comparisons show the advantages of C-OFDM over normal OFDM and F-OFDM.

5.3.2 Power Penalties

The results of the analysis of the optical power penalty for the signals under test, as depicted in Figure 5.14, provide additional insights into C-OFDM and F-OFDM using 2-PAM for the 10^{-3} BER target. As a result, the power penalty in dB increased exponentially with the increase in the DC bias points compared to the theoretical BER curve. Additionally, there was a difference of ~ 2.5 dB between the two modulation techniques when the LED's nonlinear effect was considered.

Simulation results for the C-OFDM, FOFDM and OFDM systems indicate that C-OFDM

achieved the lowest PAPR for values of N of 16 and 64. Reductions of ~ 2 dB and 5 dB PAPR respectively were found relative to F-OFDM and OFDM. That is because DBS reduced the likelihood of the constructive superposition of the input samples. Moreover, it was apparent that the PAPR of C-OFDM was the lowest compared to the F-OFDM and OFDM. The conventional OFDM's higher PAPR for any value of N was due to the cosine and sine components. However, in C-OFDM and F-OFDM, only the cosine component contributed to the power signal. Moreover, concerning the C-transformer, more than 65% of its elements were zero, which reduced the probability of obtaining a high PAPR compared to F-OFDM. Additionally, the simulation results above demonstrate two significant improvements concerning C-OFDM over F-OFDM and conventional OFDM. Firstly, C-OFDM exhibited enhanced performance under the same signal conditions. Secondly, it obtained a lower power penalty and PAPR. Due to the limitations imposed by the non-linearity of transmission devices, the lower power penalty and PAPR are advantageous for the communication systems designed with C-OFDM.

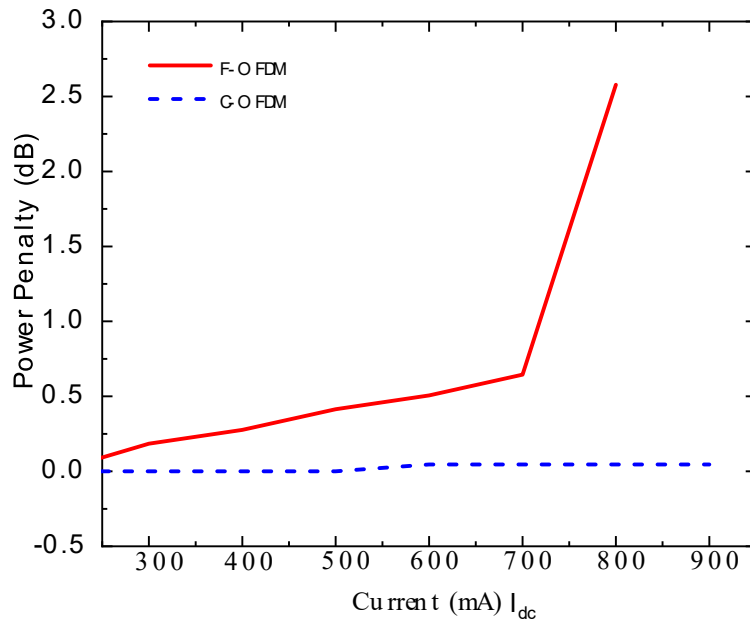


Figure 5-14: The net power penalty gains for C-OFDM over F-OFDM at 200 mA.

5.4 Conclusion

The phenomenon of LED non-linearity has been found to significantly impact the performance of optical OFDM systems. The DC bias point is one of the key characteristics that influence distortion in the information transmitted by LEDs. In this chapter, C-OFDM was proposed to investigate the influence of the nonlinear behaviour of LEDs in optical OFDM wireless communication systems. In simulations, the BER performance of C-OFDM was compared with that of F-OFDM and conventional OFDM. The results confirm that a BER of 10^{-4} could be achieved with C-OFDM at the 900 mA bias point, and that it could not be achieved with the other OFDM systems. More specifically, the linear region was extended. However, when F-OFDM was employed, the power needed to be increased by 2.5 to realise the BER at 800 mA compared to the use of C-OFDM. Consequently, the proposed system delivers a better linear region in comparison to F-OFDM and traditional OFDM. Finally, the C-OFDM system needed a lower ratio of energy-per-bit to noise spectral density (E_b/N_o) than the standard systems, according to the simulation data. As a result, across the LED's nonlinear regions, a multi-carrier system using the proposed technique would benefit from lower PAPR and E_b/N_o requirements.

Chapter 6

Performance of C-OFDM with a Multipath Channel

This chapter introduces a novel optical multicarrier system for visible light communication (VLC). It utilises a transform with low computational complexity which combines the Walsh-Hadamard transform (WHT) and discrete cosine transform (DCT) into a single, orthogonal C-transform. The proposed transform uses a novel method of optical orthogonal frequency division multiplexing (C-OFDM) and is simulated for multipath channels and various forms of modulation. Furthermore, performance in terms of BER as a function of the ratio of energy-per-bit to noise power spectral density (E_b/N_o) is evaluated by simulating systems with different multipath channel models and modulation formats. The simulation results are compared to schemes using the discrete cosine transform (DCT), fast OFDM, and conventional OFDM with the Fast Fourier transform (FFT).

6.1 Introduction

The literature review highlights the increasing mobile data traffic, with a majority occurring indoors, leading to congestion in wireless networks. To address this, optical wireless communication (OWC) using visible light communication (VLC) appears promising, although challenges like limited bandwidth due to LEDs and non-linearity must be overcome. Orthogonal frequency-division multiplexing (OFDM) is a widely used technique to improve spectral efficiency in communication systems. However, OFDM faces challenges such as peak-to-average power ratio (PAPR) and frequency offset issues. Certain modifications, like ACO-OFDM and C-transform, show potential in enhancing OFDM's robustness in dispersive channels. Developing low-cost, energy-efficient, and high-speed indoor wireless access solutions based on OWC and addressing OFDM limitations can help alleviate congestion and enhance wireless connectivity.

6.2 Channel Model

It is well-known that the design of any communication network, including in VLC, must adequately appreciate the limitations caused by the channel environment in which it functions. In particular, the VLC channel has a significant impact on the determination of the overall performance of the communication link. To achieve a high-quality communication system, it is vital to correctly define the VLC channel's specifications. Furthermore, appropriate channel modelling is critical in being able to guarantee that a VLC channel model is stable, secure, and efficient while also delivering acceptable levels of performance [96].

There are several important parameters that need to be considered in the VLC channel, as it is a free space channel where the link is either line of sight (LOS) or non-line of sight (NLOS). In the LOS scenario, the optical power depends on the distance and angle between the transmitter and the receiver. Since a room's ceiling is covered with LEDs, there will be non-directed LOS components as well owing to reflections off the wall and ceiling. Therefore, the room's dimensions, wall materials and the multipath of the light between the transmitter and the receiver are all key parameters that need to be taken into account in designing a **solid** VLC channel [16, 96]. Therefore, both LOS and diffuse components should be included within a VLC multipath channel.

6.2.1 Differences in Propagation Modes

In the literature the indoor links have been defined in mainly three categories of directed LOS, non-directed LOS and diffuse system as shown in Figure 6.1 [1, 16, 37, 130]. In the LOS scenario, the Tx and Rx have been aligned and have a narrow beam angle and field of view (FoV) respectively, as in Figure 6.1(a), and therefore accurate alignment is required. However, individuals moving around the room or the presence of items within the room might cause these links to become blocked. In the non-directed LOS scenario, the Tx has a wide beam angle and the Rx based somewhere within the room has a wide FoV, as illustrated in Figure 6.1(b). Meanwhile the diffuse mode may be one of the most widely and commonly employed systems and is illustrated in Figure 6.1(c). Here, the source's location is significant in determining the power levels at various positions inside a room. In this scheme, the Tx has a wide semi-angle at half power and the Rx has a wide FoV. In practice, its wide FoV allows the Rx to collect reflected light from everywhere in the room [37, 96].

Although NLOS or diffuse configurations reduce the beam blockage effect and increase mobility, they entail the cost of lower data rates. Non-direct LOS is most typically used for generic VLC systems but, due to the high optical power received at the Rx, most speed links in

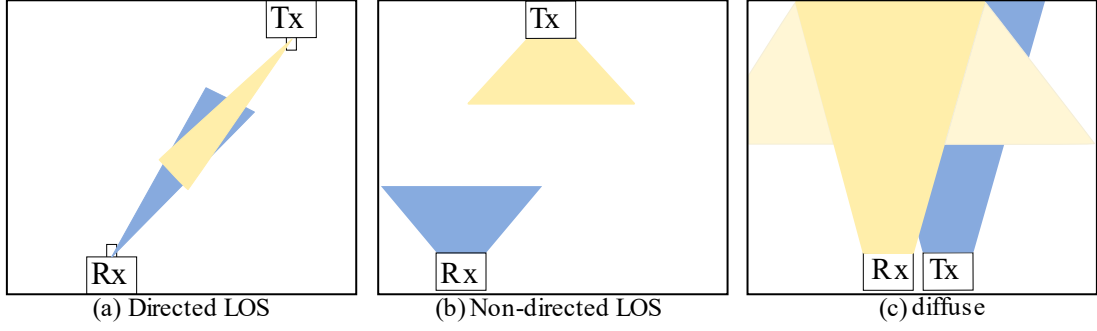


Figure 6-1: Different link configurations (a) directed LOS, (b) non-directed LOS, (c) diffuse

the literature use direct LOS. In particular, the LOS mode has a considerably greater received light intensity, with a higher signal-to-noise ratio (SNR) that may be exchanged to enhance the data rate or connection span, and also minimises inter-symbol interference (ISI). Data rates in the Gb/s regions have been found when utilising a direct LOS link [32, 131]. However, the costs involved can include restricted mobility or a greater likelihood of shadowing and beam blockage [1].

6.2.2 VLC Channel Model

In general, the channel DC gain $H(0)$ is given as a continuous integral of the channel impulse response $h(t)$ as follows:

$$H(0) = \int_{-\infty}^{\infty} h(t) dt. \quad (6.1)$$

In a static VLC channel, the total received optical power consists of two components from the direct (LOS) and reflected (NLOS) paths. The total optical power at the receiver can then be given as [1, 132]

$$P_{Rx} = P_{Tx} H_{LOS} + \int P_{Tx} H_{NLOS}. \quad (6.2)$$

where H_{LOS} and H_{NLOS} are the gains of the DC channel from the LOS and NLOS respectively, P_{Tx} is the transmitting LED's optical power, and P_{Rx} is the received power.

The length of the link for an indoor optical wireless communication link with LED sources is relevantly short. As a result, the effect of attenuation because of absorption and scattering can be neglected [16]. The DC channel gain of line of sight (LOS) for a photodetector

(PD) as a receiver located at a distance d and angle θ away from the transmitter as described in Figure 6.2 is given as [133]

$$H_{LOS} = \begin{cases} \frac{A_r(m_l+1)}{2\pi d^2} \cos^{m_l}(\theta) T_s(\psi) g(\psi) \cos(\psi) & 0 \leq \psi \leq \psi_{FOV} \\ 0, & \psi > \psi_{FOV} \end{cases} \quad (6.3)$$

Moreover, the DC channel gain for a multipath model can be approximated by [1, 132, 133]:

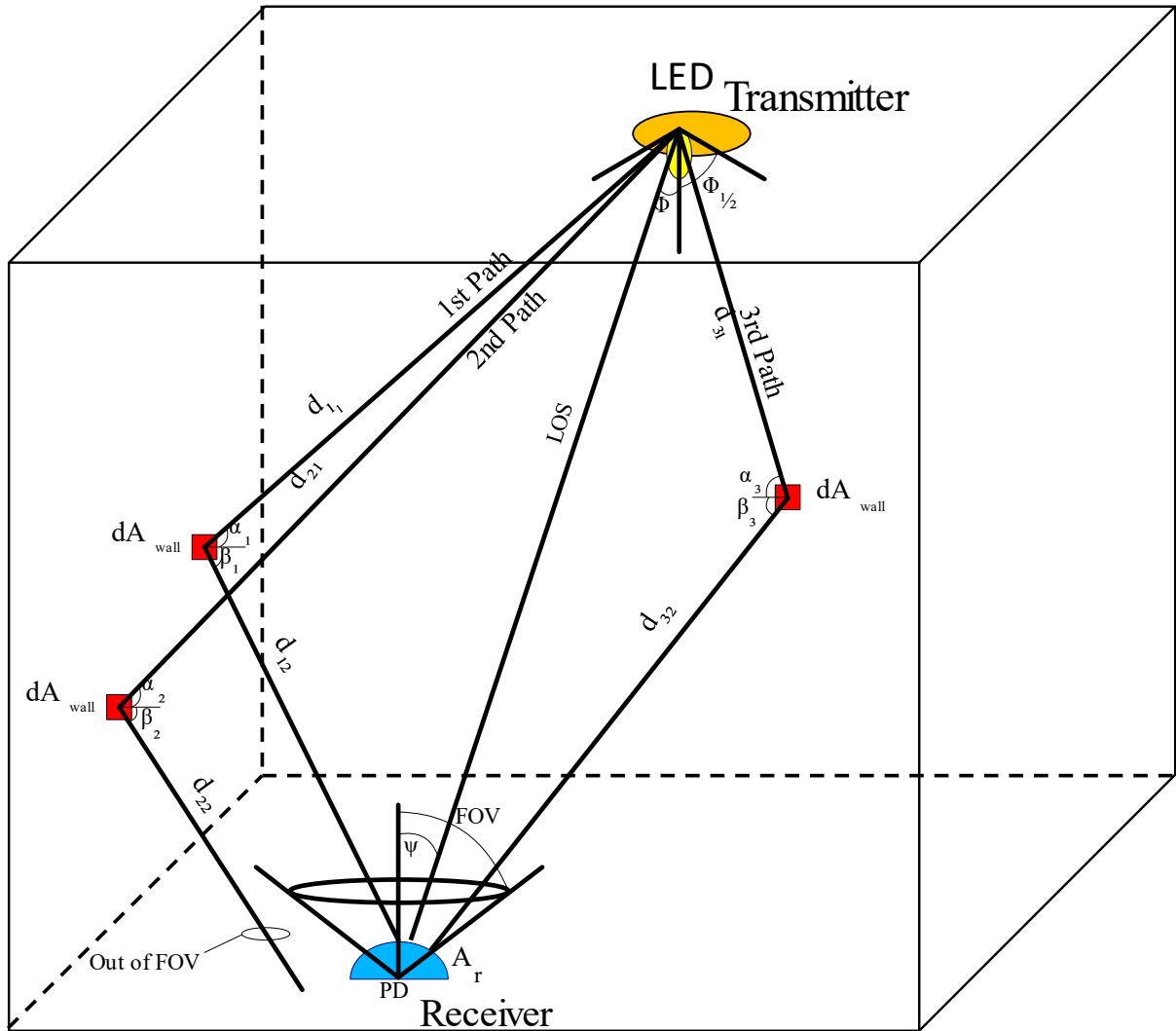


Figure 6-2: Geometry of LOS and NLOS propagation model.

$$H_{NLOS} = \begin{cases} \frac{A_r(m_l + 1)}{2(\pi d_1 d_2)^2} \rho dA_{wall} \cos^{m_l}(\phi) \cos(\alpha) \cos(\beta) T_S(\psi) g(\psi) \cos(\psi) & 0 \leq \psi \leq \psi_{FOV} \\ 0, & \psi > \psi_{FOV} \end{cases} \quad (6.4)$$

There are various additional parameters in an NLOS system; for instance, the reflectance coefficient, angle of incidence at the wall, and angle of irradiance from the wall are ρ , α and β respectively. Furthermore, d_1 is the distance between the transmitter and reflection point and d_2 is that between the reflection point and receiver. Finally, a small reflective area on the wall is dA_{wall} . Also, an optical filter $T_S(\psi)$ and concentrator $g(\psi)$ would be included as coefficients in equations 6.3 and 6.4 but are neglected here to reduce complexity. All of the parameters are illustrated in Table 6.1.

From Equations 6.3 and 6.4, the Lambertian order m_l is a significant parameter since it specifies the overall emitted radiation beam. The Lambertian order is given by [16, 130, 134]:

$$m_l = \frac{-\ln(2)}{\ln[\cos(\phi_{1/2})]} \quad , \quad (6.5)$$

Therefore, the semi-angle at half power can be written as follows:

$$m_l \ln[\cos(\phi_{1/2})] = -\ln(2)$$

$$\ln[\cos(\phi_{1/2})] = \frac{-\ln(2)}{m_l}$$

$$e^{\ln[\cos(\phi_{1/2})]} = e^{\frac{-\ln(2)}{m_l}}$$

$$\cos(\phi_{1/2}) = e^{(\ln(2))^{\frac{-1}{m_l}}}$$

$$\cos(\phi_{1/2}) = 2^{\frac{-1}{m_l}}$$

$$\phi_{1/2} = \cos^{-1}(2^{-1/m_l}). \quad (6.6)$$

Equations 6.5 and 6.6 show the relationship between m_l and the semi-angle at half power $\phi_{1/2}$. As m_l approaches 1 or ∞ , the emission becomes omnidirectional or more directional respectively, as can be seen in Figure 6.3. As $m_l = \infty$, the optical power becomes

Table 6.1: Parameters for an indoor VLC system

Parameter	Symbol	Value
LED transmitted optical power	P_{Tx}	100 mW
Semi-angle at half power	$\phi_{1/2}$	60°
Angle of irradiance	ϕ	-
Angle of incidence	ψ	-
FOV of the receiver	ψ_{FOV}	85°
Effective collection area of the PD	A_r	$16 * 10^{-6} m^2$
Small reflective area on the wall	dA_{wall}	-
Gain of an optical filter	$T_S(\psi)$	1
Optical concentrator gain	$g(\psi)$	1
Angle of incidence at the wall	α	-
Angle of irradiance from the wall	β	-
Reflectance factor	ρ	0.8
Distance between transmitter and reflection point	d_1	-
Distance between reflection point and receiver	d_2	-
Lambertian order	m_l	1
LED position	LED	(2.5, 2.5, 3)
Receiver plane height	-	0.7
Room size	Room	(5, 5, 3)

more directed, such as in laser diodes which typically have high values of m_l . LEDs, on the other hand, have lower values of m_l , leading to a huge range of patterns. Furthermore, the parameter A_r represents the photodiode's active area whereas ψ_{FOV} denotes its field of view, as shown by equations 6.3 and 6.4.

To ensure effective detection, the received signal must be within the range of the FOV of the photodiode but will not be recognised if it is outside the FOV of the receiver. The signal-to-noise ratio (SNR) in the traditional RF domain is proportional to the average received power. However, in the optical domain, SNR is proportional to the square of the average received power P_{Rx} [16]. Therefore, the received SNR is given as follows [69, 135]:

$$SNR = \frac{\mathfrak{R}^2 P_{Rx}^2}{R_b N_o} . \quad (6.7)$$

where \mathfrak{R} , R_b , N_o are the responsivity of the PD, bit rate per second and noise spectral density respectively. Therefore, higher optical power and low path loss are required to achieve the same performance as in a RF system. Consequently, OWC technology, and particularly VLC, is a promising contender for future short-range communications [69].

Figure 6.2 illustrates the basic indoor VLC scenario considering both LOS and NLOS channel models. In both LOS and NLOS scenarios, the mathematical equations obtained for the impulse response are presented in equations 6.3 and 6.4. Simulation results for the distribution of received optical power P_{Rx} and SNR for the indoor VLC technology utilising one and four lighting source configurations are shown in the following figures. The specification parameters for the indoor VLC system are listed in Table 6.1.

Figure 6.4 to Figure 6.7 show the distribution of received power and SNR for an LED

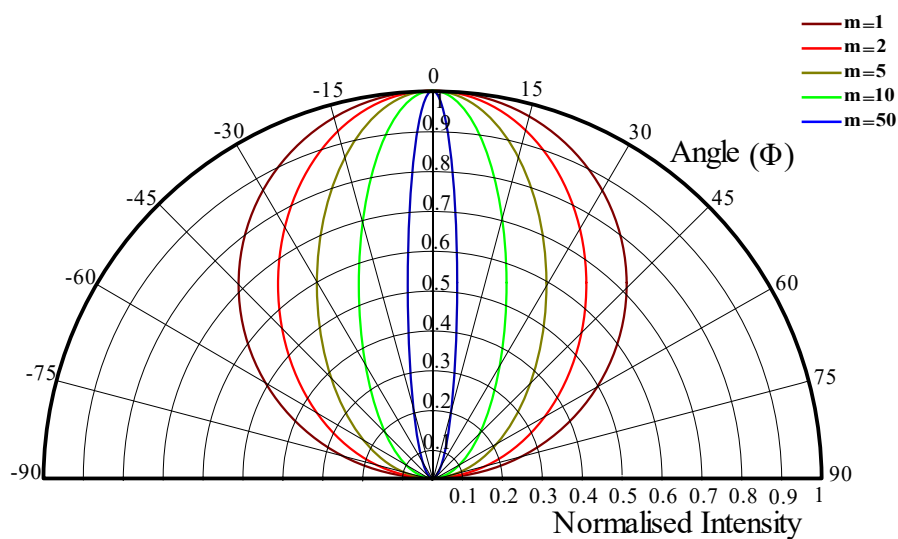


Figure 6-3: Radiation emission patterns for several Lambertian orders [1].

set-up for cases with various angles of the semi-angle at half capacity. Figure 6.4 and Figure 6.5 indicate that the optical power varies between -9.5 to -17.5 dBm and 0.8 to -80 dBm in the case of $\theta_{1/2} = 60^\circ$, 12.5° and the corresponding $m_l = 1$ respectively. Similarly, Figure 6.5 and Figure 6.7 depict the SNR distribution using one LED semi-angle at half power of 60° and

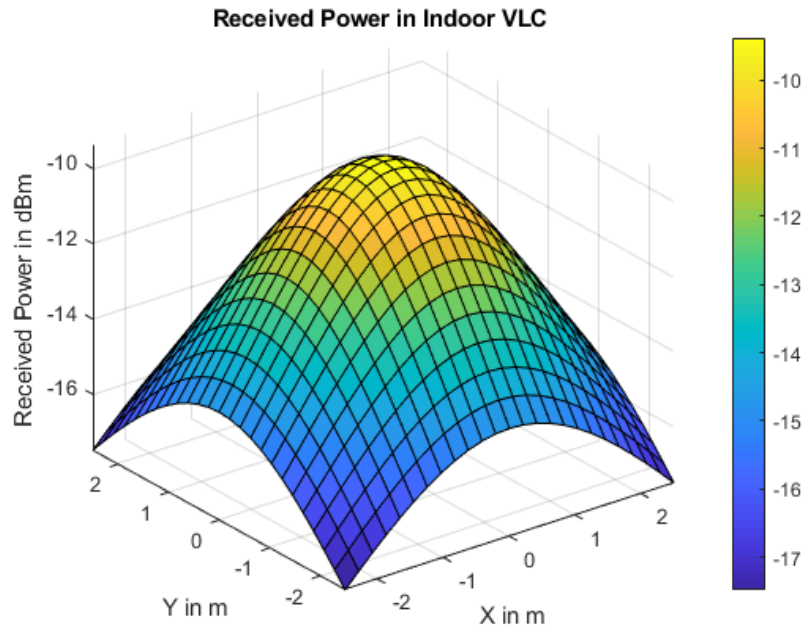


Figure 6-4: Received power distribution for single LED with $\theta_{1/2} = 60^\circ$ semi-angle at half power illumination.

12.5° . Comparing Figure 6.6 and Figure 6.7 it can be noticed that the SNR varies between -34.5 to -43.5 dB and -19.8 to -120 dB. In cases of the utilisation of multiple illuminating LEDs, the received optical power and SNR distributions are presented in Figure 6.8 to Figure 6.11 with changing semi-angles at half power and responding m_l . The received optical power changes between -7.8 to -12.5 dBm for $\theta_{1/2} = 60^\circ$ as shown in Figure 6.8 and within the range 0.75 to -40 dBm for $\theta_{1/2} = 12.5^\circ$ in Figure 6.9. That improves the receiving power by 8.5 dBm when optimising the Lambertian order. Moreover, Figure 6.10 and Figure 6.11 show the SNR distribution and, from a comparison of the two figures, it is observed that there is a significant improvement in SNR. This means that the LED optical power is more discernible with higher SNR levels.

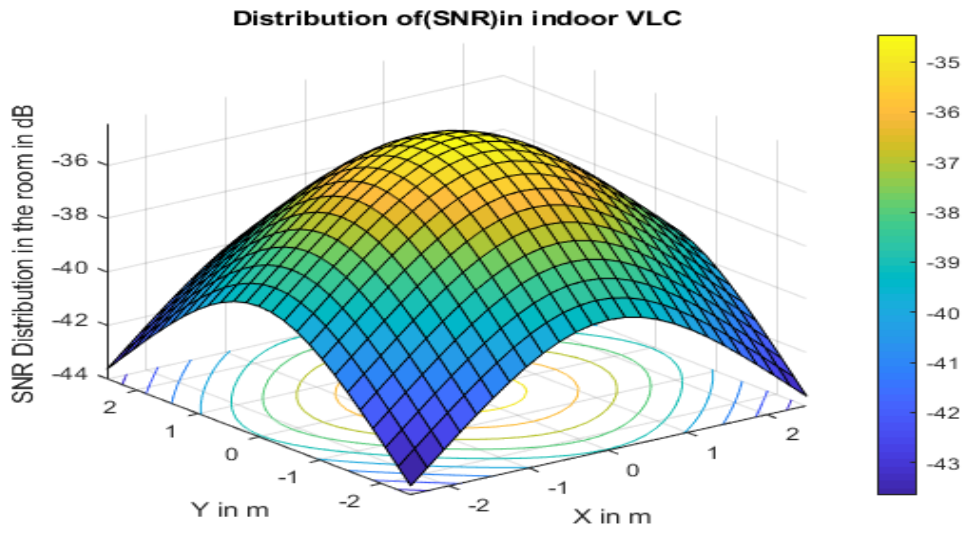


Figure 6-6: Signal-to-noise ratio (SNR) distribution for one LED with 60° semi-angle at half power illumination.

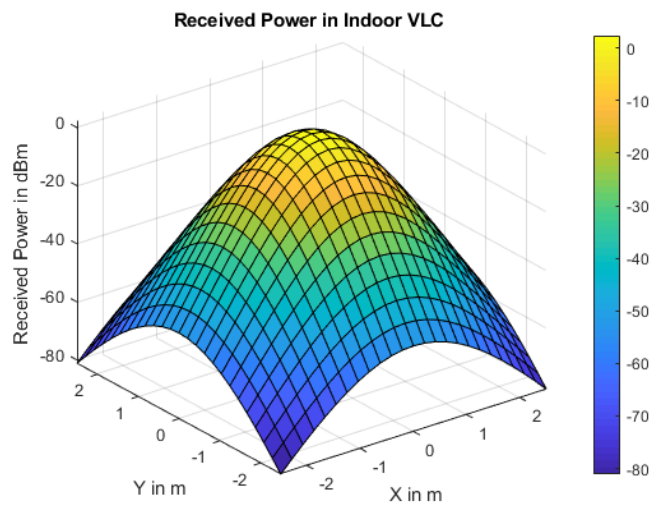


Figure 6-5: Received power distribution for single LED with =12.5 semi-angle at half power illumination.

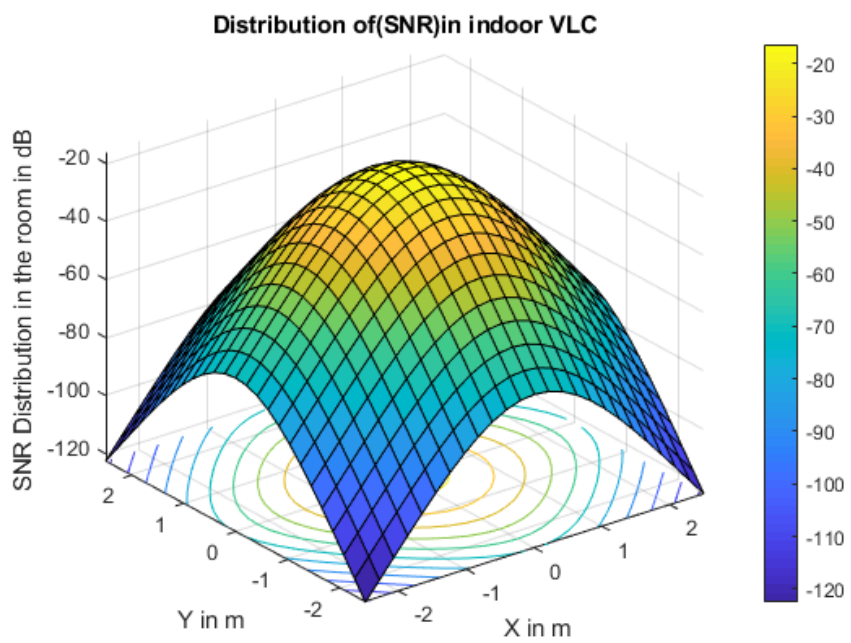


Figure 6-7: Signal-to-noise ratio (SNR) distribution for one LED with 12.5° semi-angle at half power illumination.

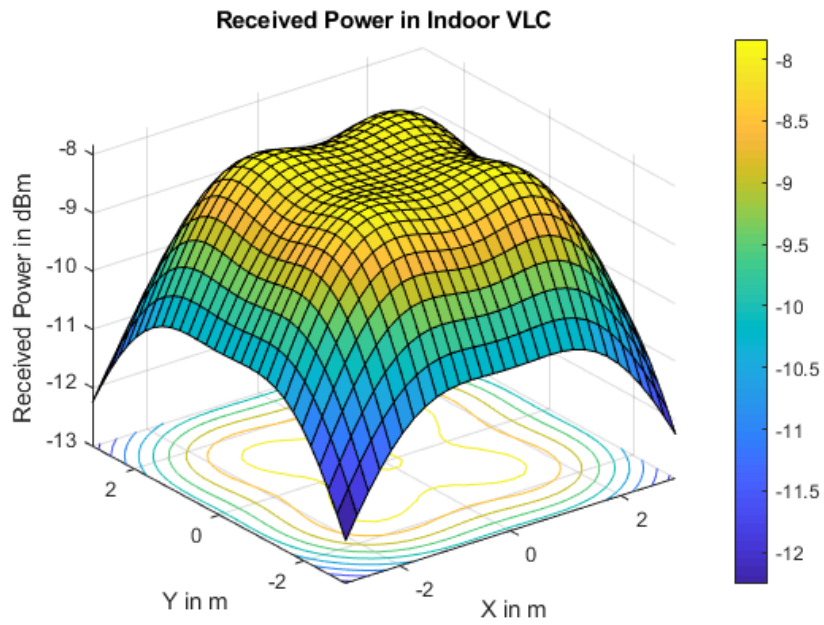


Figure 6-8: Received power distribution for multiple LEDs with 60° semi-angle at half power illumination.

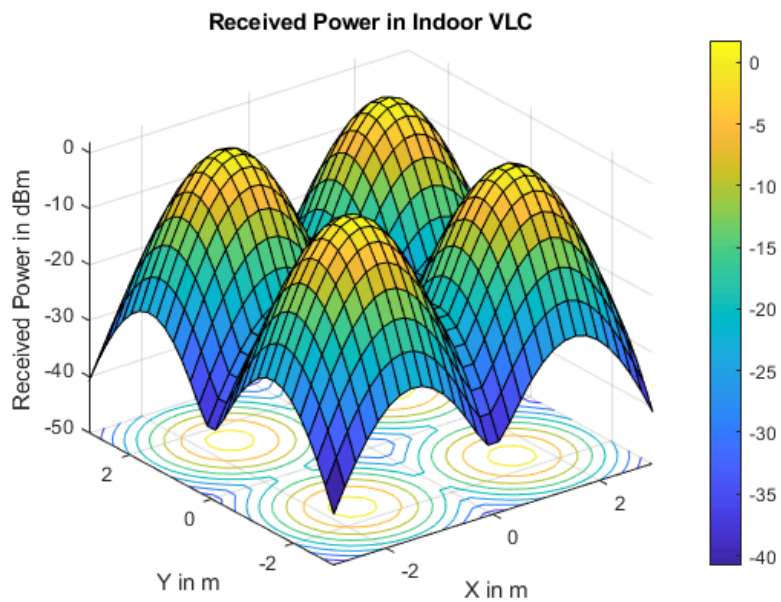


Figure 6-9 Received power distribution for multiple LEDs with 12.5° semi-angle at half power illumination.

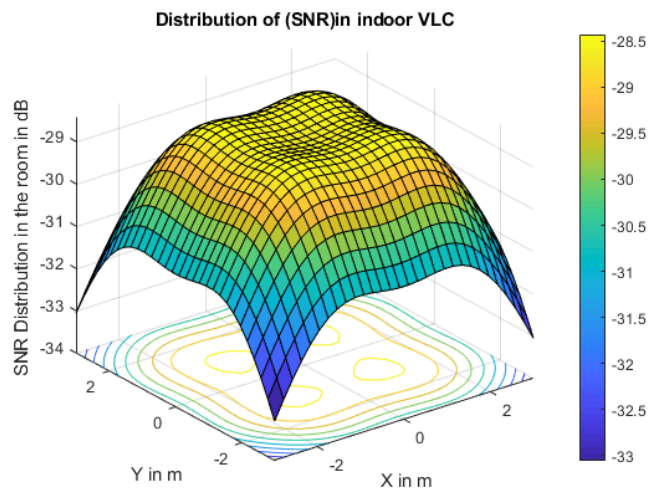


Figure 6-10: Signal-to-noise ratio (SNR) distribution for multiple LEDs with 60° semi-angle at half power illumination.

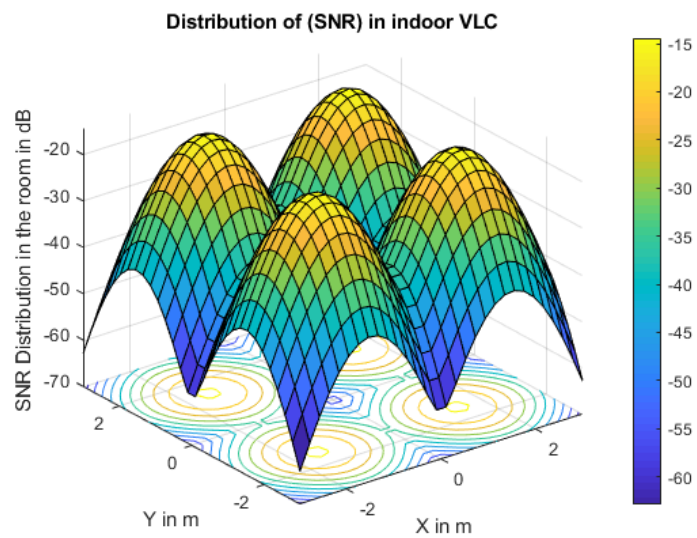


Figure 6-11: Signal-to-noise ratio (SNR) distribution for multiple LEDs with 12.5° semi-angle at half power illumination.

6.3 Multipath Channel

Especially in indoor environments, a signal delivered through wireless networks might travel across numerous channel routes with varying degrees of spreading, delays and attenuation. The signal sent is reflected by walls, ceilings, furniture, and other barriers, resulting in these routes. As seen in Figure 6.2, this phenomenon is described in terms of multipath channels which can be either line-of-sight (LOS) or non-LOS. Due to ISI, phase shift, and the attenuation of the received signals, multipath transmission significantly degrades system performance.

6.3.1 Channel Impulse Response (CIR)

In Figure 6.12 (a) the NLOS's are considered, and the optical power received is 4.5×10^{-8} with

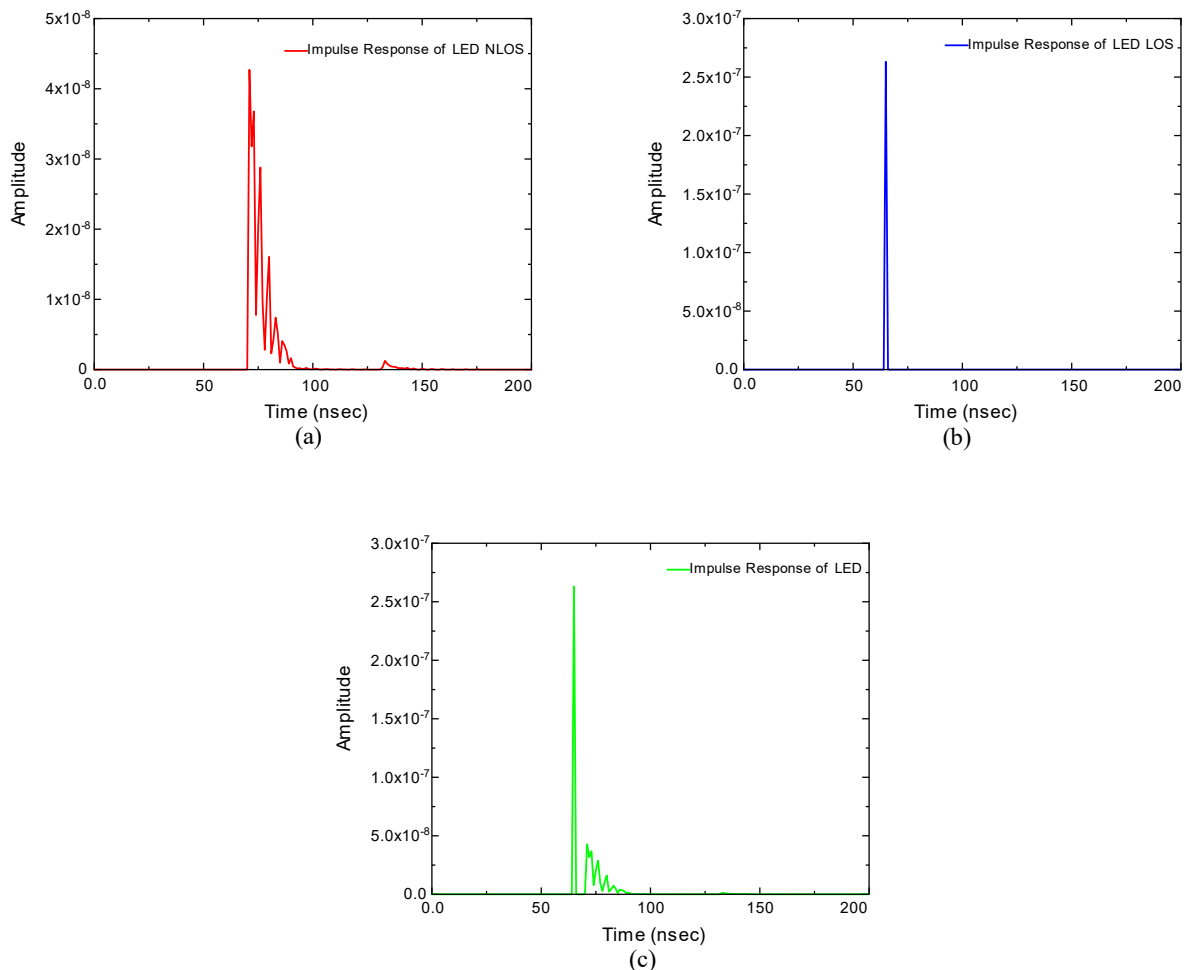


Figure 6-12: Impulse responses of VLC channels: (a) LED NLOS; (b) LED LOS (c) LED (NLOS+LOS).

delay spread from 75 to 90 ns. On the other hand, in Figure 6.12 (b), only LOS is considered. It is observed that a peak exists in CIR, which is related to LED lighting. The peak corresponds to the LOS of LED, which has optical power $\cong 2.7 \times 10^{-7}$ watt. Finally, Figure 6.12 (c) present the NOLS and LOS. There are two peaks; the large one corresponds to the NOS and the second one is the contribution of several NLOS. Even if the LOS is blocked, the PD still receives optical power.

6.4 System Model

A block diagram of the established systems is presented in Figure 6.13. At the top of the figure, the proposed C-OFDM is shown in blue, the F-OFDM is in red in the centre of the formation using IDCT and traditional OFDM using IFFT is at the bottom in green. Multiple modulation methods such as pulse-amplitude modulation (PAM) and quadrature-amplitude modulation (QAM) may be used at the transmitter side to map the incoming data, d . PAM with a real modulation format is used, since the ICT and IDCT are utilised to produce a real time-domain signal for C-OFDM and F-OFDM respectively. On the other hand, the data is mapped using QAM for conventional OFDM. Then, the mapping data, c , traverses the serial-to-parallel converter. In the next step, the parallel vector X is distributed in a number of subcarriers, N , for C-OFDM, F-OFDM, and OFDM. As mentioned earlier, to obtain a real output from the IFFT, HS must be used for IM OFDM. The HS symbols, which are denoted as X^* , are passed through an IFFT to obtain a real signal $x(t)$. However, the use of HS (as explained in Chapter 2) comes at the cost of half the bandwidth not being used for the transmission of new data, as well as an additional block being required compared to C-OFDM and F-OFDM. Then, the time-domain signal is passed through cyclic prefix (CP) or zero padding (ZP), which has been proposed as an attractive alternative to the cyclic prefix (CP) [86, 87]. Accomplished before parallelisation and transmission $x(t)$ by the LED, this technique has been described as a first-order low-pass filter response in the literature and is adopted in this work.

The proposed C-OFDM scheme replaces the IFFT and IDCT with the C-transform (ICT) in order to reduce the system's complexity. The CT is a unitary transform that uses the WHT in conjunction with the DCT.

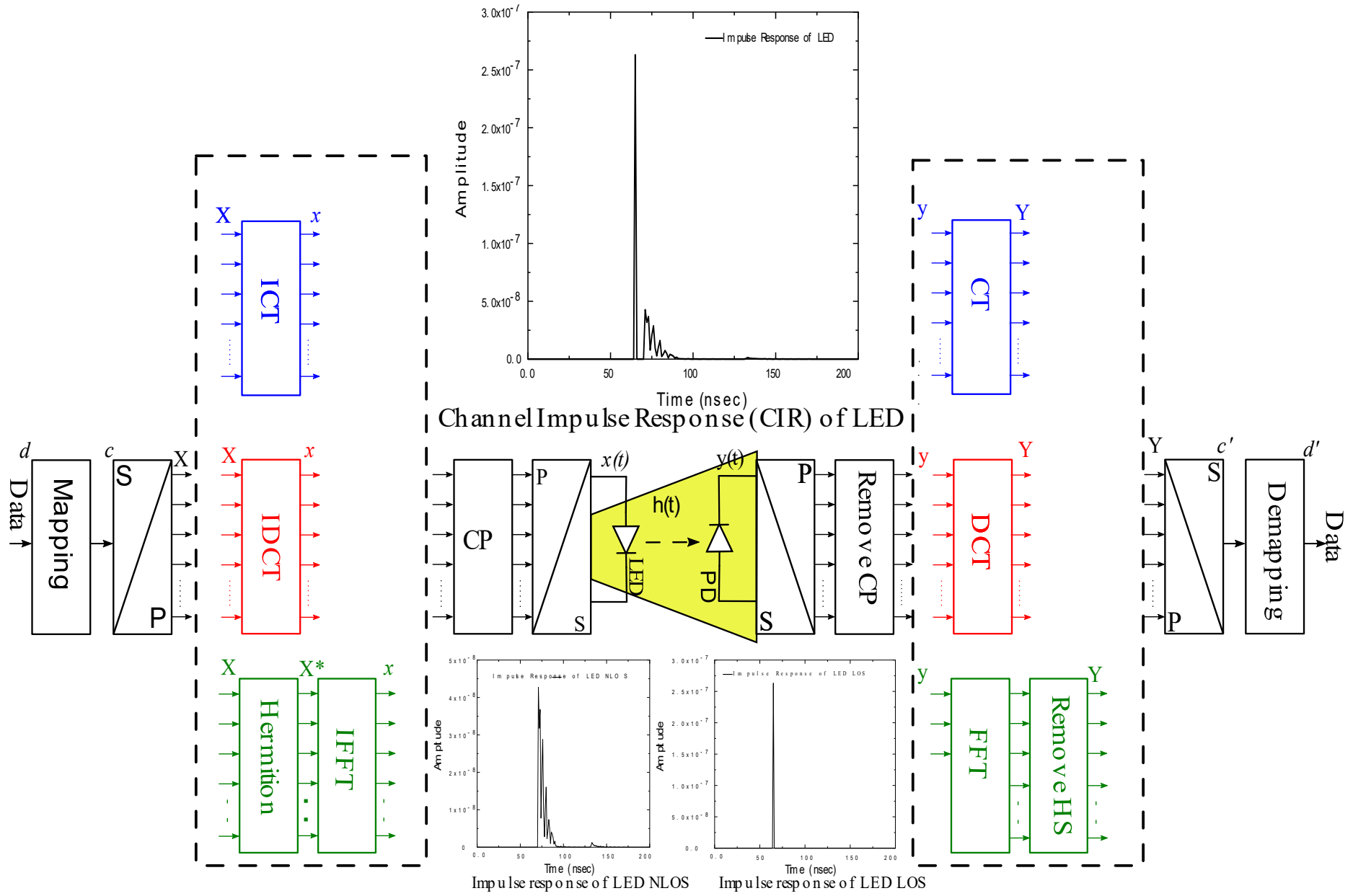


Figure 6-13: Block diagram for the OFDM schemes tested over the VLC CIR.

6.5 Simulation Results and Discussion

This section presents the results of a performance analysis of the C-OFDM, F-OFDM, and conventional OFDM systems across the multipath channel and AWGN channel models in order to analyse the BER performance of the proposed C-OFDM. Furthermore, the ratio of energy-per-bit to noise power spectral density, E_b/N_o , is assessed by simulating various multipath and AWGN channel models and modulation schemes and is used to determine the BER performance of all of the OFDM systems. It is worth noting that the proposed scheme's signal bandwidth is half that of standard OFDM due to the DCT's reduction in subcarrier spacing by half, as shown in Figure 4.1.

6.5.1 BER Performance over VLC AWGN Channel

Figure 6.14 illustrates the BER performance of the C-OFDM, F-OFDM, and standard OFDM systems employing 512 subcarriers (N) and QAM 4, 16, and 64 over the AWGN channel. It demonstrates that all of these systems work in identical ways over the AWGN channel. As predicted, the proposed technique's BER performance in an AWGN channel fulfils the Shannon theory. This proves that the WHT does not affect the AWGN noise power, which is already evenly distributed among all subchannels. Additionally, the WHT has not affected the signal

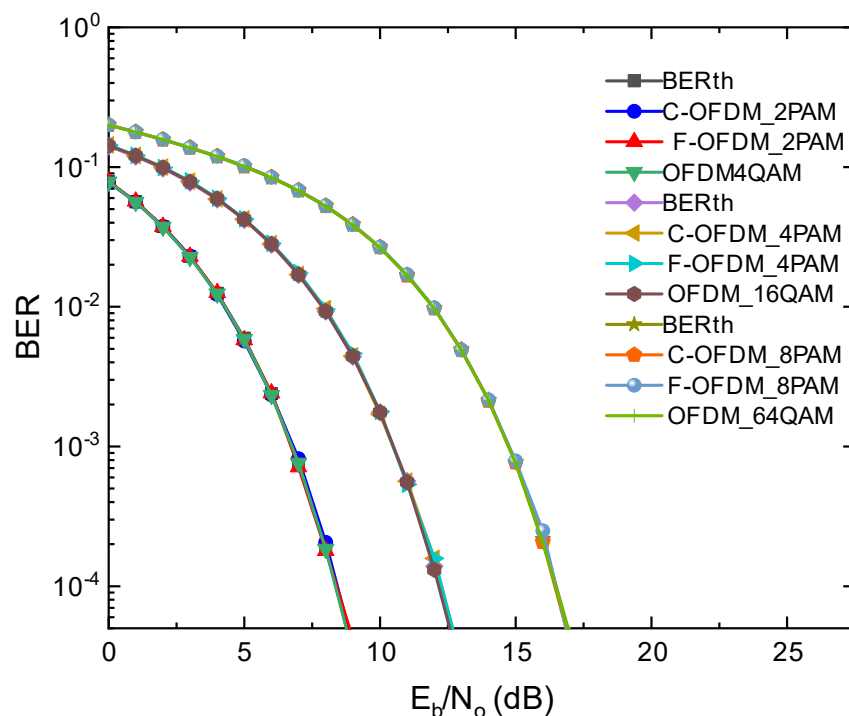


Figure 6-14: BERs of the proposed C-OFDM, F-OFDM and OFDM systems through the AWGN channel

strength since it is a unit transformation. However, it is unclear how the system would operate when exposed to an indoor VLC channel environment with the LED bandwidth constraint.

6.5.2 BER Performance over VLC Multipath Channel

In addition to reducing PAPR, the use of the C-transform in OFDM systems allows for more channel diversity to be exploited, which is especially useful when transmitting across multipath channels. Figure 6.15 illustrates the BER performance of the C-OFDM, F-OFDM using PAM and OFDM using QAM over an indoor VLC channel 1(nsec). Compared to the theoretical BER curve, the E_b/N_o is increased by $\cong 3$ dB to achieve the BER target of 5×10^{-5} in the case of C-OFDM. However, this BER target has not been achieved by F-OFDM and OFDM, and they perform at BER 10^{-3} at the cost of $E_b/N_o \cong 2$ dB when compared with the theoretical curve. Furthermore, the worst BER curve is for DCT-OFDM, as is seen in Figure 6.15. However, the C-OFDM exhibits the best BER performance, proving that the addition of the WHT to the DCT improves the OFDM system.

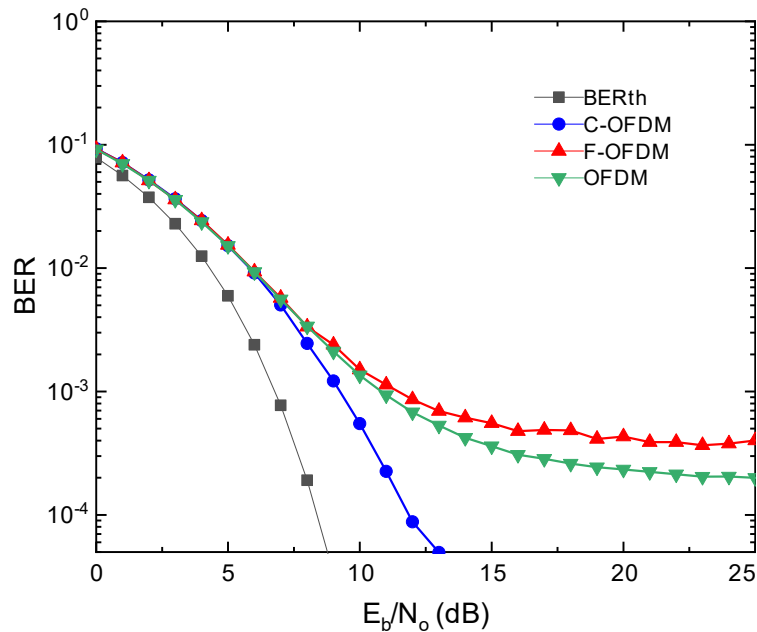


Figure 6-15: BER performance as a function of E_b/N_o for C-OFDM, F-OFDM and OFDM under VLC channel characteristics.

6.5.2.1 BER Performance against the Bandwidth Limitations of the LED.

In this section, the aforementioned OFDM systems are investigated under various bandwidth limitations of the LED. Figure 6.16 shows the BER curves for C-OFDM, F-OFDM, and conventional OFDM for $f_c = [1, 0.75, 0.5]$ and with 512 subcarriers over the VLC channel. The most crucial feature of Figure 6.16 is that C-OFDM, but not F-OFDM or OFDM, have reached the 5×10^{-5} BER target. However, this achievement comes at the cost of values of E_b/N_o at 4, 4.5 and 6 dB, with values of f_c/B at 1, 0.75 and 0.5, respectively. On the other hand, all of the OFDM systems have reached the BER target of 10^{-3} , with values of E_b/N_o slightly higher than C-OFDM. The proposed C-OFDM system improves the value of E_b/N_o by several dBs for $f_c=1B$, $0.75B$ and $0.5B$ compared to F-OFDM and OFDM, which shows that the C-OFDM is a spectrally efficient technique.

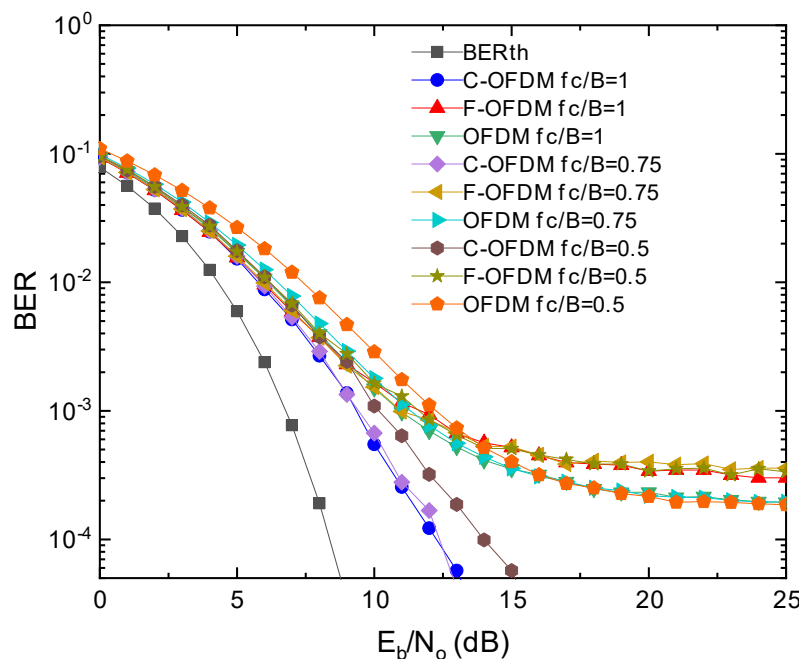


Figure 6-16: BER performance as a function of E_b/N_o for C-OFDM, F-OFDM and OFDM with $F_c/B = 1, 0.75,$ and 0.5 .

6.5.3 Power Penalties

Additional information may be acquired by examining the electrical power cost associated with the test signals, as indicated in Figure 6.19 for C-OFDM and F-OFDM using PAM and OFDM using QAM for the 10^{-3} BER objective. As the results in Figure 6.19 show, the power penalty in dB for the BER objectives grows almost exponentially with a linear decrease in bandwidth. When $f_c/B = 0.4$ for OFDM, F-OFDM, and C-OFDM, the highest attenuations encountered at a BER of 10^{-3} were 13, 11.7, and 11.25 dB respectively. However, when the f_c/B is 1, the OFDM signal is not affected by the LED band limitation; the power penalties are now 11, 11.5 and 9.4 dB for OFDM, F-OFDM and C-OFDM. In other words, when $f_c/B=1$, Figure 6.19 shows the effect of the VLC channel on the OFDM systems. The difference in power penalty between these modulation formats increases in this range because the ISI experienced by OFDM becomes higher as f_c/B reaches 0.4. It is clearly seen that the proposed C-OFDM system is an efficient energy scheme, which is advantageous for VLC since it has been reported that the majority of VLC connections have high signal-to-noise ratios [136].

For the BER target of 10^{-3} , Figure 6.20 shows the observed E_b/N_0 gain with C-OFDM in contrast to those of F-OFDM and OFDM. For identical band-limitation circumstances, the negative index implies that C-OFDM consumes less power than both F-OFDM and OFDM. As f_c/B becomes more significant and the system becomes more band-limited, the benefit of C-OFDM having half the bandwidth of OFDM begins to prevail, and a power penalty is noted.

The above findings demonstrate the superiority of C-OFDM over F-OFDM and OFDM. Additionally, C-OFDM has a significant BER benefit over F-OFDM and OFDM in band-limited systems. As a result, it is concluded that C-OFDM is a promising candidate for future exploration in VLC systems as a potential alternative to traditional OFDM.

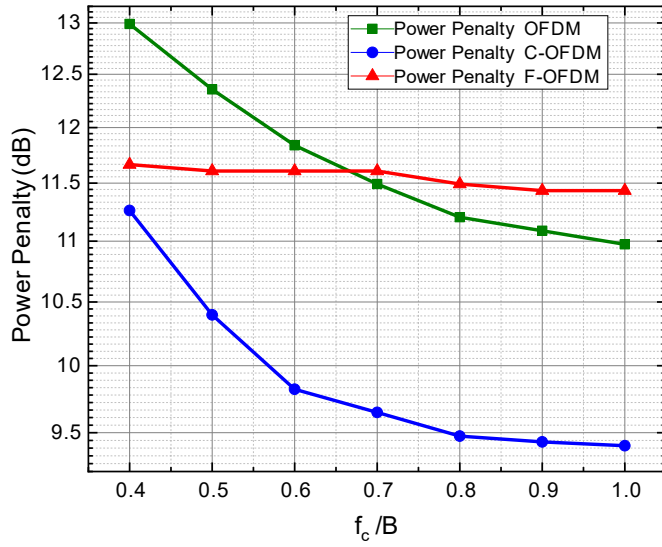


Figure 6-17: Measured electrical power penalties for C-OFDM, F-OFDM and OFDM for the BER target of 10^{-3} .

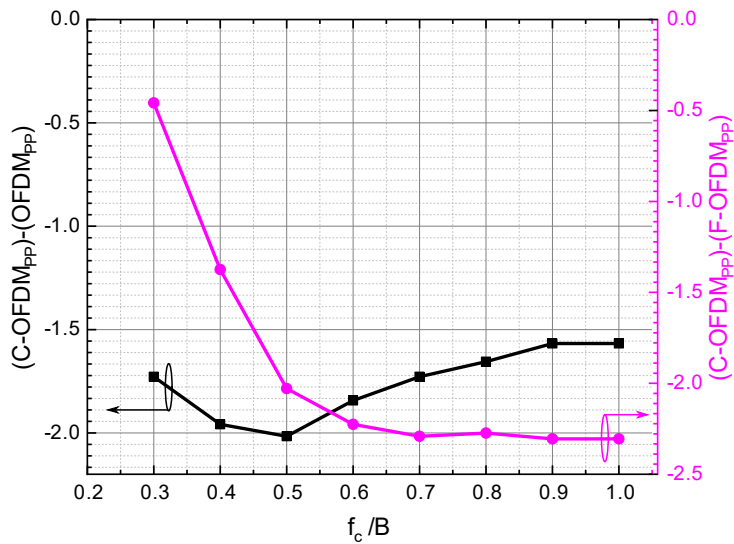


Figure 6-18: Net power penalty gain for C-OFDM over F-OFDM and OFDM.

6.6 Conclusion

In this chapter, the performance of the proposed CT is investigated by comparing it with conventional and fast OFDM variants in terms of BER and power penalties. Moreover, the BER over the AWGN channel has the same curve compared with traditional OFDM and F-OFDM. In addition, C-OFDM is proposed for the first time for VLC channel environments with high LED band limitations. The BER performance of C-OFDM has been compared against that of typical OFDM and F-OFDM in a VLC channel environment with an increasing bandwidth limitation, and it is shown that, when the signal bandwidth is larger than the LED modulation bandwidth, a BER target of 5×10^{-5} can be reached at the cost of a 4-6 dB optical power penalty, whereas both OFDM and F-OFDM failed to meet the target. However, this achievement comes at the expense of slightly increased computational complexity compared to F-OFDM when $N = 32$.

Chapter 7

Conclusion and future work

The dissertation that was given discussed several difficulties with communicating using visible light. This chapter summarises this thesis and the subsequent research.

7.1 Conclusion

Recent research has focused heavily on improving the performance of the OFDM modulation system in IM/DD-based VLC systems, despite the fact that doing so incurs significant increases in computational complexity and PAPR, worse BERs, and wasted power. In comparison to RF, VLC has significant benefits such as license-free operation, the ability to be deployed in electromagnetically sensitive environments like aeroplanes and hospitals, and a bandwidth of 400 THz which is around 10^4 times greater than that in RF. Therefore, VLC merits further study so that it may reach its full potential. However, the fundamental obstacle to the adoption of a high-performance throughput VLC-based system is the constrained LED bandwidth. Therefore, this study aimed to solve the VLC system restrictions brought about primarily by the constrained LED bandwidths, which serve as the primary roadblock to deploying a high-performance throughput VLC-based infrastructure. In order to accomplish this goal, a novel and promising modulation scheme, C-OFDM, was introduced into the VLC technological environment and its potential to enhance the performance of VLC systems was examined. The study's findings show that the C-OFDM method has great potential to increase the throughput in VLC networks. This research aimed to build a proposed C-OFDM system for the VLC technique using a new transform rather than the IFFT/FFT by combining the Walsh-Hadamard transform (WHT) and the discrete cosine transform (DCT) into a single orthonormal unitary transform. Prominent characteristics of the C-transform (CT) include its low complexity, diversity, sparsity, and unitary diagonal structure.

The technical difficulties encountered, the reasons for performing this investigation, and new insights were discussed in the first chapter of this thesis. Following this, Chapter 2 detailed

the fundamentals of VLC systems, including the transmitter and receiver devices. Furthermore, the most significant difficulties associated with a VLC system were noted and addressed. This chapter also discussed the most widely used multi-carrier modulation techniques for VLC systems. Chapter 3 then covered the basics of the C-transform used to achieve the goals of this research. The chapter also explained the lower complexity of the C-OFDM in comparison with that of F-OFDM and conventional OFDM systems, and it was shown that the computational complexity of the C-OFDM system is 52-75% lower compared to the traditional OFDM.

In Chapter 4, numerical simulations were provided to show how the C-OFDM system should be implemented. Additionally, compared to F-OFDM and OFDM, C-OFDM has the capacity to minimise high peak power in the OFDM system within a range of 5 dB and 2 dB owing to the lowering of the superposition among the SCs via the C-transform. Also, the simulation results illustrated that the proposed C-OFDM system achieves the same BER curve over AWGN compared to the other systems. Furthermore, the BER performance under the condition of the band limitations of the LED was simulated, and the results show that the C-OFDM offers an improvement of several dBs E_b/N_o for $f_c=1B$ and $0.5B$.

In most visible light communication systems, light-emitting diodes provide an electro-optic output that is inherently non-linear. This is especially troublesome when employing modern modulation schemes with high peak-to-average power ratios, owing to clipping and distortion, such as in orthogonal frequency-division multiplexing (OFDM). Therefore, Chapter 5 introduced the system architecture of the novel so-called C-transform, which deterministically spreads the information and lowers the PAPR by using a Walsh-Hadamard matrix and a discrete cosine transform. This chapter treated and demonstrated the effects of the LED's non-linearity on the BER performance of a proposed OFDM system. Therefore, the novel transform was contrasted with more conventional formulations of OFDM at a number of bias sites along the electro-optic transfer function. It was concluded that the C-transform-based OFDM produced the best BER findings and showed the most significant independence of LED non-linearity. The results demonstrated that C-OFDM at the 900 mA bias point could achieve a BER of 10^{-4} , whereas the aforementioned OFDM systems could not. In other words, the linear area was specifically expanded. In comparison to OFDM, a decrease in the power penalty was found of 2.5 dB at a BER of 10^{-4} . Consequently, compared to F-OFDM and conventional OFDM, the proposed system produced a superior linear region. Finally, modelling results showed that the C-OFDM system required a lower ratio energy-per-bit to noise spectral density (E_b/N_o) than traditional and fast OFDM systems. Therefore, a multi-carrier system adopting the proposed

approach would benefit from a reduced PAPR and had lower E_b/N_o requirements throughout LED non-linear zones.

The BER performance of C-OFDM over a multipath channel has been examined in Chapter 6 by addressing the impact of the C-transform on the effectiveness of the proposed system under multipath transmission conditions. Additionally, by simulating various multipath channel models and modulation schemes, bit error rate (BER) performance as a function of the ratio of energy-per-bit to noise power spectral density (E_b/N_o) was assessed. Simulation findings for the discrete cosine transform (DCT), fast OFDM, and fast Fourier transform (FFT) standard OFDM were contrasted with those for C-OFDM. The results show that the novel C-OFDM performed better for multipath channels than both fast and conventional OFDM. Furthermore, the suggested method reduced the peak-to-average power ratio (PAPR) compared to the OFDM schemes mentioned above because the proposed transform's diagonal block structure (DBS) minimises input signal superposition.

Additionally, it was demonstrated that C-OFDM has a smaller power penalty than F-OFDM and OFDM while maintaining a comparable level of spectral efficiency for a particular set of band restrictions. Additionally, the BER over the AWGN channel follows the same curve as in F-OFDM and conventional OFDM. C-OFDM was then proposed for the first time for use in VLC channel situations with severe LED band constraints. In a VLC channel environment with increasing bandwidth limitations, the BER performance of C-OFDM was compared to that of typical OFDM and F-OFDM. The results demonstrated that, when the signal bandwidth is greater than the LED modulation bandwidth, a BER target of 5×10^{-5} can be reached using C-OFDM at the cost of a 4-6 dB optical power penalty, whereas both OFDM and F-OFDM failed to achieve this. However, compared to F-OFDM when $N > 32$, this accomplishment comes at the cost of slightly higher computational complexity.

7.2 Future Work

On the basis of the results and conclusions of the present study, significant topics for future research have been identified. It should also be understood that this project was never intended to result in a finished standalone product. The following recommendations are therefore made:

1. The method used to create the C-transform may also be used to build new transforms from other transformations, including the Hartley transform, the Hilbert transform, the number theoretic transform, the Fermat number transform, and the Haar transform. Because of this, the benefits of two cascaded transforms may be combined and used with other types of communication.
2. This study examined the BER performance of C-OFDM across AWGN, multipath channel models, and the impact of LED non-linearity. Meanwhile, in order to increase human activity in the ocean, underwater wireless communication (UWC) is essential. Due to its inherent benefits of high transmission data rates and low latency compared to the widely utilised underwater acoustic communication (UAC), underwater optical wireless communication (UOWC) has attracted much interest. UOWC provides inexpensive, eye-safe devices that may be utilised for point-to-multipoint cell networks and short links based on light-emitting diodes (LEDs). In order to address the drawbacks of their usage in the UOWC channel, another novel optical form of C-OFDM might be investigated.
3. It is possible that the hardware system might be adapted to use the proposed approaches. Real-time experimental demonstrations would be essential in assessing the potential of C-OFDM transmission.
4. Future work should focus on important technical topics such as error correction codes in order to further enhance the performance of C-OFDM in VLC systems.

References

- [1] P. A. Haigh, *Visible Light Data communications and applications*. London: IOP, 2020.
- [2] P. A. Haigh *et al.*, "Wavelength-multiplexed polymer LEDs: Towards 55 Mb/s organic visible light communications," *IEEE Journal on Selected Areas in Communications*, vol. 33, no. 9, pp. 1819-1828, 2015.
- [3] H. Koumaras *et al.*, "A SDN-based WiFi-VLC Coupled System for Optimised Service Provision in 5G Networks," in *2018 IEEE 19th International Symposium on "A World of Wireless, Mobile and Multimedia Networks"(WoWMoM)*, 2018: IEEE, pp. 14-17.
- [4] W. Saad, M. Bennis, and M. Chen, "A vision of 6G wireless systems: Applications, trends, technologies, and open research problems," *IEEE network*, vol. 34, no. 3, pp. 134-142, 2019.
- [5] C. V. N. Index, "Global Mobile Data Traffic Forecast Update, 2010–2015, white paper.«," *Retrieved February*, vol. 1, 2011.
- [6] Ericsson. "Ericsson Mobility Report." <https://www.ericsson.com/en/mobility-report/reports> (accessed 10/8/2021).
- [7] A. Osseiran *et al.*, "Scenarios for 5G mobile and wireless communications: the vision of the METIS project," *IEEE communications magazine*, vol. 52, no. 5, pp. 26-35, 2014.
- [8] Statista. "IoT: Number Of Connected Devices Worldwide 2012-2025 " <https://www.statista.com/statistics/471264/iot-number-of-connected-devices-worldwide/> (accessed 25 August 2020).
- [9] B. Bangerter, S. Talwar, R. Arefi, and K. Stewart, "Networks and devices for the 5G era," *IEEE Communications Magazine*, vol. 52, no. 2, pp. 90-96, 2014.
- [10] U. Cisco, "Cisco annual internet report (2018–2023) white paper," *Cisco: San Jose, CA, USA*, 2020.
- [11] M. A. Uusitalo *et al.*, "Hexa-X The European 6G flagship project," in *2021 Joint European Conference on Networks and Communications & 6G Summit (EuCNC/6G Summit)*, 2021: IEEE, pp. 580-585.
- [12] S. Goyal, N. Sharma, I. Kaushik, B. Bhushan, and N. Kumar, "A green 6G network era: Architecture and propitious technologies," in *Data Analytics and Management: Springer*, 2021, pp. 59-75.

- [13] B. Zong, C. Fan, X. Wang, X. Duan, B. Wang, and J. Wang, "6G technologies: Key drivers, core requirements, system architectures, and enabling technologies," *IEEE Vehicular Technology Magazine*, vol. 14, no. 3, pp. 18-27, 2019.
- [14] T. Huang, W. Yang, J. Wu, J. Ma, X. Zhang, and D. Zhang, "A survey on green 6G network: Architecture and technologies," *IEEE Access*, vol. 7, pp. 175758-175768, 2019.
- [15] K. David and H. Berndt, "6G vision and requirements: Is there any need for beyond 5G?," *IEEE Vehicular Technology Magazine*, vol. 13, no. 3, pp. 72-80, 2018.
- [16] Z. Ghassemlooy, W. Popoola, and S. Rajbhandari, *Optical wireless communications: system and channel modelling with Matlab®*. CRC press, 2019.
- [17] K. Fan, T. Komine, Y. Tanaka, and M. Nakagawa, "The effect of reflection on indoor visible-light communication system utilizing white LEDs," in *The 5th International Symposium on Wireless Personal Multimedia Communications*, 2002, vol. 2: IEEE, pp. 611-615.
- [18] S. Haruyama and M. Nakagawa, "A basic study of optical OFDM system for indoor visible communication utilizing plural white LEDs as lighting," 2001.
- [19] Y. Tanaka, S. Haruyama, and M. Nakagawa, "Wireless optical transmissions with white colored LED for wireless home links," in *11th IEEE International Symposium on Personal Indoor and Mobile Radio Communications. PIMRC 2000. Proceedings (Cat. No. 00TH8525)*, 2000, vol. 2: IEEE, pp. 1325-1329.
- [20] Y. Tanaka, T. Komine, S. Haruyama, and M. Nakagawa, "Indoor visible communication utilizing plural white LEDs as lighting," in *12th IEEE International Symposium on Personal, Indoor and Mobile Radio Communications. PIMRC 2001. Proceedings (Cat. No. 01TH8598)*, 2001, vol. 2: IEEE, pp. F-F.
- [21] T. Komine and M. Nakagawa, "Fundamental analysis for visible-light communication system using LED lights," *IEEE transactions on Consumer Electronics*, vol. 50, no. 1, pp. 100-107, 2004.
- [22] K. Cui, G. Chen, Z. Xu, and R. D. Roberts, "Line-of-sight visible light communication system design and demonstration," in *2010 7th International Symposium on Communication Systems, Networks & Digital Signal Processing (CSNDSP 2010)*, 2010: IEEE, pp. 621-625.

- [23] J. Song *et al.*, "Indoor hospital communication systems: An integrated solution based on power line and visible light communication," in *2014 IEEE Faible Tension Faible Consommation*, 2014: IEEE, pp. 1-6.
- [24] P. A. Haigh *et al.*, "Multi-band carrier-less amplitude and phase modulation for bandlimited visible light communications systems," *IEEE Wireless Communications*, vol. 22, no. 2, pp. 46-53, 2015.
- [25] S. Dimitrov and H. Haas, *Principles of LED light communications: towards networked Li-Fi*. Cambridge University Press, 2015.
- [26] J. Vučić, C. Kottke, K. Habel, and K.-D. Langer, "803 Mbit/s visible light WDM link based on DMT modulation of a single RGB LED luminary," in *2011 Optical Fiber Communication Conference and Exposition and the National Fiber Optic Engineers Conference*, 2011: IEEE, pp. 1-3.
- [27] F. Wu *et al.*, "Performance comparison of OFDM signal and CAP signal over high capacity RGB-LED-based WDM visible light communication," *IEEE Photonics Journal*, vol. 5, no. 4, pp. 7901507-7901507, 2013.
- [28] P. A. Haigh and I. Darwazeh, "Visible light communications: Fast-orthogonal frequency division multiplexing in highly bandlimited conditions," in *2017 IEEE/CIC International Conference on Communications in China (ICCC Workshops)*, 2017: IEEE, pp. 1-8.
- [29] P. A. Haigh *et al.*, "A multi-CAP visible-light communications system with 4.85-b/s/Hz spectral efficiency," *IEEE Journal on Selected Areas in Communications*, vol. 33, no. 9, pp. 1771-1779, 2015.
- [30] Z. Ghassemlooy, S. Arnon, M. Uysal, Z. Xu, and J. Cheng, "Emerging optical wireless communications—advances and challenges," *IEEE journal on selected areas in communications*, vol. 33, no. 9, pp. 1738-1749, 2015.
- [31] P. A. Haigh, Z. Ghassemlooy, S. Rajbhandari, I. Papakonstantinou, and W. Popoola, "Visible light communications: 170 Mb/s using an artificial neural network equalizer in a low bandwidth white light configuration," *Journal of lightwave technology*, vol. 32, no. 9, pp. 1807-1813, 2014.
- [32] F. Hu *et al.*, "High-speed Visible Light Communication Systems Based on Si-substrate LEDs with Multiple Superlattice Interlayers," 2021.

- [33] J. Li, P. Zou, X. Ji, X. Guo, and N. Chi, "High-speed visible light communication utilizing monolithic integrated PIN array receiver," *Optics Communications*, vol. 494, p. 127027, 2021.
- [34] R. Bian, I. Tavakkolnia, and H. Haas, "15.73 Gb/s visible light communication with off-the-shelf LEDs," *Journal of Lightwave Technology*, vol. 37, no. 10, pp. 2418-2424, 2019.
- [35] M. Wieckowski, J. Jensen, I. T. Monroy, J. Siuzdak, and J. Turkiewicz, "300 Mbps transmission with 4.6 bit/s/Hz spectral efficiency over 50 m PMMA POF link using RC-LED and multi-level carrierless amplitude phase modulation," in *National Fiber Optic Engineers Conference, 2011: Optical Society of America*, p. NTuB8.
- [36] Y. Wang *et al.*, "Efficient MMSE-SQRD-based MIMO decoder for SEFDM-based 2.4-Gb/s-spectrum-compressed WDM VLC system," *IEEE Photonics Journal*, vol. 8, no. 4, pp. 1-9, 2016.
- [37] S. Vappangi, V. V. Mani, and M. Sellathurai, *Visible Light Communication: A Comprehensive Theory and Applications with MATLAB®*. 2021.
- [38] X. Li, R. Mardling, and J. Armstrong, "Channel capacity of IM/DD optical communication systems and of ACO-OFDM," in *2007 IEEE International Conference on Communications*, 2007: IEEE, pp. 2128-2133.
- [39] Roke.co.uk. "The Roke United Kingdom Frequency Allocation Table - Roke." [Online]. Available: <https://roke.co.uk/expertise/sensors-and-communications/the-roke-united-kingdom-frequency-allocation-table> (accessed 23 May, 2022).
- [40] Z. Ghassemlooy, L. N. Alves, S. Zvanovec, and M.-A. Khalighi, *Visible light communications: theory and applications*. CRC press, 2017.
- [41] A. Halder and A. D. Barman, "Nonlinear compensation of LEDs for improved performance in CSK based indoor visible light communication," in *2015 6th International Conference on Computers and Devices for Communication (CODEC)*, 2015: IEEE, pp. 1-4.
- [42] R. Hui, "XPM and FWM in OFDM optical systems," in *LEOS 2001. 14th Annual Meeting of the IEEE Lasers and Electro-Optics Society (Cat. No. 01CH37242)*, 2001, vol. 1: IEEE, pp. 281-282.

- [43] M. Rodrigues and I. Darwazeh, "Fast OFDM: A proposal for doubling the data rate of OFDM schemes," in *Proceedings of the International Conference on Telecommunications*, 2002, vol. 3, pp. 484-487.
- [44] S. D. Dissanayake, K. Panta, and J. Armstrong, "A novel technique to simultaneously transmit ACO-OFDM and DCO-OFDM in IM/DD systems," in *2011 IEEE GLOBECOM Workshops (GC Wkshps)*, 2011: IEEE, pp. 782-786.
- [45] J. Armstrong, "OFDM for optical communications," *Journal of lightwave technology*, vol. 27, no. 3, pp. 189-204, 2009.
- [46] S. D. Dissanayake and J. Armstrong, "Comparison of aco-ofdm, dco-ofdm and ado-ofdm in im/dd systems," *Journal of lightwave technology*, vol. 31, no. 7, pp. 1063-1072, 2013.
- [47] H. Haas, M. S. Islam, C. Chen, and H. Abumarshoud, *An Introduction to Optical Wireless Mobile Communication*. Artech House, 2021.
- [48] M. Giordani, M. Polese, M. Mezzavilla, S. Rangan, and M. Zorzi, "Toward 6g networks: Use cases and technologies," *IEEE Communications Magazine*, vol. 58, no. 3, pp. 55-61, 2020.
- [49] P. Sharma, "Evolution of mobile wireless communication networks-1G to 5G as well as future prospective of next generation communication network," *International Journal of Computer Science and Mobile Computing*, vol. 2, no. 8, pp. 47-53, 2013.
- [50] A. U. Gawas, "An overview on evolution of mobile wireless communication networks: 1G-6G," *International Journal on Recent and Innovation Trends in Computing and Communication*, vol. 3, no. 5, pp. 3130-3133, 2015.
- [51] R. Green, H. Higgins, and M. Leeson, "Recent developments in indoor optical wireless [Optical]," 2008.
- [52] I. Akasaki, H. Amano, and S. Nakamura, "Blue LEDs—Filling the world with new light," *The Royal Swedish Academy of Sciences—The Nobel Prize in Physics*, 2014.
- [53] C. Wang, G. Li, Y. Ha, S. Han, and N. Chi, "A 2.5 Gb/s Real-Time Visible-Light Communication System Based on Phosphorescent White LED," in *2019 7th International Conference on Information, Communication and Networks (ICICN)*, 2019: IEEE, pp. 140-145.

- [54] R. X. Ferreira *et al.*, "High bandwidth GaN-based micro-LEDs for multi-Gb/s visible light communications," *IEEE Photonics Technology Letters*, vol. 28, no. 19, pp. 2023-2026, 2016.
- [55] M. S. Islim *et al.*, "Towards 10 Gb/s orthogonal frequency division multiplexing-based visible light communication using a GaN violet micro-LED," *Photonics Research*, vol. 5, no. 2, pp. A35-A43, 2017.
- [56] E. Xie *et al.*, "Over 10 Gbps VLC for long-distance applications using a GaN-based series-biased micro-LED array," *IEEE Photonics Technology Letters*, vol. 32, no. 9, pp. 499-502, 2020.
- [57] H. Le Minh, Z. Ghassemlooy, A. Burton, and P. A. Haigh, "Equalization for organic light emitting diodes in visible light communications," in *2011 IEEE GLOBECOM Workshops (GC Wkshps)*, 2011: IEEE, pp. 828-832.
- [58] I. D. Samuel *et al.*, "Ultrafast OLEDs enable visible light communication at a gigabit per second," in *Organic and Hybrid Light Emitting Materials and Devices XXIV*, 2020, vol. 11473: International Society for Optics and Photonics, p. 114730P.
- [59] K. Yoshida *et al.*, "245 MHz bandwidth organic light-emitting diodes used in a gigabit optical wireless data link," *Nature communications*, vol. 11, no. 1, pp. 1-7, 2020.
- [60] K. A. Werfli, "Experimental Investigation of the Generalised Multi-Band Carrier-Less Amplitude and Phase Modulation in Visible Light Communications," University of Northumbria at Newcastle (United Kingdom), 2018.
- [61] J. Armstrong and B. J. Schmidt, "Comparison of asymmetrically clipped optical OFDM and DC-biased optical OFDM in AWGN," *IEEE communications letters*, vol. 12, no. 5, pp. 343-345, 2008.
- [62] A. Bergh and J. Copeland, "Optical sources for fiber transmission systems," *Proceedings of the IEEE*, vol. 68, no. 10, pp. 1240-1247, 1980.
- [63] P. Haigh, "Using equalizers to increase data rates in organic photonic devices for visible light communications systems," University of Northumbria, 2014.
- [64] P. A. Haigh *et al.*, "Exploiting equalization techniques for improving data rates in organic optoelectronic devices for visible light communications," *Journal of lightwave technology*, vol. 30, no. 19, pp. 3081-3088, 2012.

- [65] I. Stefan, H. Elgala, and H. Haas, "Study of dimming and LED nonlinearity for ACO-OFDM based VLC systems," in *2012 IEEE Wireless Communications and Networking Conference (WCNC)*, 2012: IEEE, pp. 990-994.
- [66] D. Falconer, "Carrierless am/pm," *Bell Laboratories, NJ, USA, Bell Laboratories Technical Memorandum, Tech. Rep*, 1975.
- [67] L.-L. Yang, *Multicarrier communications*. John Wiley & Sons, 2009.
- [68] E. Basar, M. Wen, R. Mesleh, M. Di Renzo, Y. Xiao, and H. Haas, "Index modulation techniques for next-generation wireless networks," *IEEE access*, vol. 5, pp. 16693-16746, 2017.
- [69] A. Al-Kinani, C.-X. Wang, L. Zhou, and W. Zhang, "Optical wireless communication channel measurements and models," *IEEE Communications Surveys & Tutorials*, vol. 20, no. 3, pp. 1939-1962, 2018.
- [70] M. I. Olmedo *et al.*, "Multiband carrierless amplitude phase modulation for high capacity optical data links," *Journal of Lightwave Technology*, vol. 32, no. 4, pp. 798-804, 2013.
- [71] K. Sankar. "Raised cosine filter for transmit pulse shaping." <https://dsplog.com/2008/04/22/raised-cosine-filter-for-transmit-pulse-shaping/> (accessed 19/07, 2023).
- [72] S. B. Weinstein, "The history of orthogonal frequency-division multiplexing [History of Communications]," *IEEE Communications Magazine*, vol. 47, no. 11, pp. 26-35, 2009.
- [73] N. LaSorte, W. J. Barnes, and H. H. Refai, "The history of orthogonal frequency division multiplexing," in *IEEE GLOBECOM 2008-2008 IEEE Global Telecommunications Conference*, 2008: IEEE, pp. 1-5.
- [74] R. W. Chang, "Orthogonal frequency multiplex data transmission system," ed: Google Patents, 1970.
- [75] R. Lassalle and M. Alard, "Principles of modulation and channel coding for digital broadcasting for mobile receivers," *EBU Tech. Rev*, vol. 224, no. 1, pp. 68-190, 1987.
- [76] M. Kornfeld and G. May, "DVB-H and IP datacast—broadcast to handheld devices," *IEEE Transactions on Broadcasting*, vol. 53, no. 1, pp. 161-170, 2007.
- [77] J. S. Chow, J. C. Tu, and J. M. Cioffi, "A discrete multitone transceiver system for HDSL applications," *IEEE journal on selected areas in communications*, vol. 9, no. 6, pp. 895-908, 1991.

- [78] E. Telatar, "Capacity of multi-antenna Gaussian channels," *European transactions on telecommunications*, vol. 10, no. 6, pp. 585-595, 1999.
- [79] I. E. Telatar and R. G. Gallager, "Combining queueing theory with information theory for multiaccess," *IEEE Journal on Selected Areas in Communications*, vol. 13, no. 6, pp. 963-969, 1995.
- [80] L. Cimini, "Analysis and simulation of a digital mobile channel using orthogonal frequency division multiplexing," *IEEE transactions on communications*, vol. 33, no. 7, pp. 665-675, 1985.
- [81] M. Rodrigues and I. Darwazeh, "A spectrally efficient frequency division multiplexing based communications system," in *Proc. 8th Int. OFDM Workshop*, 2003, pp. 48-49.
- [82] W. Y. Zou and Y. Wu, "COFDM: An overview," *IEEE transactions on broadcasting*, vol. 41, no. 1, pp. 1-8, 1995.
- [83] J. G. Andrews, A. Ghosh, and R. Muhamed, *Fundamentals of WiMAX: understanding broadband wireless networking*. Pearson Education, 2007.
- [84] O. Saied, "Orthogonal Frequency Division Multiplexing for Indoor Visible Light Communication Links," Northumbria University, 2018.
- [85] M. S. Ahmed, "OFDM base T-transform for wireless communication networks," Newcastle University, 2012.
- [86] B. Muquet, Z. Wang, G. B. Giannakis, M. De Courville, and P. Duhamel, "Cyclic prefixing or zero padding for wireless multicarrier transmissions?," *IEEE Transactions on communications*, vol. 50, no. 12, pp. 2136-2148, 2002.
- [87] W. Ozan, R. Grammenos, and I. Darwazeh, "Zero Padding or Cyclic Prefix: Evaluation for Non-Orthogonal Signals," *IEEE Communications Letters*, 2020.
- [88] A. R. Bahai, B. R. Saltzberg, and M. Ergen, *Multi-carrier digital communications: theory and applications of OFDM*. Springer Science & Business Media, 2004.
- [89] I. B. Djordjevic, *Advanced optical and wireless communications systems*. Springer, 2018.
- [90] A. Peled and A. Ruiz, "Frequency domain data transmission using reduced computational complexity algorithms," in *ICASSP'80. IEEE International Conference on Acoustics, Speech, and Signal Processing*, 1980, vol. 5: IEEE, pp. 964-967.

- [91] A. A. Al-jzari, I. Kostanic, and K. H. M. Mabrok, "Effect of variable cyclic prefix length on OFDM system performance over different wireless channel models," *Univers. J. Commun. Networ*, vol. 3, no. 1, pp. 7-14, 2015.
- [92] A. K. Jagannatham, "NOC: Principles of Modern CDMA/MIMO/OFDM Wireless Communications," ed, 2015.
- [93] M. Zhang and Z. Zhang, "An optimum DC-biasing for DCO-OFDM system," *IEEE Communications Letters*, vol. 18, no. 8, pp. 1351-1354, 2014.
- [94] S. Dimitrov and H. Haas, "Information rate of OFDM-based optical wireless communication systems with nonlinear distortion," *Journal of Lightwave Technology*, vol. 31, no. 6, pp. 918-929, 2012.
- [95] S. Deka, P. Saengudomlert, and S. Baruah, "Dimming consideration for OFDM-based visible light communications," *ADBU Journal of Engineering Technology*, vol. 2, no. 1, 2015.
- [96] S. Vappangi and V. M. Vakamulla, "Channel estimation in ACO-OFDM employing different transforms for VLC," *AEU-International Journal of Electronics and Communications*, vol. 84, pp. 111-122, 2018.
- [97] H. G. Myung, J. Lim, and D. J. Goodman, "Peak-to-average power ratio of single carrier FDMA signals with pulse shaping," in *2006 IEEE 17th international symposium on personal, indoor and mobile radio communications*, 2006: IEEE, pp. 1-5.
- [98] H. Burchardt, N. Serafimovski, D. Tsonev, S. Videv, and H. Haas, "VLC: Beyond point-to-point communication," *IEEE Communications Magazine*, vol. 52, no. 7, pp. 98-105, 2014.
- [99] R. Rathore and N. Kaur, "Comparison study of DIT and DIF radix-2 FFT algorithm," *Int. J. Comput. Appl.*, vol. 150, pp. 25-28, 2016.
- [100] H. A. Leftah and S. Boussakta, "Novel OFDM based on C-transform for improving multipath transmission," *IEEE Transactions on Signal Processing*, vol. 62, no. 23, pp. 6158-6170, 2014.
- [101] N. Ahmed, T. Natarajan, and K. R. Rao, "Discrete cosine transform," *IEEE transactions on Computers*, vol. 100, no. 1, pp. 90-93, 1974.
- [102] K. R. Rao and P. Yip, *Discrete cosine transform: algorithms, advantages, applications*. Academic press, 2014.

- [103] J. L. Walsh, "A closed set of normal orthogonal functions," *American Journal of Mathematics*, vol. 45, no. 1, pp. 5-24, 1923.
- [104] H. C. Andrews, A. Tescher, and R. P. Kruger, "Image processing by digital computer," *IEEE spectrum*, vol. 9, no. 7, pp. 20-32, 1972.
- [105] M. Maqusi, *Applied Walsh Analysis*. Heyden, 1981.
- [106] N. Ahmed and K. R. Rao, *Orthogonal transforms for digital signal processing*. Springer Science & Business Media, 2012.
- [107] S. Boussakta and A. Holt, "Fast algorithm for calculation of both Walsh-Hadamard and Fourier transforms (FWFTs)," *Electronics Letters*, vol. 25, no. 20, pp. 1352-1354, 1989.
- [108] M. T. Hamood and S. Boussakta, "Fast walsh–hadamard–fourier transform algorithm," *IEEE Transactions on Signal Processing*, vol. 59, no. 11, pp. 5627-5631, 2011.
- [109] D. Hein and N. Ahmed, "On a real-time Walsh-Hadamard/cosine transform image processor," *IEEE Transactions on Electromagnetic Compatibility*, no. 3, pp. 453-457, 1978.
- [110] J. Abdulwali, P. A. Haigh, and S. Boussakta, "New Visible Light Communication Using C-OFDM," in *2020 12th International Symposium on Communication Systems, Networks and Digital Signal Processing (CSNDSP)*, 2020: IEEE, pp. 1-5.
- [111] Q. Wen, Y. Xiao, P. Cheng, C. Zhang, and S. Li, "S-PTS for PAPR reduction in OFDM systems," in *2008 4th International Conference on Wireless Communications, Networking and Mobile Computing*, 2008: IEEE, pp. 1-4.
- [112] E. Chu and A. George, *Inside the FFT black box: serial and parallel fast Fourier transform algorithms*. CRC press, 1999.
- [113] R. Srinivasan and K. Rao, "An approximation to the discrete cosine transform for N=16," *Signal Processing*, vol. 5, no. 1, pp. 81-85, 1983.
- [114] V. Britanak, P. C. Yip, and K. R. Rao, *Discrete cosine and sine transforms: general properties, fast algorithms and integer approximations*. Elsevier, 2010.
- [115] L. Yang, K.-K. Soo, Y.-M. Siu, and S. Li, "A low complexity selected mapping scheme by use of time domain sequence superposition technique for PAPR reduction in OFDM system," *IEEE transactions on Broadcasting*, vol. 54, no. 4, pp. 821-824, 2008.

- [116] P. Tan and N. C. Beaulieu, "A comparison of DCT-based OFDM and DFT-based OFDM in frequency offset and fading channels," *IEEE Transactions on Communications*, vol. 54, no. 11, pp. 2113-2125, 2006.
- [117] W.-L. Chin, "Maximization of effective signal power in DCT window for symbol time synchronization in optical fast OFDM," *Journal of lightwave technology*, vol. 31, no. 5, pp. 740-748, 2012.
- [118] J. Zhou *et al.*, "FOFDM based on discrete cosine transform for intensity-modulated and direct-detected systems," *Journal of lightwave technology*, vol. 34, no. 16, pp. 3717-3725, 2016.
- [119] P. A. Haigh, A. Burton, Z. Ghassemlooy, and I. Darwazeh, "Visible Light Communications: Simplified Co-Equalisation of Fast OFDM in a Multiple-Input Multiple-Output Configuration," in *2019 26th International Conference on Telecommunications (ICT)*, 2019: IEEE, pp. 46-50.
- [120] J. Zhao and A. Ellis, "A novel optical fast OFDM with reduced channel spacing equal to half of the symbol rate per carrier," in *Optical Fiber Communication Conference*, 2010: Optical Society of America, p. OMR1.
- [121] L. Zhao, J. He, Z. Zhou, R. Deng, and L. Chen, "The research of optical fast OFDM based on channel estimation algorithm," *IEEE Photonics Journal*, vol. 8, no. 3, pp. 1-5, 2016.
- [122] T. Jiang and Y. Wu, "An overview: Peak-to-average power ratio reduction techniques for OFDM signals," *IEEE Transactions on broadcasting*, vol. 54, no. 2, pp. 257-268, 2008.
- [123] H. Elgala, R. Mesleh, and H. Haas, "Non-linearity effects and predistortion in optical OFDM wireless transmission using LEDs," *International Journal of Ultra Wideband Communications and Systems*, vol. 1, no. 2, pp. 143-150, 2009.
- [124] S. H. Han and J. H. Lee, "An overview of peak-to-average power ratio reduction techniques for multicarrier transmission," *IEEE wireless communications*, vol. 12, no. 2, pp. 56-65, 2005.
- [125] H. Zhang, Y. Yuan, and W. Xu, "PAPR reduction for DCO-OFDM visible light communications via semidefinite relaxation," *IEEE Photonics Technology Letters*, vol. 26, no. 17, pp. 1718-1721, 2014.

- [126] O. Saied, X. Li, and K. M. Rabie, "DFT Spread-Optical Pulse Amplitude Modulation for Visible Light Communication Systems," *IEEE Access*, vol. 10, pp. 15956-15967, 2022.
- [127] W. O. Popoola, Z. Ghassemlooy, and B. G. Stewart, "Pilot-assisted PAPR reduction technique for optical OFDM communication systems," *Journal of Lightwave Technology*, vol. 32, no. 7, pp. 1374-1382, 2014.
- [128] K. Bandara, P. Niroopan, and Y.-H. Chung, "PAPR reduced OFDM visible light communication using exponential nonlinear companding," in *2013 IEEE International Conference on Microwaves, Communications, Antennas and Electronic Systems (COMCAS 2013)*, 2013: IEEE, pp. 1-5.
- [129] H. Elgala, R. Mesleh, and H. Haas, "An LED model for intensity-modulated optical communication systems," *IEEE Photonics Technology Letters*, vol. 22, no. 11, pp. 835-837, 2010.
- [130] J. M. Kahn and J. R. Barry, "Wireless infrared communications," *Proceedings of the IEEE*, vol. 85, no. 2, pp. 265-298, 1997.
- [131] H. Le Minh *et al.*, "A 1.25-Gb/s indoor cellular optical wireless communications demonstrator," *IEEE Photonics Technology Letters*, vol. 22, no. 21, pp. 1598-1600, 2010.
- [132] P. Chvojka, S. Zvanovec, P. A. Haigh, and Z. Ghassemlooy, "Channel characteristics of visible light communications within dynamic indoor environment," *Journal of Lightwave Technology*, vol. 33, no. 9, pp. 1719-1725, 2015.
- [133] A. Burton, H. Le Minh, Z. Ghassemlooy, S. Rajbhandari, and P. A. Haigh, "Performance analysis for 180 receiver in visible light communications," in *2012 Fourth International Conference on Communications and Electronics (ICCE)*, 2012: IEEE, pp. 48-53.
- [134] P. H. Pathak, X. Feng, P. Hu, and P. Mohapatra, "Visible light communication, networking, and sensing: A survey, potential and challenges," *IEEE communications surveys & tutorials*, vol. 17, no. 4, pp. 2047-2077, 2015.
- [135] A. Gupta and P. Garg, "Statistics of SNR for an indoor VLC system and its applications in system performance," *IEEE Communications Letters*, vol. 22, no. 9, pp. 1898-1901, 2018.

- [136] I. Stefan, H. Burchardt, and H. Haas, "Area spectral efficiency performance comparison between VLC and RF femtocell networks," in *2013 IEEE international conference on communications (ICC)*, 2013: IEEE, pp. 3825-3829.